

RESONATING VALENCE BOND STATES – A QUANTUM INFORMATION PERSPECTIVE

By
SUDIPTO SINGHA ROY
PHYS08201204007

Harish-Chandra Research Institute, Allahabad

A thesis submitted to the
Board of Studies in Physical Sciences
In partial fulfillment of requirements
for the Degree of
DOCTOR OF PHILOSOPHY
of
HOMI BHABHA NATIONAL INSTITUTE



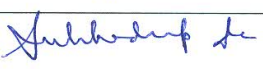
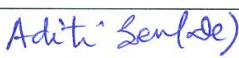



September, 2017

Homi Bhabha National Institute¹

Recommendations of the Viva Voce Committee

As members of the Viva Voce Committee, we certify that we have read the dissertation prepared by Mr. Sudipto Singha Roy entitled "Resonating Valence Bond States – A Quantum Information Perspective" and recommend that it may be accepted as fulfilling the thesis requirement for the award of Degree of Doctor of Philosophy.

Chairman – Prof. Pinaki Majumdar		Date: 14/2/18
Guide / Convener – Prof. Ujjwal Sen		Date: 19/2/18
Examiner – Prof. Subhadeep De		Date: 19/02/2018
Member 1- Prof. Aditi Sen (De)		Date: 19.02.18
Member 2- Prof. Arun Kumar Pati		Date: 19.2.18
Member 3- Prof. Santosh Kumar Rai		Date:

Final approval and acceptance of this thesis is contingent upon the candidate's submission of the final copies of the thesis to HBNI.

I/We hereby certify that I/we have read this thesis prepared under my/our direction and recommend that it may be accepted as fulfilling the thesis requirement.

Date: February 19, 2018

Place: Allahabad

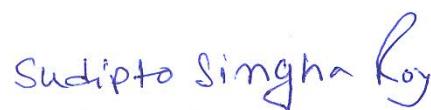

Prof. Ujjwal Sen

¹ This page is to be included only for final submission after successful completion of viva voce.

STATEMENT BY AUTHOR

This dissertation has been submitted in partial fulfillment of requirements for an advanced degree at Homi Bhabha National Institute (HBNI) and is deposited in the Library to be made available to borrowers under rules of the HBNI.

Brief quotations from this dissertation are allowable without special permission, provided that accurate acknowledgement of source is made. Requests for permission for extended quotation from or reproduction of this manuscript in whole or in part may be granted by the Competent Authority of HBNI when in his or her judgment the proposed use of the material is in the interests of scholarship. In all other instances, however, permission must be obtained from the author.


Sudipto Singha Roy

DECLARATION

I, hereby declare that the investigation presented in the thesis has been carried out by me. The work is original and has not been submitted earlier as a whole or in part for a degree / diploma at this or any other Institution / University.

Sudipto Singha Roy
Sudipto Singha Roy

List of Publications arising from the thesis

Journal

1. “Diverging scaling with converging multisite entanglement in odd and even quantum Heisenberg ladders”, Sudipto Singha Roy, Himadri Shekhar Dhar, Debraj Rakshit, Aditi Sen(De), and Ujjwal Sen, *New Journal of Physics*, **2016**, *18*, 023025-1-023025-9.
2. “Analytical recursive method to ascertain multisite entanglement in doped quantum spin ladders”, Sudipto Singha Roy, Himadri Shekhar Dhar, Debraj Rakshit, Aditi Sen(De), and Ujjwal Sen, *Physical Review B*, **2017**, *96*, 075143-1-075143-10.

Preprints

1. “Response to defects in multi- and bipartite entanglement of isotropic quantum spin networks”, Sudipto Singha Roy, Himadri Shekhar Dhar, Debraj Rakshit, Aditi Sen(De), and Ujjwal Sen, arXiv:1607.05195 [quant-ph].
2. “Fibonacci sequence and valence bond entanglement entropy in quantum spin ladders”, Sudipto Singha Roy, Himadri Shekhar Dhar, Aditi Sen(De), and Ujjwal Sen, arXiv:1712.02726 [quant-ph].

Further publications of candidate not used substantially in the thesis

Journal

1. “Beating no-go theorems by engineering defects in quantum spin model”, Debasis Sadhukhan, Sudipto Singha Roy, Debraj Rakshit, Aditi Sen(De), and Ujjwal Sen, *New Journal of Physics*, **2015**, *17*, 043013-1-043013-2.
2. “Quantum discord length is enhanced while entanglement length is not by introducing disorder in a spin chain”, Debasis Sadhukhan, Sudipto Singha Roy, Debraj Rakshit, R Prabhu, Aditi Sen(De), and Ujjwal Sen, *Physical Review E*, **2016**, *93*, 012131-1-012131-8.

3. “Conclusive Identification of Quantum Channels via Monogamy of Quantum Correlations”, Asutosh Kumar, Sudipto Singha Roy, Amit Kumar Pal, R Prabhu, Aditi Sen(De), and Ujjwal Sen, *Physical Letters A*, **2016**, 380, 3588-3594.
4. “Generalized Geometric Measure of Entanglement for Multiparty Mixed States”, Tamoghna Das, Sudipto Singha Roy, Shrobona Bagchi, Avijit Misra, Aditi Sen(De), and Ujjwal Sen, *Physical Review A*, **2016**, 94, 022336-1-022336-8.
5. “Multipartite Entanglement Accumulation in Quantum States: Localizable Generalized Geometric Measure”, Debasis Sadhukhan, Sudipto Singha Roy, Amit Kumar Pal, Debraj Rakshit, Aditi Sen(De), and Ujjwal Sen, *Physical Review A*, **2017**, 95, 022301-1-022301-14.
6. “Detecting phase boundaries of quantum spin1/2 XXZ ladder via bipartite and multipartite entanglement transitions”, Sudipto Singha Roy, Himadri Shekhar Dhar, Debraj Rakshit, Aditi Sen(De), and Ujjwal Sen, *Journal of Magnetism and Magnetic Materials*, **2017**, 444, 227-235.
7. “Quantum discord and its allies: a review of recent progress”, Anindita Bera, Tamoghna Das, Debasis Sadhukhan, Sudipto Singha Roy, Aditi Sen(De), and Ujjwal Sen, *Report on Progress in Physics*, **2018**, 81, 024001-1-024001-59.
8. “Effects of cavity-cavity interaction on the entanglement dynamics of a generalized double Jaynes-Cummings model”, Mahasweta Pandit, Sreetama Das, Sudipto Singha Roy, Himadri Shekhar Dhar, and Ujjwal Sen, *Journal of Physics B: Atomic, Molecular and Optical Physics*, **2018**, 51 , 045501-1-045501-7.

Preprints

1. “Emergence of adiabatic freezing of genuine multipartite entanglement with insertion of defects in one-dimensional Hubbard model”, Sreetama Das, Sudipto Singha Roy, Himadri Shekhar Dhar, Debraj Rakshit, Aditi Sen(De), and Ujjwal Sen, arXiv:1708.07005 [quant-ph].

2. “Wave-particle duality employing quantum coherence in superposition with non-distinguishable pointers”, Sreetama Das, Chiranjib, and Ujjwal Sen, arXiv: 1705.04343 [quant-ph].
3. “Benford analysis of quantum critical phenomena: First digit provides high finite-size scaling exponent while first two and further are not much better”, Anindita Bera, Utkarsh Mishra, Sudipto Singha Roy, Anindya Biswas, Aditi Sen(De), and Ujjwal Sen, arXiv: 1711.00758 [quant-ph].

Conferences/visits

1. *School on Topological Quantum Matter, Harish-Chandra Research Institute, India, February 2015*, Poster presentation on “Enhancement of Quantum Correlation Length in Quenched Disordered Spin Chains”
2. *Young Quantum-2015 (YouQu-15), Harish-Chandra Research Institute, India, February 2015*, Oral presentation on “Beating no-go theorems by engineering defects in quantum spin models”.
3. *International School and Conference on Quantum Information (ISCQI-16), February 2016, Institute of Physics (IOP), Bhubaneswar, India*, Poster presentation on “Diverging scaling with converging multisite entanglement in odd and even quantum Heisenberg ladders”.
4. *Conference on Entanglement and Non-Equilibrium Physics of Pure and Disordered Systems, July 2016, International Centre for Theoretical Physics, Trieste, Italy*, Poster presentation on “Analytical recursive method to ascertain multisite entanglement in doped quantum spin ladders”.

Sudipto Singha Roy

Sudipto Singha Roy

To my parents and sisters

ACKNOWLEDGEMENTS

It gives me immense pleasure to acknowledge all the people who have supported me during the course of my PhD research. First and foremost, my deepest gratitude goes out to my supervisor, Prof. Ujjwal Sen, for his guidance throughout my doctoral study. He has provided me with critical insights and, at the same time, given me the freedom to formulate my ideas. I am equally grateful to Prof. Aditi Sen (De) for her valuable suggestions, support and encouragement during my research life. I would be remiss if I did not recognize their approachability, sincerity and warmth that made my research life enjoyable and rewarding. My heartfelt thanks to Prof. Arun Kumar Pati and the members of my advisory committee for always being available for any discussion and assistance.

I would also like to take this opportunity to express my sincerest gratitude to all the faculties and researchers at HRI. Academic debates with my fellow colleagues of the Quantum Information and Computation (QIC) Group have further enriched my research. I also had the opportunity of interacting with several physicists across the world, who have been kind enough to share their knowledge and expertise with me. I would like to thank Prof. German Sierra at IFS, Madrid, Spain, Prof. Didier Poilblanc at CNRS, Toulouse, France, Prof. Stefan Wessel at RWTH, Aachen, Germany. Prof. Rosario Fazio at ICTP, Trieste, Italy, Prof. David Rossini at SNS, Pisa, Italy.

I thank the Department of Atomic Energy, Government of India and HBNI for financial support during my doctoral research. My sincere thanks to the HRI administrative body, the computer centre, the cluster computation facility and the library for providing me a conducive environment for research. I would also like to thank to all other nonacademic staffs, mess staffs, gardeners, security staffs, cleaning staffs at HRI.

My years as a doctoral student would not have been interesting if not for fellow researchers who made my journey easier. My love and gratitude goes out to all the members, past and present, of the QIC group, other friends at HRI, Belur and IIT Bombay who made life outside academics, fun and memorable. A special thanks to Anindita, Arnab, Arka, Debasis, Tanmay, Ritwik, Himadri da, Suthopa di, Sunil Maharaj and Khadiza for always being there and for supporting me in all aspects of my life. Many thanks to my childhood friends Abhigyan, Uttam, Mriganka for their support and encouragement.

I would also like to thank all my relatives for their constant support and wishing the best for me. Thanks and lots of love to my sisters, Manashi and Tapasi, and my brothers-in-law Sanjay da and Pradipta da, for being a constant source of affection and encouragement. I will forever be indebted to my mother, Mala Singha Roy and father, Hiran Singha Roy for their unconditional love and support during all these years. I thank them for giving me a wonderful childhood and guiding me in all aspects of my life.

Contents

SYNOPSIS	v
LIST OF FIGURES	xi
1 Introduction	1
2 Quantum entanglement measures	11
2.1 Introduction	11
2.2 Bipartite entanglement measures	12
2.2.1 Valence bond entanglement entropy	12
2.2.2 Logarithmic negativity	14
2.2.3 Multipartite entanglement measures	15
2.3 Summary	16
3 Fibonacci sequence and valence bond entanglement entropy	17
3.1 Introduction	17
3.2 Resonating valence bond ladder and the Fibonacci sequence	19
3.3 Multi-legged quantum spin ladders and recursion relations	23
3.4 Doped RVB ladders	28
3.5 Summary	34
4 Multipartite entanglement in undoped quantum spin ladders	37
4.0.1 Introduction	37
4.1 Characterization of genuine multisite entanglement in Heisenberg ladders	39
4.1.1 Odd-legged ladders	40

4.1.2	Even-legged ladders	41
4.2	Density matrix recursion method (DMRM)	43
4.3	Characterization of genuine multisite entanglement in RVB ladders	52
4.4	Diverging scaling with converging multisite entanglement	53
4.5	Summary	55
5	Multipartite entanglement in doped quantum spin ladders	57
5.1	Introduction	57
5.2	Recursion method to generate doped RVB states	60
5.3	Recursion relation for reduced density matrices	66
5.3.1	Open ladder	66
5.3.2	Periodic ladder	70
5.4	Genuine multiparty entanglement in quantum ladders	72
5.5	Trends of genuine multisite entanglement: GS of t - J ladder vs doped RVB state	75
5.6	Summary	79
6	Isotropic quantum spin networks in two-dimensions	81
6.1	Introduction	81
6.2	Isotropic spin network	82
6.3	Single- and two-node Reduced states of the spin network	84
6.4	Bound on bipartite entanglement	91
6.5	Genuinely multipartite entanglement	94
6.6	Summary	96
7	Summary	99
	Bibliography	105

SYNOPSIS

Over the past few decades, developments in the field of quantum information have led to the discovery of quantum computation and communication networks that transcend the capabilities of classical systems. Natural candidates to implement an efficient and scalable quantum network include interacting spin lattices. In order to avail such quantum many-body systems as resources for quantum information processing tasks, an important primary investigation would be necessary to uncover the intricate details of the distribution of quantum correlations among the subparts of the systems. In particular, distribution of quantum entanglement in the ground state configuration of a many-body system provides useful insights on various co-operative phenomena associated with it. For instance, in noncritical one-dimensional systems, the entanglement entropy between a contiguous block and the rest of the system scales with the boundary of the bipartition— an area law. On the other hand, when the system remains close to a quantum phase transition point, a significant change in the scaling behavior is observed which includes additional logarithmic corrections.

Down the avenue, several attempts have been made to characterize bipartite as well as multipartite entanglement properties associated with various strongly correlated systems which undoubtedly emphasize the role of entanglement in detecting co-operative phenomena. However, quantification and characterization of quantum entanglement in a complex quantum many-body system is not an easy task to perform. One of the primary reasons behind this is the lack of exact analytical form of the minimum energy configuration of the system. There are only a few cases for which exact analytical form of the ground state configuration can be obtained and one needs to rely on various approximation methods, when the size of the system becomes even moderately large. In this regard, resonating valence bond states have been emerged as an efficient ansatz capturing the behavior of frustrated quantum

spin systems, in particular, Heisenberg antiferromagnets. For instance, the superconducting states of the t - J ladder can be represented using the short-range doped resonating valence bond ansatz, which were introduced to describe Mott-insulators in spin-1/2 Heisenberg antiferromagnets. Over the years, notable progress has been made which uncover other important aspects of resonating valence bond states, which includes topological order. While there have been efforts to characterize quantum correlations, in particular, multipartite quantum entanglement, present in resonating valence bond states, there is still much that is left to understand and interpret. In this thesis, we shed light on the bipartite and multipartite entanglement properties of the doped as well as undoped resonating valence bond states, on multi-legged spin-1/2 quantum ladders and isotropic networks in two-dimension and highlight its importance in quantum information processing tasks.

Following are the main results that are included in this thesis.

- We derive analytical recursion methods to generate resonating valence bond states defined on doped and undoped multi-legged spin-1/2 quantum ladders. Subsequently, we investigate the scaling behavior of the valence bond entanglement entropy for these multi-legged quantum ladders, consisting of a large number of lattice sites. **The detailed descriptions are reported in Ref. [1].**
- We detect a dichotomy between even- and odd-legged ladders using genuine multiparty entanglement present in the ground state configuration of Heisenberg ladders of moderate size, using exact diagonalization technique. Thereafter, using the resonating valence bond states ansatz, we detect the diverging scaling properties of multiparty entanglement for odd- and even-legged quantum ladders, in the asymptotic limit. **The detailed descriptions are reported in Ref. [2].**
- We investigate the trends of genuine multipartite entanglement in the ground

state configuration of a Hubbard model with large onsite interactions (t - J model) of moderate size, using exact diagonalization. We subsequently formulate an analytical recursion method to efficiently estimate multiparty entanglement in doped resonating valence bond ladders of large size. The doped resonating valence bond state is shown to have high fidelity in the relevant ranges of the Hubbard model for moderate size. **The detailed descriptions are reported in Ref. [3].**

- We consider an isotropic quantum network of spin-1/2 particles with a finite fraction of defects and studied its bipartite as well as multipartite entanglement characteristics. **The detailed descriptions are reported in Ref. [4].**

The content of the thesis is split into seven Chapters.

In Chapter 1 (Introduction), we will briefly highlight the importance of characterization of quantum correlations present in interacting quantum-many-body systems. In Chapter 2 (Quantum entanglement measures), we will discuss a few measures of bipartite as well as multipartite quantum entanglement which we will later use in the proposed thesis. Thereafter, in Chapter 3 (Fibonacci sequence and valence bond entanglement entropy), we derive analytical recursive methods to construct resonating valence bond states on doped and undoped multi-legged spin-1/2 quantum ladders [1]. We then investigate the behavior of valence bond entanglement entropy between a contiguous block to the rest of the system with the increase of the size of the block. This provides useful information regarding the distribution of entanglement in the ground state configuration. Our results in Chapter 3 are contained in Ref. [1].

In Chapter 4 (Multipartite entanglement in undoped quantum spin ladders), we consider the ground state of Heisenberg spin ladders and investigate the odd-even dichotomy of genuine multiparty entanglement [2]. We found that when the size of the system remains small, multiparty entanglement measure can capture the even-

odd dichotomy present in the ground state of the system. However, as the size of the system is increased to a moderately large value, this even-odd dichotomy of multiparty entanglement is difficult to analyze due to increase in computational load. Interestingly, using the short-ranged resonating valence bond state ansatz, which emerges as possible ground state of the Heisenberg spin ladders in some parameter range, we show that though multiparty entanglement measure itself fails to capture the odd-even dichotomy, its scaling behavior is capable to distinguish the odd-even dichotomy in Heisenberg ladders, even in the asymptotic limit. The results of this Chapter are published in Ref. [2].

In Chapter 5 (Multipartite entanglement in doped quantum spin ladders), we investigate the trends of genuine multipartite entanglement in the ground states of a Hubbard model with large onsite interactions– the t - J model–via exact diagonalization [3]. Subsequently, for finite hole doping, the short-range resonating valence bond state is considered to be the ground state of the Hubbard model. We prove that doped resonating valence bond ladder states are always genuine multipartite entangled. We then formulate an analytical recursion method for the wave function, which allows us to efficiently estimate the entanglement as well as other physical quantities in large doped resonating valence bond ladders. The results of this Chapter are published in Ref. [3].

In Chapter 6 (Isotropic quantum spin networks in two dimensions), we consider an isotropic quantum network of spin-1/2 particles with a finite fraction of defects, where the corresponding wave function of the network is rotationally invariant under the action of local unitaries. By using quantum information-theoretic concepts like strong subadditivity of von Neumann entropy and approximate quantum telecloning, we prove analytically that in the presence of defects, the network sustains genuine multisite entanglement, and at the same time may exhibit a finite amount of bipartite entanglement, in contrast to the network with no defects. Our result in this Chapter

are contained in Ref. [4].

In Chapter 7 (Summary), we provide a brief summary of the results presented in the thesis.

We believe that the results obtained in the proposed thesis will be important to strengthen the bridge across the traditional boundaries between the two disciplines—quantum information theory and quantum many-body physics.

List of Figures

2.1	A dimer covered quantum spin ladder with a bipartition across $\tilde{L} : \tilde{N} - \tilde{L}$. The sites on different bipartite lattices, A and B have been distinguished using two different colors and the arrow represents dimer connecting two sites one from lattice A and another from lattice B. The covering contains $a_i = 2$ dimers across the boundary, shared between the blocks of \tilde{L} and $\tilde{N} - \tilde{L}$, which contributes to the valence bond entanglement entropy in Eq. (2.4). The above dimer arrangement constitutes a single covering in the valence bond basis $\{ \phi_i\rangle\}$. For any given ladder, Z_N such coverings are possible, each with a_i singlets present across the boundary.	13
3.1	The dimer coverings (represented by the arrows) in the state $ \bar{2}\rangle$, $ \bar{3}\rangle$ and $ \bar{4}\rangle$. The sites on different bipartite lattices, A and B, have been distinguished using two different colors.	20
3.2	The naturally occurring patterns on the Molluscan shell roughly follows the golden spiral, with the areas of the square blocks following the Fibonacci sequence.	21

- 3.3 Valence bond entanglement entropy in undoped RVB ladders. We exhibit here the variation of the valence bond entanglement entropy ($S_{\tilde{L}}$), with increasing block size of \tilde{L} rungs, for two- (black circles), three- (red squares) and four- (blue diamonds) legged undoped RVB ladders. The horizontal axis is dimensionless while the vertical one is in ebits, with the singlet being normalized to $\ln 2$ ebits of entanglement. The plots display the valence bond entanglement entropy for partitions where \tilde{L} are even number of rungs. For the three-legged ladder, we do not have values for $\tilde{L}:N-\tilde{L}$ partition, where \tilde{L} is odd. However, for the even-legged ladders, the values for odd \tilde{L} partitions *decreases* before converging. Importantly, the converged values are the same at large \tilde{L} , irrespective of the small- \tilde{L} variations between odd and even \tilde{L} . The saturation of the valence bond entanglement entropy implies that a straight line fit is appropriate in this case. . . . 22
- 3.4 The dimer coverings (represented by the arrows) in the state $|\eta_1\rangle, |\eta_2\rangle, |\xi_1\rangle$, and $|\xi_2\rangle$. The states, $|\eta_i\rangle$ and $|\xi_i\rangle$, for $i > 2$, can be generated upon increasing the rungs by inserting floating horizontal singlets at the non-edge sites such that no non-singlet sharing blocks are formed. This can be observed in the above figures by looking at how $|\eta_2\rangle$ ($|\xi_2\rangle$) is generated from $|\eta_1\rangle$ ($|\xi_1\rangle$). The sites on different bipartite lattices, A and B , have been distinguished using two different colors. 24
- 3.5 The changing face of the generalized Fibonacci sequences with increase in dopants. We exhibit here the rate of increase of the number of coverings $Z_{N,k}$, given by $\alpha_{N,k}$, for different hole concentration n_h . For each doped RVB ladder, with a different number of legs, there is a critical value of hole concentration, n_{hc} , where $\alpha_{N,k}$ is maximum. All quantities are dimensionless. 31
- 3.6 Valence bond entanglement entropy in doped RVB ladders. We plot here the variation of the valence bond entanglement entropy, S_L , with increasing block size of L rungs, for two- (black circles), three- (red squares) and four- (blue diamonds) legged doped RVB ladders. The four subfigures correspond to different doping concentrations, with $n_h = 0.1$ (top-left), $n_h = 0.3$ (top-right), $n_h = 0.5$ (bottom-left), and $n_h = 0.8$ (bottom-right). The horizontal axes are dimensionless while the vertical axes are in ebits. 32

4.1	Schematic diagram of an \mathcal{L} -legged and \mathcal{M} -rung ladder, with $M (= \mathcal{M})$ and $L (= \mathcal{L})$ number of spin sites along the legs and rungs, respectively. The boundary condition is shown by a solid line that connects the first and last sites on a specific leg.	38
4.2	The behavior of GGM (\mathcal{G}), with increasing even number of rungs (\mathcal{M}) for odd \mathcal{L} -legged ladders, in ground states obtained by exact diagonalization of the Heisenberg Hamiltonian. The red and blue circles represent the behavior obtained for $\mathcal{L} = 1$ and $\mathcal{L} = 3$ legs, respectively. The solid lines show fits to the data values using Eq. (4.24). The dashed line serves as a guide to the eye. From the plots one can conclude that with even rungs, \mathcal{G} increases for odd-legged ladders while decreases for even ones. All quantities are dimensionless.	41
4.3	The behavior of GGM (\mathcal{G}), with increasing even number of rungs (\mathcal{M}) for odd \mathcal{L} -legged ladders, in ground states obtained by exact diagonalization of the Heisenberg Hamiltonian. The solid lines show fits to the data values using Eq. (4.24). The dashed line serves as a guide to the eye. From the plots one can conclude that with even rungs, \mathcal{G} increases for even-legged ladders while decreases for even ones. All quantities are dimensionless.	42
4.4	Schematic diagram of two possible bipartitions of a multi-legged quantum spin ladder (one denoted by solid lines and the other one by broken lines), sharing a common node and comprised of same number of sites.	45
4.5	A two-dimensional bipartite lattice, with sublattices A (blue-circles) and B (yellow-circles).	46
4.6	The dimer coverings in the state $ 1\rangle$, $ \bar{2}\rangle$ and $ 2\rangle$. The sites on different bipartite lattices, A and B, have been distinguished using two different colors.	48
4.7	Schematic diagram of the additional term $ \mathcal{M}\rangle_{2,m+1} \bar{2}\rangle$ appeared in Eq. (4.11), due to periodic boundary condition. The sites on different bipartite lattices, A and B, have been distinguished using two different colors.	49

4.8	The behavior of GGM (\mathcal{G}), with increasing number of rungs (\mathcal{M}) in one- and three-legged ladders, using short-range RVB states. The solid lines show fits to the data values using the equation given in Eq. (4.24). The dashed line serves as a guide to the eye. The “two-rung” case for the one-legged ladder is just a singlet-instead of superpositions over several coverings of singlets, and also correspondingly provides a value that is drastically different from the higher-rung cases of the same ladder. We therefore ignore this case from the one-legged ladder case.	52
4.9	The behavior of GGM (\mathcal{G}), with increasing number of rungs (\mathcal{M}) in two- and four-legged ladders using short-range RVB states. The solid lines show fits to the data values using the equation given in Eq. (4.24). The dashed line serves as a guide to the eye.	53
4.10	Diverging scaling with converging multisite entanglement. The behavior of the asymptotic GGM ($\mathcal{G}_c(\mathcal{L})$) and the scaling exponent ($x(\mathcal{L})$) with increasing \mathcal{L} . We observe that even though, the $\mathcal{G}_c(\mathcal{L})$ for odd- and even-legged ladders, converge with increasing \mathcal{L} , the scaling $x(\mathcal{L})$ diverge. All axes are dimensionless. The data point corresponding to the case of only two “rungs” on the one-legged ladder is not considered for the fitting. Please see the caption of Fig 4.8 in this regard.	54
5.1	Schematic diagram of a two-legged doped quantum ladder. The sites on different bipartite lattice A and B , have been distinguished using two different colors.	58
5.2	Schematic diagram of the blocks L , R , and J in the spin lattice. To compute \mathcal{G} , we obtain the reduced density matrix (ρ_{red}) corresponding to the sites 1-4 in the R block. The rest of the lattice is traced out. Numerical studies show that the reduced state ρ_{red} is sufficient to compute \mathcal{G} in doped RVB states.	62
5.3	Schematic diagram of the states: a) $ \chi_2\rangle$, b) $ \chi_3\rangle$, c) $ \chi_3\rangle$, and the periodic terms: d) $ \xi\rangle$, and e) $ \gamma_1\rangle$ and $ \gamma_2\rangle$, used in the recursion relations.	63
5.4	Schematic diagram of the scheme to build a doped-RVB state from a lattice filled with holes, for an 8 site RVB ladder, as given by the process: $ 4, 0\rangle \xrightarrow{k=1} 3, 1\rangle$, described in Eq. (5.4).	64
5.5	Schematic diagram of the blocks L , R , and J in the spin lattice with periodic boundary condition.	69

5.6	Genuine multisite entanglement in doped RVB ladder. Variation of \mathcal{G} with n_{el} in doped RVB ladder states, for $2N = 40$ (blue circles) and 200 (red diamonds) lattice sites. The top inset magnifies the encircled region in the plot. The bottom inset shows the scaling of n_c with the $\log_{10} N$. The inset shows that as N increases (plotted up to 300 sites), n_c converges to 0.56. This is to be compared to the result for the systems described by the t - J model in the superconducting regime, in Fig. 5.7.	76
5.7	Genuine multisite entanglement in the t - J ladder. Variation of \mathcal{G} with n_{el} for the exact GS of the t - J ladder Hamiltonian, given in Eq. (5.29), for $N = 10, 12$, and 14. \mathcal{G} reaches its maximum value at $n_c \approx 0.65$. Here $J/t = 0.66$. All quantities plotted are dimensionless.	77
6.1	Schematic diagram of a two-dimensional quantum lattice with dimer coverings.	82
6.2	A two-dimensional bipartite honey- comb lattice, with defects (red-circles) in the network. The nodes in sublattice \mathcal{A} (blue-circles) and \mathcal{B} (yellow-circles), are occupied by spin-1/2 particles.	84
6.3	Another instance of a two-dimensional bipartite honeycomb lattice, with defects (red-circles) spread in the network.	85
6.4	(Color online). a) Single node containing a spin-1/2 belonging to a dimer, b) Single node containing a defect, c) A NN two-node containing a dimer, and d) A NN two-node containing a pair of defects. . . .	87
6.5	(Color online). a) A NN two node containing a spin-1/2 belonging to a dimer in sublattice \mathcal{B} and a defect in sublattice \mathcal{A} , b) same two node now containing a spin-1/2 belonging to a dimer in \mathcal{A} and a defect in \mathcal{B} , c)-d) Another instance of the arrangement a)-b), respectively, at a different pair of nodes.	89
6.6	Possible two-node reduced states, represented by Eq. (6.18), between a central node (encircled red) and a set of \mathcal{M} distant nodes, separated by approximately x edges. The central node belongs to sublattices \mathcal{A} , with the distant nodes belonging to sublattice \mathcal{B} . These two-node states form the channel for the quantum telecloning protocol discussed in the main text.	94

6.7	Maximum permissible bipartite entanglement. We show the upper bound on entanglement due to quantum telecloning, quantified using logarithmic negativity ($E(\rho)$), for the two-party reduced state $\rho_{AB_i}^{(2)}$, for $\mathcal{M} = 4, 20, 100$, and ∞ , as a function of $1 - p'_3$. The plot shows that the maximum permissible entanglement decreases as \mathcal{M} increases. Interestingly, in the absence of defects ($p'_3 = 1$) no bipartite entanglement is present as $\mathcal{M} \rightarrow \infty$. The vertical axis is in ebits, while the horizontal one is dimensionless.	95
-----	--	----

CHAPTER 1

Introduction

“Quantum information is like the information in the dream. If you start even trying to share it with one person besides yourself and talking about it, you start forgetting the dream and you only remember what you said about it”—Charles H. Bennett.

One of the fundamental features that distinguish the quantum theory of nature from the classical one is superposition of quantum states. Absence of information, even in principle, about the system’s actual state prior to the measurement, validates that the concept of superposition has no classical analogue. Apart from establishing itself as a suitable framework for studying and understanding the microscopic details of physical systems, quantum theory has opened up several revolutionary ideas in the field of information theory [5–9]. A key feature that is useful in quantum information protocols is that any superposition of valid quantum states is itself a valid quantum state. This naturally leads to non-orthogonal states, which model nondistinguishable physical situations. Hence, information can be encoded in nondistinguishable elements as well. In a traditional computer, information is encoded in a series of bits, and these bits are then manipulated in order to get the desired results. On the other hand, in the case of a quantum computer, the basic unit of information is a superposition of bits, referred to as a ‘qubit’, which is manipulated by executing a series of quantum gates, made of unitary operators [5–9].

In principle, it is always possible to simulate a physical system using a classical computer. However, it turns out that due to the exponential growth in the number of degrees of freedom, the system becomes computationally intractable even after moderate increase in size. Richard Feynman was among the first to mention that efficient simulation of a quantum mechanical system can indeed be achieved using

a machine which works on the quantum mechanical principles [10]. In subsequent years, David Deutsch and Richard Jozsa [11, 12] came up with a remarkable algorithm which further strengthened Feynman’s intuition. They explicitly show that by taking advantage of quantum superposition, an exponential speedup in the computation over any classical machine can be achieved. This brought the attention of the community to look for further computational tasks where the concepts of quantum theory can be applied. In 1994, Peter Shor proposed an algorithm to efficiently find the prime factors of large integers [13]. Till date, no efficient classical algorithm for the prime factorization of a large number is known. In general, we call an algorithm is efficient if its execution time i.e. the number of elementary operations required is asymptotically polynomial in the length of its input. To factor an integer N , Shor’s proposed algorithm requires $O((\log N)^2(\log \log N)(\log \log \log N))$ numbers of operations. Hence, the algorithm runs in a polynomial in time. In the following years, a few other quantum algorithms were introduced, such as the Grover’s search algorithm [14, 15].

Apart from the above notable progress made in the field of computation, at almost the same time, a parallel interest was also growing which considered the possible application of quantum mechanical concepts to communication process [5–7, 9]. A celebrated example in this regard is quantum cryptography [16–21]. Conventional cryptography [22], using classical methods to send secret classical information, consists of three main steps, viz, sharing of a secret classical key between the sender and the receiver, encryption of the secure message using secret keys by the sender and decryption of it using the same by the observer which receives that through a classical channel. The security of the information transfer relies on the secrecy of the classical key. If an eavesdropper has prior knowledge about the classical key, invading the classical channel, s/he can retrieve the information without leaving any trace. However, in a quantum setting, in order to have the knowledge about the classical information encoded in the quantum states, the eavesdropper has to perform some measurements which will cause disruption in the system and inevitably leave some trace.

Another significant development in the realm of quantum information was marked by the emergence of entanglement, in theory and in practice [23]. Though the non-intuitive notion of quantum entanglement was brought to light long back in 1935, by Einstein, Podolsky, Rosen, and Schrödinger [24, 25], it took several years to realize

that entanglement can indeed be used as a resource to perform quantum information processing tasks. In their seminal paper on the EPR paradox [24], Einstein, Podolsky, and Rosen described quantum entanglement as a ‘spooky action at a distance’, which led to properties that violated certain intuitively satisfactory tenets of a physical theory, namely reality and locality, when considered in conjunction. This was put in an experimentally verifiable form by Bell [26–32].

The idea to use this counter-intuitive feature of quantum theory as a resource for some physical tasks was not clear until the early 1990s. In particular, in 1993, Bennett, Brassard, Crepeau, Jozsa, Peres, and Wootters introduced a very simple and astonishing protocol known as quantum teleportation [33]. The scheme includes a direct use of quantum entanglement. It demonstrated that using shared quantum entanglement along with a finite amount of classical communication, an unknown quantum state can be transferred-“teleported”- from one physical laboratory to another. A year earlier, quantum superdense coding [34] was proposed by Bennett and Wiesner, which uses shared quantum entanglement and one qubit of quantum information, in order to transmit two bits of classical information. Furthermore, in 1991, Ekert proposed a variant of quantum key distribution using entanglement [35].

In recent years, development in entanglement theory has not only enriched the field of quantum information science and made this a vibrant area of research, it has also affected research in several other streams of study [36–42]. One such area, where the tools of quantum information theory, in particular, quantum entanglement, has been useful, is the study of quantum many-body systems [37, 38, 40, 41]. Over the years, quantum many-body theory has flourished as an independent area of research, equipped with tools capable of explaining many important concepts, especially related to low energy physics. Recent developments in the field of quantum information has been recognized as a new paradigm to understand large complex quantum systems in a more efficient way. Traditionally, many-body systems are studied by the characteristic changes in their properties as responses to external perturbations [43–45]. Study of the ground state properties of many-body systems using the tools developed in quantum information may uncover novel physics in these systems. To this end, in the past decade, several works have been reported which enhance the importance of quantum entanglement in efficiently detecting quantum phase transition points [38, 40, 46–58, 58–61]. For instance, in the seminal papers by Osterloh *et al.* [47], and Osborne and Nielsen [50] it has been shown that nonana-

lyticity in the first derivative of the nearest-neighbor bipartite entanglement, with respect to the field parameter in the zero-temperature state of the quantum transverse Ising model, can capture the QPT present in this model. Here, the notable fact is that from the knowledge of few-site entanglement properties, the behavior of the physical system near the phase transition point can be well-captured. In addition to this, there are plenty of examples where bipartite as well as multipartite entanglement properties have been used along with the conventional order parameters, to gain complete information about the zero-temperature phase diagram of a complex quantum system [40, 46, 48–58, 58–63]. For instance, there are physical models for which conventional order parameters become inadequate and some important properties related to the phase boundaries remain elusive [62–64].

Apart from the information obtained via the nonanalytic behavior of quantum entanglement, there are other changes in behavior of entanglement which signal quantum phase transition points. For example, studies related to ground state entanglement properties of low dimensional gapped quantum systems reveal the fact that the entanglement between a contiguous block and the rest of the spins, of the system, scales with the boundary of the bipartition and follows an area law. Contrastingly, in critical systems, the scaling behavior deviates from the area law [65] and has additional logarithmic corrections. Hence, looking at the scaling behavior of entanglement, one can predict whether or not the system is close to a critical point. Moreover, in recent years, several works which highlight the role of monogamy of quantum entanglement in characterizing various properties of many-body systems have also been reported [66].

In addition to the study of the equilibrium properties related to the quantum many-body systems, considerable interest have been shown to characterize the trends of bipartite as well as multipartite properties when the physical system interacts with its environment [67–70]. Attempts have been made to characterize statistical mechanical properties like ergodicity [71–75] of bipartite entanglement, dynamics of quantum entanglement under sudden quench [70], etc.

Along with the study of the entanglement properties of complex many-body systems, the concept of quantum entanglement has recently been used to develop numerical techniques in order to efficiently simulate complex quantum systems [76–81]. In general, the dimension of the Hilbert space of a complex many-body system scales

rapidly with the increase of system size. Hence, in order to access the ground state properties of the system, it is necessary to restrict oneself to a moderate-sized system only. However, in order to examine how fast the properties of the physical system converges with the size of the system and finally mimics the thermodynamical limit, one needs to carry out finite-size scaling analysis. Therefore, development of an efficient tool to simulate complex many-body systems also at relatively large system sizes is a need of utmost importance. In 1992, S. White *et al.* came up with an efficient simulation technique, known as density matrix renormalization group [76], where it has been argued that importance should be given to those degrees of freedoms which are more ‘relevant’ for the description of the system. This indeed reduces the computational cost to a very low value. It turns out that the number of parameters required to describe the systems, in this cases, scales linearly with the size of the system.

The formalism of density matrix renormalization group was introduced as a generalization to the existing renormalization group methods, and for quite a long time it was not clear why such efficient description of the given complex many-body system is possible by using relatively less number of parameters. However, very recently, a plausible explanation in terms of quantum entanglement has been proposed [77]. It has been realized that in order to simulate a physical system, the relevant components considered must have a small amount of entanglement. Since its emergence, density matrix renormalization group has turned out to be a powerful tensor network theory, and have given birth to many variants [77–81]. In general, such a wide application of an approximation technique may seem quite astonishing. However, various studies related to ground state entanglement properties of general many-body systems reveal that in general, the ground state of a quantum many-body system possess very low amount of entanglement and hence obeys the area law of entanglement entropy [65]. This opens up the possibility of efficient representation, even with a low number of parameters.

Over the years, in these and several other ways quantum entanglement has played a crucial role in building a bridge between quantum information and quantum many-body theory. So far, we have mainly discussed the important aspect of studying the interface between quantum information theory and the quantum many-body systems, where tools from quantum information have been used to get a deeper insight into the properties of complex quantum systems. However, it is clear that in order

to realize a quantum information protocol in the laboratory, one needs to look for suitable physical systems. For that purpose, quantum many-body systems are potential candidates. Unprecedented quantum control over large numbers of atoms, as has recently been attained, opens up the possibility of implementing promising applications in quantum information processing by using these systems [37, 82–87].

For an efficient use of many-body systems for quantum information processing tasks, it is important to obtain a complete characterization of quantum correlations, present in the subparts of the quantum system. For instance, if one designs protocols which demand long-range quantum correlation in some intermediate step of the scheme, the corresponding physical model needs to be chosen carefully. It may happen that for certain choices of physical models, the long-range quantum correlation between its various subparts remains suppressed, for all possible values of the system parameters. And, there are examples which show that presence of disorder in the system parameters sustain more entanglement than the ordered one [88–96], which is potentially useful in a communication task.

Along with the characterization of quantum correlation, a challenging task in designing a reliable quantum network is to prevent it from environmental perturbation or from the presence of defects in the system. This is due to the fact that complete isolation of a physical system is not possible and in a practical scenario, it is also very difficult to have an impurity-free quantum system. In general, quantum correlations are extremely fragile under the effect of environmental perturbation and decreases to zero very rapidly [97–100]. Thereby, the physical system may become useless for quantum information processing tasks. Similarly, there are instances where the introduction of disorders into the system causes significant reduction of quantum correlation. Hence, it is important to explore the response on quantum correlations due to the influence of environmental perturbation or impurity.

In this thesis, we consider a rich class of quantum many-body systems, known as resonating valence bond (RVB) states and characterize their bipartite as well as multipartite entanglement properties. RVB states were first introduced by Linus Pauling in 1938 [101], in the context of organic materials like benzene and later extended to metals. Paul Anderson revived the interest in this concept in 1973 [102–105] while trying to explain the physics of Mott insulators, where an expected long-range anti-ferromagnetic order was absent.

The theory of resonating valence bond states, got an important boost when for the first time, superconductivity was observed for some unexpected oxides like $\text{La}_{1-x}\text{Ba}_x\text{CuO}_4$ [106]. It was argued that in copper oxide lattices, electrons from neighboring copper atoms interact to form a valence bond, which locks them in place. However, with doping, these electrons can act as mobile Cooper pairs and are able to superconduct [105, 107–110]. Soon after this discovery, two key approaches were developed to deal with these strongly correlated systems: RVB mean field theory (BZA theory) [104] and a gauge theory [111]. The approach of BZA theory turned out to be very appealing as it naturally leads to a spectrum of fermionic excitations which is indeed known to be the correct spectrum in a one-dimensional model.

In the following years, several other studies came up, where resonating valence bond states have been considered as a framework to study ground state properties of various physical systems. One such example is the ground-state properties of the antiferromagnetic Heisenberg model in two dimensions [112]. The conventional understanding of spin systems interacting via the Heisenberg antiferromagnetic Hamiltonian is that the ground state is close to the Néel state [113]. The Néel state is gapless to spin excitations. Soon it was realized that for spin-1/2 and low dimensional lattices with significant frustration, this picture is incorrect. For higher dimensional lattices, based on numerical analysis with small lattice sizes, support towards the presence of long-range order was reported [114]. At that time, studies related to various other lattice geometries, confirms the absence of long-range order [115]. Hence, the true nature of ground state for higher dimensional antiferromagnets remained ambiguous. In this regard, notable success has been achieved when the ground state is modeled using the short-ranged resonating valence bond state ansatz for various lattice geometries [116–120].

Several analytical and numerical studies support the fact that the importance of resonating valence bond states is not limited to its use as an ansatz, and there are physical models for which the system possesses an RVB liquid phase for a finite region of parameter space [121–125]. In low dimensional systems, one such example is the ground state configuration of the J_1 - J_2 model at the Majumdar-Ghosh (MG) point [121]. For higher dimensional lattices like Kagomé [124, 126] and triangular lattices [127], similar results have also been reported.

In subsequent years, considerable interest has also grown for considering variants of resonating valence bond states. This includes long-ranged resonating valence bond states as frameworks to study various properties of higher dimensional systems. As an example, Lee and Feng in Ref. [128] studied numerically how a paramagnetic RVB state can be modified to become a long-range antiferromagnetically ordered state by introducing an additional variational parameter. In addition to this, an RVB spin liquid was proposed as a ground state on a square lattice with further-neighbor hopping as well as on a triangular lattice [129]. Moreover, a long-range resonating valence bond state is proposed as a variational wave function for the ground-state of the $S = 1/2$ antiferromagnetic Heisenberg model on the honeycomb lattice. Using a recursive method, which constructs dimer and non-dimer variational ansatz states for the two-legged ladder, properties such as the energy density and spin-correlation functions have been efficiently computed [130, 131].

Apart from the modeling of ground state or near-ground state wave functions using resonating valence bond theory, studies related to the topological order of resonating valence bond states have also received attention [132–136]. In general, topological properties of a system play important roles when the characterization of quantum phases are not possible using conventional order parameters. It has been argued that the resonating valence bond state has topological long-range order. In recent years, making use of simple tensor-network representations, topological properties of both critical and gapped topologically ordered RVB wave functions have been extensively studied [133, 135–137]. The valence bond character of the RVB wave function suggests the presence of certain types of topological excitations.

Despite its importance, there has not been significant efforts to characterize quantum correlations, in particular, multipartite quantum entanglement, present in resonating valence bond states. However, as mentioned earlier, in order to use this very rich and complex many-body system for quantum information processing and computation, characterization of the quantum correlations present among its various subparts is extremely important. Entanglement properties of resonating-valence-bond states on two-and higher- dimensional lattices have been studied by Chandran *et al.* [138]. It was found that though the network is genuinely multipartite entangled, it possesses only a negligible amount of bipartite entanglement. In Ref [139], an attempt has been made to investigate entanglement properties of doped resonating valence bond states in relatively small-sized ladders and plaquettes. However, under-

standing the behavior of entanglement in these systems require further investigation.

Very recently, Dhar *et al.* in Ref. [140, 141] have proposed an analytical method to calculate the genuine multipartite entanglement on a square lattice with an arbitrary number of sites. In addition to this, in Ref. [142] a comparative study between the bipartite as well as multipartite entanglement behavior of quantum ladders and two-dimensional lattices have been carried out which shows that geometry can play an important role in determining the entanglement properties of multiparty quantum states.

In this thesis, we attempted to shed further light on this aspect and tried to reveal some important concepts related to the entanglement properties of the resonating valence bond states, which were not explored before. In Chapter 2, we present a brief review of the bipartite and multipartite entanglement measures that we have considered in our work. Subsequently, in Chapter 3, we introduce the resonating valence bond state which we have considered for our purpose. In the literature, several variants of resonating valence bond states are available, and it is important to clearly define the resonating valence bond state that has been considered. Thereafter, we derive analytical recursive methods to construct resonating valence bond states in doped and undoped multi-legged spin-1/2 quantum ladders. We then investigate the behavior of valence bond entanglement entropy between a contiguous block to the rest of the system with the increase of the size of the block.

In Chapter 4, we consider the ground state of Heisenberg spin ladders and investigate the odd-even dichotomy of genuine multiparty entanglement. We found that when the size of the system remains small, multiparty entanglement can capture the even-odd dichotomy present in the system. However, as the size of the system is increased to a moderately large value, this dichotomy of multiparty entanglement appears to become elusive. Interestingly, we show that though multiparty entanglement measure itself fails to capture the odd-even dichotomy, its scaling behavior is capable of distinguishing it in Heisenberg ladders, even in the asymptotic limit.

In Chapter 5, we investigate the trends of genuine multipartite entanglement in the ground states of a Hubbard model with large onsite interactions, obtained by exact diagonalization technique. We find the connection of this model with doped resonating valence bond ladder states. We show that the latter are always genuine

multipartite entangled. We then formulate an analytical recursion method for generating the local density matrices of the wave function, which allows us to efficiently estimate the entanglement as well as other physical quantities in large doped resonating valence bond ladders. Thereafter, in Chapter 6, we consider an isotropic quantum network of spin-1/2 particles with a finite fraction of defects, where the corresponding wave function of the network is rotationally invariant under the action of local unitaries. By using quantum information-theoretic concepts like strong subadditivity of von Neumann entropy and approximate quantum telecloning, we prove analytically that in the presence of defects, the network sustains genuine multisite entanglement, and at the same time may exhibit a finite amount of bipartite entanglement, in contrast to the network with no defects. In Chapter 7, we provide a brief summary of the results presented in the thesis.

Quantum entanglement measures

2.1 Introduction

In the resource theory of quantum entanglement, separable states are treated as free resources, whereas entangled states are considered to be the expensive ones [23]. This follows from the realization that local quantum operations and classical communications between the local laboratories are easy to implement in practice, while operations outside this class are difficult. The set of local operations and classical communication is denoted by LOCC.

A pure quantum state, $|\psi\rangle_{AB}$, is said to be entangled across the bipartition $A : B$, if it cannot be written as

$$|\phi\rangle_A \otimes |\phi\rangle_B, \tag{2.1}$$

where $|\phi\rangle_A$ and $|\phi\rangle_B$ are the quantum states of the local subsystems A and B respectively. However, as is often the case, complete information about the physical system may not be available, so that a pure state description of the joint physical system is not possible. In such a scenario, the joint system must be described by using the density matrix formalism. A bipartite quantum state, ρ_{AB} , is said to be entangled if it cannot be written as a convex sum over product states [143],

$$\rho_{AB} = \sum_k p_k \rho_A^k \otimes \rho_B^k, \tag{2.2}$$

where $\rho_A^k(\rho_B^k)$ are the quantum states of the subsystem $A(B)$, $p_k \geq 0$, and $\sum_k p_k = 1$.

However, characterization of quantum entanglement, e.g. in complex many-body systems, demands its proper quantification alongside its detection. Towards that aim, one needs to search for computable measures of bipartite as well as multipartite entanglement. In this Chapter, we briefly review a few of such measures of quantum entanglement, which we later use in the thesis. These measures do not increase, on average, under local quantum operations and classical communication and their values become zero when the quantum state is separable. Below we first discuss about bipartite entanglement measures, which is then followed by the discussions related to a multiparty entanglement measure.

2.2 Bipartite entanglement measures

A bipartite entanglement measure, \mathcal{E} , is a map which takes a density operator, ρ , to a real positive number (in \mathbb{R}^+). For any pure quantum state, a good measure of bipartite entanglement always reduces to the entropy of entanglement [144]. Below we discuss the necessary details of a few computable measures of bipartite entanglement which we have used for our purpose.

2.2.1 Valence bond entanglement entropy

The scaling behavior of entanglement entropy in the ground state of strongly correlated systems has been widely researched in recent years to study critical phenomena [47, 56, 57, 65, 145, 146]. Entanglement entropy is a measure of entanglement in bipartitions of a pure quantum state, and defined as $S(\rho) = -\text{Tr}(\rho \ln \rho)$, where ρ is the reduced density matrix of any one of the subparts [23, 147]. In noncritical low-dimensional quantum systems, say of \tilde{N} spins, the entanglement entropy in a ground state, between a contiguous block of \tilde{L} spins and the rest, consist of $\tilde{N} - \tilde{L}$ spins, of the system often scales with the boundary of the bipartition and follows an area law [148]. For instance, in one-dimensional spin systems, entanglement entropy often saturates with increasing \tilde{L} , as the boundary remains constant for all bipartitions. In contrast, for critical systems, the scaling behavior deviates from the area law, and has additional logarithmic corrections [56, 57]. In general quantum many-body systems, scaling of entanglement entropy and deviation from area law are believed to be closely related to critical phenomena and also to the ground state

topology [47, 65, 145, 146]. Although intrinsic to the characteristics of a physical system, entanglement entropy is not easily computable in all systems. To obtain the scaling behavior, it is imperative to consider larger systems beyond the realm of exact diagonalization. Moreover, tensor network approaches such as density matrix renormalization group [76] and matrix product states [78] seem unsuitable in dimensions higher than one.

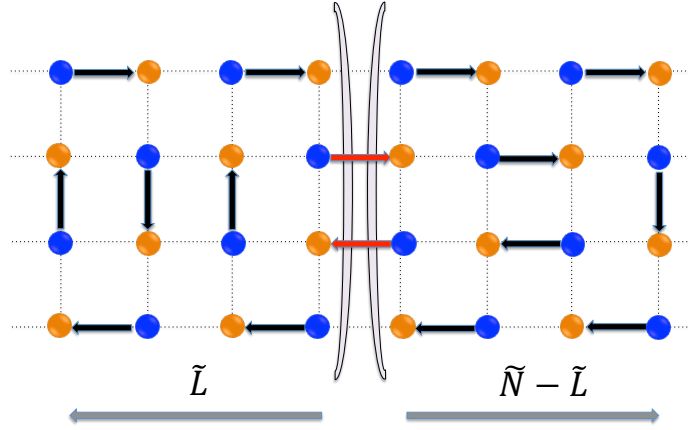


Figure 2.1: A dimer covered quantum spin ladder with a bipartition across $\tilde{L} : \tilde{N} - \tilde{L}$. The sites on different bipartite lattices, A and B have been distinguished using two different colors and the arrow represents dimer connecting two sites one from lattice A and another from lattice B. The covering contains $a_i = 2$ dimers across the boundary, shared between the blocks of \tilde{L} and $\tilde{N} - \tilde{L}$, which contributes to the valence bond entanglement entropy in Eq. (2.4). The above dimer arrangement constitutes a single covering in the valence bond basis $\{|\phi_i\rangle\}$. For any given ladder, Z_N such coverings are possible, each with a_i singlets present across the boundary.

An alternative approach to estimate the scaling behavior of entanglement entropy in the case when the relevant state is representable as a superposition over singlet coverings possibly interspersed with holes, is by defining a measure called the valence bond entanglement entropy (VBEE) [149, 150], which is defined as an average number of dimers that cross the boundary between two bipartitions. Though not directly comparable, the VBEE has been used to effectively predict the scaling properties of entanglement entropy in the different phases of the 2D spin-1/2 Heisenberg model [149–153], using Quantum Monte Carlo simulations in the valence bond basis [154], although the predicted corrections to the area law at criticality does not seem to be comparable [151]. To define the VBEE, we depict the ground state (GS)

of the \tilde{N} -spin system (\tilde{N} is even) in the dimer-covered valence bond basis ($\{|\phi_i\rangle\}$), such that

$$|\Psi\rangle_{\text{GS}} = \sum W_i |\phi_i\rangle, \quad (2.3)$$

where W_i are the coefficients of each valence bond covering, ‘ i ’. In doped spin lattices, each element of the basis represents a complete hole-dimer covering. Let us consider the ground state, in a bipartition, given by $\tilde{L} : \tilde{N} - \tilde{L}$, such that for the basis state $|\phi_i\rangle$ in the ground state, a_i singlets are shared between \tilde{L} and $\tilde{N} - \tilde{L}$, i.e., a_i singlets cross the boundary (see Fig. 2.1). The valence bond entropy is then defined as [149]

$$S_{\tilde{L}} = \frac{1}{\sum |W_i|} \sum_i a_i |W_i|. \quad (2.4)$$

For a given set of parties, Eq. 2.4 provides a bipartite entanglement measure. However, the set of their values for different \tilde{L} , especially when then scaling with respect to \tilde{L} is considered, provides information about the state’s multiparty entanglement as well.

2.2.2 Logarithmic negativity

In order to quantify the amount of bipartite entanglement present in a general two-qudit system on $\mathbb{C}^d \otimes \mathbb{C}^d$, one can use negativity (\mathcal{N}) as a measure of bipartite entanglement. The negativity of a bipartite quantum system is an easily computable entanglement measure, which is an entanglement monotone- it does not increase under local operations and classical communications (LOCC) [155]. However, there exists positive partial transposed (PPT) entangled quantum states [156, 157], for which negativity fails to detect the presence of entanglement and becomes zero.

For a bipartite quantum state, ρ_{AB} , its negativity [158–161] $\mathcal{N}(\rho_{AB})$, is defined as the absolute value of the sum of the negative eigenvalues of $\rho_{AB}^{T_A}$, where $\rho_{AB}^{T_A}$ denotes the partial transpose [156, 157] of ρ_{AB} with respect to the subsystem A . Alternatively, it can also be expressed as

$$\mathcal{N} = \frac{||\rho_{AB}^{T_A}||_1 - 1}{2}, \quad (2.5)$$

where $||M||_1$ is the trace norm of the matrix M .

Using the above definition of negativity, one can obtain the logarithmic negativity

(\mathcal{E}), which is given by

$$\mathcal{E}(\rho) = \log_2(2\mathcal{N} + 1). \quad (2.6)$$

Logarithmic negativity is an upper bound of distillable entanglement [160]. Neither negativity nor logarithmic negativity reduce to the entanglement entropy for pure states [144].

2.2.3 Multipartite entanglement measures

In the case of a multiparty pure quantum state of $n > 2$ parties, quantification of entanglement across its various bipartitions does not always provide complete information about its actual entanglement content. It may turn out that across some bipartitions, the quantum state is separable, while at the same time may possess nonzero amount of entanglement across other bipartitions. Therefore, in terms of entanglement content, some of the bipartitions become more important than the others. We restrict ourselves to the case when we are mainly interested to know whether or not the given multiparty pure quantum state is genuinely multiparty entangled. A multiparty pure quantum state is said to be genuinely multiparty entangled if it cannot be written as a product in any bipartition.

In general, computation of genuine multiparty entanglement, even for pure quantum states is a nontrivial task. In this section, we discuss a computable measure of genuine multisite entanglement for pure quantum states, known as the generalized geometric measure (GGM) [64, 162] (see also. [163–171]). However, apart from a few exemplary cases [172], computability for general mixed quantum states is yet to be achieved.

For an n -party pure quantum state, $|\psi_n\rangle$, the GGM, \mathcal{G} is defined as an optimized fidelity-based distance of the given state from the set of all states that are not genuinely multiparty entangled:

$$\mathcal{G}(|\psi_n\rangle) = 1 - \Lambda_{\max}^2(|\psi_n\rangle), \quad (2.7)$$

where $\Lambda_{\max}(|\psi_n\rangle) = \max |\langle\chi|\psi_n\rangle|$ with $|\chi\rangle$ being an n - party state not genuinely multiparty entangled. For an n -party pure quantum state, $|\psi_n\rangle$, consisting of the

parties A_1, A_2, \dots, A_n , Eq. (5.11) can be shown to be equivalent to the form [64, 162]

$$\mathcal{G} = 1 - \max\{\lambda_{K:L}^2 | K \cup L = \{A_i\}_{i=1}^n, K \cap L = \emptyset\}, \quad (2.8)$$

where $\lambda_{K:L}$ is the maximal Schmidt coefficient in the bipartite split $K : L$ of $|\psi_n\rangle$.

We note that all possible bipartitions, $K : L$, of the system are considered in Eq. (2.8), with the K subsystem in the above bipartition containing all possible combinations of A_i , for $i = 1, 2, \dots, n$. The computation of GGM depends on the efficient generation of arbitrary reduced density matrices across all possible bipartitions of the given physical system. For states where the reduced density matrices can be efficiently generated, the GGM turns out to be an efficiently computable measure of genuine multisite entanglement. Additional leverage is obtained if the state is known to be symmetric and/or the maximal Schmidt coefficient is known to arise from a selected subset of all possible bipartitions.

2.3 Summary

In this Chapter, we have discussed computational details of a few bipartite and multipartite entanglement measures, which we have used in our work.

Fibonacci sequence and valence bond entanglement entropy

3.1 Introduction

Over the years, entanglement entropy [23, 147] has been an important indicator to investigate critical behavior [56, 57] and topological order [145, 146] in the ground states of low-dimensional quantum many-body systems [37, 38, 41, 65]. In particular, in one-dimensional quantum spin systems, the scaling behavior of entanglement entropy between a contiguous block and rest of the system is different for noncritical and critical systems [56, 57]. For a large class of quantum spin systems, a more recently introduced estimator of the scaling characteristics of block entanglement entropy is the valence bond entanglement entropy [149, 150], which is defined as the average number of dimers (singlets) shared between the relevant blocks of the system. We have already introduced the measure in Chapter 2. In the valence bond basis, valence bond entanglement entropy can be computed in antiferromagnetic (AFM) spin systems in higher dimensions where the entanglement entropy is not numerically accessible [149–151].

An important class of systems where the valence bond entanglement entropy is of direct significance is the dimer covered states of the spin-1/2 AFM Heisenberg model. These states, also known as resonating valence bond states (RVB) [102], were introduced to study Mott insulators [103] and high- T_c superconductivity in cuprates [104, 107, 110, 173]. Over the years, the RVB states of strongly-correlated systems have provided ingredients for investigation of exotic quantum phenom-

ena ranging from spin liquids, topological phases [127, 132, 174, 175], and quantum correlations [2, 3, 133, 136, 138–142]. An interesting feature of the RVB state in Heisenberg ladders, with nearest-neighbor (NN) dimers, is that the quantum state for arbitrary number of spins can be recursively generated from smaller states [2, 3, 130, 131, 140, 141, 176], with the number of possible dimer coverings given by the *Fibonacci sequences* [177, 178]. More precisely, the number of coverings in the valence bond basis, for an N -rung RVB ladder state, is the sum of the possible coverings for $(N - 1)$ - and $(N - 2)$ -rung RVB ladders [130, 131]. This has a direct bearing on the computation of the valence bond entanglement entropy of the system. For instance, in RVB states on a spin ladder which have equal-weight superposition of all possible NN dimer coverings, the valence bond entanglement entropy across any bipartition can be derived as a function of the number of coverings in each contiguous block on either side of the bipartition. These numbers are then obtained directly from the Fibonacci sequence, which for large N increases with the *golden ratio*, Φ [179].

In this Chapter, we derive recursion relations and look at possible generalizations of the Fibonacci sequence for dimer covered quantum spin-1/2 ladders with multiple legs, and with or without the presence of dopants. Using specific spin lattices in ladder configurations, such as doped and undoped two-, three-, and four-legged ladders, we show that a recursion relation for these RVB states, in terms of the number of coverings in the valence bond basis, can be generated to build larger N -rung states from smaller rung states [2, 3, 140, 141]. For an equal-weight RVB superposition, a generalized sequence for the number of coverings in these states can be estimated. These sequences predictably deviate from the usual Fibonacci sequence, which corresponds to the case for undoped two-leg RVB ladders. Nonetheless, the generalized sequence allows us to calculate the valence bond entanglement entropy for these states, and highlight the scaling characteristics for both doped and undoped multi-legged Heisenberg ladders. In particular, we observe that the valence bond entanglement entropy saturates with block size, for both types of dimer covered ladders, which shows that these states follow the “area law” and are thus noncritical systems [65]. Further, the entanglement between the blocks, as commensurate with valence bond entanglement entropy, is dependent on the doping, i.e., it decreases with increased doping as the average number of shared dimers between the blocks decreases. However, the scaling behavior remains unaffected, thus showing that the criticality of the system is independent of the variation in doping concentration.

This Chapter is organized as follows. In Sec. 3.2 we define the RVB state we have considered for our work and formulate recursion relation for two-legged ladders. Thereafter, in Sec. 3.3, we derive the recursion relations for multi-legged ladders and present the scaling behavior of valence bond entanglement entropy. In Sec. 3.4 we carried out the same analysis in presence of dopants in the lattice sites. We present a summary in Sec. 3.5.

3.2 Resonating valence bond ladder and the Fibonacci sequence

In this work, the principal systems of interest are the nearest-neighbor dimer-covered states, also called the short-range resonating valence bond states, of the spin-1/2 Heisenberg ladders [102]. We begin by defining a bipartite lattice, with two sublattices, \mathcal{A} and \mathcal{B} , which is a lattice where each site on sublattice \mathcal{A} (\mathcal{B}) is surrounded by NNs on sublattice \mathcal{B} (\mathcal{A}). A dimer or a singlet is formed between any pair of NN spins belonging to different sublattices, and can be written as $[e_k, e_l] = \frac{1}{\sqrt{2}}(|\uparrow_k \downarrow_l\rangle - |\downarrow_k \uparrow_l\rangle)$, such that $k \in \mathcal{A}$ and $l \in \mathcal{B}$. A single unique covering of the ladder lattice, with NN dimers, is then given by $|\phi_i\rangle = ([e_1, e_2] \otimes [e_3, e_4] \otimes \dots [e_{N-1}, e_N])_i$, where the odd (even) indices belong to sublattice \mathcal{A} (\mathcal{B}), and \tilde{N} is even. All such unique coverings together form an overcomplete valence bond basis. The variational RVB state in this basis, with weights W_i , as in Eq. (2.3), can then be written as

$$|\Psi_{\text{RVB}}\rangle = \sum_{i=1}^{\tilde{Z}_{\tilde{N}}} W_i ([e_1, e_2] \otimes [e_3, e_4] \otimes \dots [e_{N-1}, e_N])_i, \quad (3.1)$$

where $\tilde{Z}_{\tilde{N}}$ is the number of all possible coverings or states in the basis $\{|\phi_i\rangle\}$. In our work, we consider the originally defined equal-weight resonating valence bond state, where $W_i = 1, \forall i$. We note that the state $|\Psi_{\text{RVB}}\rangle$ is not normalized and importantly, $\{|\phi_i\rangle\}$ is not an orthogonal basis. In general, the complexity of the RVB state is compounded by this lack of orthogonality and the exponential increase of $\tilde{Z}_{\tilde{N}}$ with the size of the system. This renders exact methods unfeasible for calculating quantities such as entanglement entropy in large RVB systems. However, for two-legged quantum spin ladders, the RVB state and the subsequent number of coverings can be recursively generated [3, 131, 140, 141], and it is observed that quantity $\tilde{Z}_{\tilde{N}}$ is related to the Fibonacci sequence. Such recursion relations have been shown to be extremely important in calculations pertaining to several important

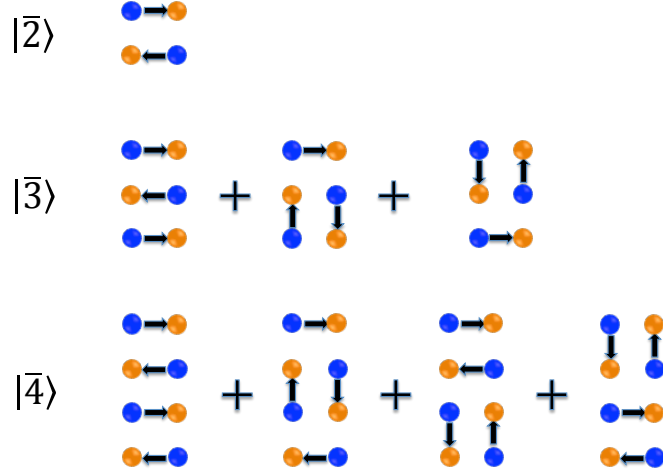


Figure 3.1: The dimer coverings (represented by the arrows) in the state $|\bar{2}\rangle$, $|\bar{3}\rangle$ and $|\bar{4}\rangle$. The sites on different bipartite lattices, A and B , have been distinguished using two different colors.

physical quantities [130, 131, 140, 141, 176], including genuine multipartite entanglement [2, 3, 140, 141]. Here we show how the Fibonacci sequence related to \tilde{Z}_N allows us to estimate the valence bond entropy in arbitrary large systems. Let us take a closer look at the two-legged RVB ladder and the Fibonacci sequence.

Consider $|N\rangle$ to be an N -rung, two-legged RVB ladder in which all the lattice sites are covered by dimers, i.e., the system has no dopants or holes. By considering the geometry of the $2 \times N$ lattice, and all the NN bonds possible, the state $|N\rangle$ can be recursively built, using the smaller-rung ladders, $|N-1\rangle$ and $|N-2\rangle$. The corresponding recursion relation reads as

$$|N\rangle = |N-1\rangle|1\rangle + |N-2\rangle|\bar{2}\rangle, \quad (3.2)$$

where $|1\rangle$ is the single rung dimer state, and $|\bar{2}\rangle$ is a 2×2 ladder with a pair of singlets connecting the horizontal NN spins (see Fig. 3.1). Therefore, the number of dimer coverings, Z_N , in a $2 \times N$ ladder is given by

$$Z_N = Z_{N-1} + Z_{N-2}. \quad (3.3)$$

We find that $Z_1 = 1$ and $Z_2 = 2$, which generates the Fibonacci sequence $\{Z_N\}$. The first few terms of the sequence are tabulated below:

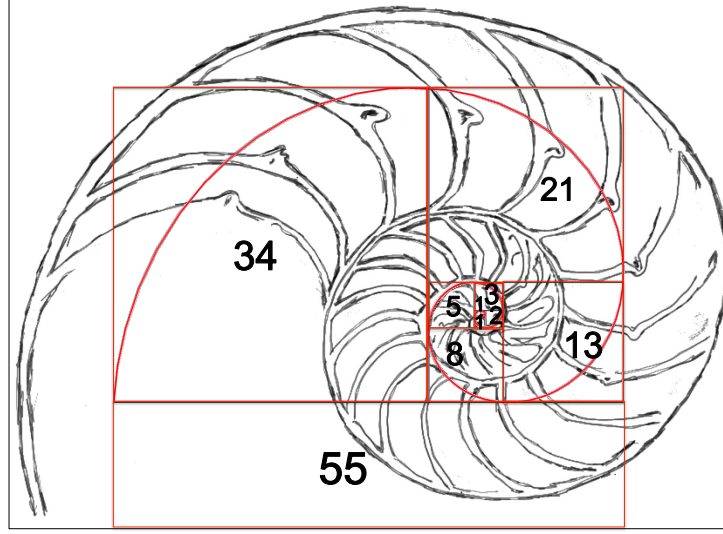


Figure 3.2: The naturally occurring patterns on the Molluscan shell roughly follows the golden spiral, with the areas of the square blocks following the Fibonacci sequence.

No. of dimer coverings Z_N									
Z_1	Z_2	Z_3	Z_4	Z_5	Z_6	Z_7	Z_8	Z_9	\dots
1	2	3	5	8	13	21	34	55	\dots

It is often said that the Fibonacci numbers are Nature’s numbering system. There exist an enormous number of examples where the basic structure of naturally occurring patterns, such as phyllotaxis and flowering in plants, arrangement in pine cones and pineapples, pedigrees in honeybees, and various shell proportions in molluscs (see Fig. 3.2) follow the Fibonacci sequence (cf. Ref. [177–179]).

An important quantity, from the perspective of general RVB states, is the rate of divergence of the series $\{Z_N\}$ at large N . For convenience of notation, we denote this rate as α , although for the Fibonacci sequence it is conventionally denoted as Φ , and referred to as the “golden ratio”. So, $\alpha = \frac{Z_N}{Z_{N-1}}$ and it quantifies the increase in the number of coverings with increasing rung. For two-legged RVB ladders, α can be derived as

$$Z_N = \alpha Z_{N-1} = \alpha^2 Z_{N-2}, \quad (3.4)$$

for sufficiently large N . Now plugging these terms into Eq. (3.3), one can obtain

$$\alpha^2 - \alpha - 1 = 0 \implies \alpha = \frac{1 + \sqrt{5}}{2} \approx 1.6180. \quad (3.5)$$

The approximate value of α is correct to four decimal places. The other value of α obtained from the equation is negative.

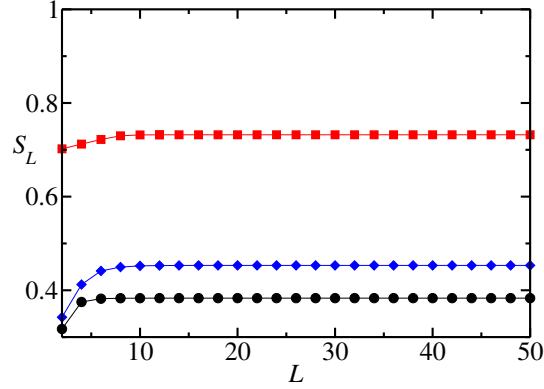


Figure 3.3: Valence bond entanglement entropy in undoped RVB ladders. We exhibit here the variation of the valence bond entanglement entropy ($S_{\tilde{L}}$), with increasing block size of \tilde{L} rungs, for two- (black circles), three- (red squares) and four- (blue diamonds) legged undoped RVB ladders. The horizontal axis is dimensionless while the vertical one is in ebits, with the singlet being normalized to $\ln 2$ ebits of entanglement. The plots display the valence bond entanglement entropy for partitions where \tilde{L} are even number of rungs. For the three-legged ladder, we do not have values for $\tilde{L}:N-\tilde{L}$ partition, where \tilde{L} is odd. However, for the even-legged ladders, the values for odd \tilde{L} partitions *decreases* before converging. Importantly, the converged values are the same at large \tilde{L} , irrespective of the small- \tilde{L} variations between odd and even \tilde{L} . The saturation of the valence bond entanglement entropy implies that a straight line fit is appropriate in this case.

We now look at how the sequence $\{Z_N\}$ can be used to estimate the valence bond entropy across an arbitrary boundary, for a two-legged RVB ladder with N rungs. Let us consider the boundary between the \tilde{L} and $\tilde{L} + 1$ rungs, such that the ladder is divided into \tilde{L} and $N - \tilde{L}$ rungs. The only coverings that contain a singlet pair across the boundary between the \tilde{L} and $\tilde{L} + 1$ rungs, are those that have the state $|\bar{2}\rangle$ at these rungs. Such coverings come from the state, $|\tilde{L} - 1\rangle \otimes |\bar{2}\rangle_{\tilde{L}, \tilde{L}+1} \otimes |N - \tilde{L} - 1\rangle$. Therefore the total number of singlets, $\sum_i a_i = 2Z_{\tilde{L}-1} \times Z_{N-\tilde{L}-1}$, and the valence

bond entropy is,

$$S_{\tilde{L}} = \frac{\sum a_i}{\sum W_i} \ln 2 = \frac{2Z_{\tilde{L}-1}Z_{N-\tilde{L}-1}}{Z_N} \ln 2, \quad (3.6)$$

as, $\sum_i W_i = Z_N$, since $W_i = 1 \ \forall \ i$.

Figure 3.3, provides the behavior of valence bond entropy for the two-legged ladder, with $N = 100$ rungs. We observe that $S_{\tilde{L}}$ saturates at a relatively low value of \tilde{L} (~ 10) rungs. The behavior shows that the valence bond entanglement entropy follows the area law and saturates with increasing \tilde{L} . This is consistent with exponentially decaying correlations in the system [180, 181], which suggests an area law for the entanglement entropy [182]. The scaling of valence bond entanglement entropy, therefore exhibits the behavior of entanglement entropy. The value at which valence bond entanglement entropy saturates (S_{sat}) can be expressed in terms of the quantity α . Consider $\tilde{L} = N/2$, in Eq. (3.6), and identify S_{sat} with $S_{N/2}$, to have

$$S_{sat} = \frac{2Z_{N/2-1} \times Z_{N/2-1}}{Z_N} \ln 2 = \frac{2Z_{N/2}}{\alpha^{N/2+2}} \ln 2 = \frac{2p}{\alpha^2} \ln 2, \quad (3.7)$$

where, from Eq. (3.4), we have used that $Z_{x+y} = \alpha^y Z_x$ for positive integers and large x and y , and that $p = \frac{Z_{N/2}}{\alpha^{N/2}}$ is a constant for large N . We will later on comment on the scaling with respect to the number of spins.

An important question that arises is whether a sequence form of the number of coverings, Z_N , can also be achieved for more complex systems. In subsequent sections we show that this can be done for higher-legged RVB ladders as well doped quantum spin ladders. Importantly, this allows us to characterize the valence bond entanglement entropy in all these systems.

3.3 Multi-legged quantum spin ladders and recursion relations

In this section, we begin with an analysis of the dimer covered states of the three- and four-legged RVB ladders. The main aim is to obtain a sequence for the number of coverings in the valence bond basis, similar to the Fibonacci sequence, which will allow us to estimate the valence bond entanglement entropy and the critical properties of these systems.

Three-legged RVB ladder– In the previous section, we found that for an undoped

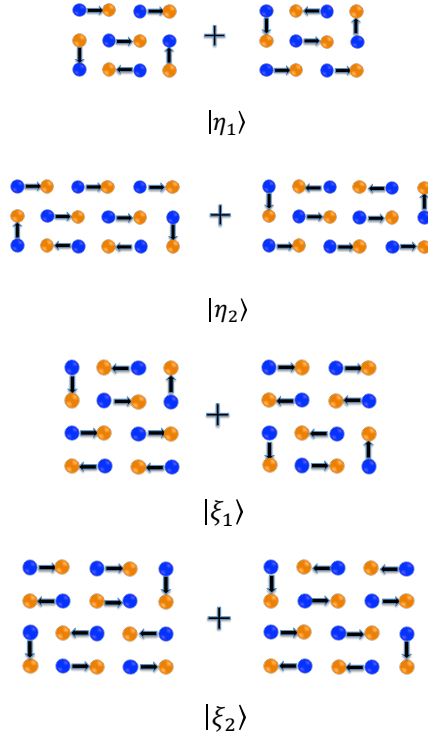


Figure 3.4: The dimer coverings (represented by the arrows) in the state $|\eta_1\rangle$, $|\eta_2\rangle$, $|\xi_1\rangle$, and $|\xi_2\rangle$. The states, $|\eta_i\rangle$ and $|\xi_i\rangle$, for $i > 2$, can be generated upon increasing the rungs by inserting floating horizontal singlets at the non-edge sites such that no non-singlet sharing blocks are formed. This can be observed in the above figures by looking at how $|\eta_2\rangle$ ($|\xi_2\rangle$) is generated from $|\eta_1\rangle$ ($|\xi_1\rangle$). The sites on different bipartite lattices, A and B , have been distinguished using two different colors.

two-legged ladder with moderately large rungs, the growth of the number of terms in the RVB state, described in Eq. (3.1), follows the Fibonacci sequence and the ratio of two successive elements in that sequence, is exactly equal to the golden ratio. In this regard, a possible generalization is to study the growth of the dimer coverings when the number of legs is more than two. For a $3 \times N$ RVB ladder, it is not possible to have odd number of rungs (N), as this shall result in odd number of spin sites which cannot accommodate complete singlets. For an even N -rung three-legged ladder, the RVB state $|N\rangle$ can recursively be generated as (not to be confused with the $|N\rangle$ in Eq. 3.2)

$$|N\rangle = |N-2\rangle|\bar{3}\rangle + \sum_{i=1}^{N/2-1} |N-2i-2\rangle|\eta_i\rangle, \quad (3.8)$$

where the additional terms $|\bar{3}\rangle$ and $|\eta_i\rangle$'s are depicted in Figs. 3.1 and 3.4, respectively. Hence, as in Eq. (3.3), the number of dimer coverings, Z_N , follow the relation

$$\begin{aligned} Z_N &= Z_{\bar{3}} \times Z_{N-2} + \sum_{i=1}^{N/2-1} Z_{N-2i-2} \times Z_{\eta_i}, \\ &= 3 Z_{N-2} + 2 \sum_{i=1}^{N/2-1} Z_{N-2i-2}, \end{aligned} \quad (3.9)$$

where, from Fig. 3.1, we observe that $Z_{\bar{3}} = 3$, and $Z_{\eta_i} = 2$, $\forall i$. Note that we are using the same notation, Z_N , for two-, three- and other multi-legged ladders, where N is the number of rungs. By rearranging the terms, the above equation can further be simplified to

$$Z_N = 4 Z_{N-2} - Z_{N-4}. \quad (3.10)$$

Hence, we observe that though the recursion relation for the three-legged RVB state does not yield the Fibonacci sequence, a generalized sequence for $\{Z_N\}$ can be obtained. The rate of divergence, at large N , is given by $\alpha'^2 = Z_N/Z_{N-2}$. Using Eq. (3.10), we obtain

$$\begin{aligned} Z_N &= \alpha'^2 Z_{N-2} = \alpha'^4 Z_{N-4} \\ \alpha'^4 - 4\alpha'^2 + 1 &= 0 \implies \alpha'^2 = 2 + \sqrt{3} \approx 3.7320, \end{aligned} \quad (3.11)$$

where the higher value of α'^2 (instead of $2 - \sqrt{3}$) is numerically observed. Here the approximate value of α' is correct to four decimal places. The quantity α'^2 can be compared with the rate of divergence in the Fibonacci sequence, when one gallops over every next term in the sequence, which is equal to $\alpha^2 = \Phi^2$ and we find that $\alpha'^2 > \alpha^2$. Hence, the three-legged ladder offers a higher rate of divergence when the number of rungs are increased, as compared to the two-legged ladder. If we wish to compare the number of coverings in the two- and three-legged ladders, when the number of spins are increased (and not the rungs), we must compare α'^2 with the number α^3 . Surprisingly, the two-legged ladder seems to be more complex, in the sense of having a larger number of coverings, than the three-legged ladder, when compared with respect to the increasing number of spins.

The valence bond entanglement entropy for the three-legged ladder bipartition across $\tilde{L}:N-\tilde{L}$ rungs can be obtained from the recursion in Eq. (3.10), by counting

the number of singlets crossing the boundary. The expression of $S_{\tilde{L}}$ is then given by

$$S_{\tilde{L}} = \frac{1}{Z_N} (5Z_{\tilde{L}-1} \times Z_{N-\tilde{L}-1} + 2 \sum_{i=1}^{N-\tilde{L}-1} Z_{\tilde{L}-2} \times Z_{N-\tilde{L}-1-i}) \ln 2. \quad (3.12)$$

The variation of $S_{\tilde{L}}$ with increasing block size \tilde{L} , is depicted in Fig. 3.3. Similar to the two-legged RVB ladder, the valence bond entropy in this case also satisfies the area law and saturates at large \tilde{L} . To obtain the saturation value of valence bond entanglement entropy, we look at the leading terms in Eq. (3.12) for the partition $\tilde{L} = N/2$. This gives us

$$\begin{aligned} S_{sat} &= \frac{5}{Z_N} Z_{\frac{N}{2}-1}^2 (1 + \frac{2}{5\alpha'^2} + \frac{2}{5\alpha'^3} + \dots) \ln 2, \\ &= 5 \times \frac{Z_{N/2}}{\alpha'^{N/2+2}} \ln 2 = \frac{5p'}{\alpha'^2} \ln 2, \end{aligned} \quad (3.13)$$

where $p' = \frac{Z_{N/2}}{\alpha'^{N/2}}$, at large N . We observe that the saturation value of valence bond entanglement entropy is higher than that of the two-legged RVB case. Therefore, an increase in the number of legs increases the average number of singlets across the block boundary, when compared on the axis of the number of rungs. See Fig. 3.3. One can make the same comparison on the axis of the number of spins, instead of rungs, and although the plots for valence bond entanglement entropy would take off in a different manner, as compared to Fig. 3.3, the saturation values would remain unaltered.

Four-legged RVB ladder– Similarly, one can proceed to obtain the series, $\{Z_N\}$, for the four-legged RVB ladder. The N -rung state, $|N\rangle$, can again be recursively be generated as,

$$|N\rangle = |N-1\rangle|1\rangle + |N-2\rangle|\bar{4}\rangle + \sum_{i=1}^{N-2} |N-i-2\rangle|\xi_i\rangle, \quad (3.14)$$

where the terms $|\bar{4}\rangle$ and $|\xi_i\rangle$'s are depicted in Figs. 3.1 and 3.4, respectively. Hence,

the number of dimer coverings follows the recursive relation

$$\begin{aligned}
Z_N &= Z_{N-1}Z_1 + Z_{N-2}Z_4 + \sum_{i=1}^{N-2} Z_{N-i-2}Z_{\xi_i}, \\
&= Z_{N-1} + 4Z_{N-2} + 2 \sum_{i=1}^{N-2} Z_{N-i-2}, \\
&= 2 Z_{N-1} + 3 Z_{N-2} - 2 Z_{N-3},
\end{aligned} \tag{3.15}$$

where we have inserted, $Z_1 = 1$, $Z_4 = 4$ and $Z_{\xi_i} = 2$, and rearranged the terms. As with two- and three-legged ladders, the rate of increase in the number of dimer coverings in four-leg RVB ladders, $\alpha'' = \frac{Z_N}{Z_{N-1}}$, for large N is given by the relation

$$\begin{aligned}
Z_N &= \alpha'' Z_{N-1} = \alpha''^2 Z_{N-2} = \alpha''^3 Z_{N-3}, \\
\alpha''^3 - 2\alpha''^2 - 3\alpha'' + 2 &= 0 \implies \alpha'' \approx 2.8136,
\end{aligned} \tag{3.16}$$

where the solution of α'' , which is positive and greater than unity, has been considered. The approximate value of α'' is correct to four decimal places. With respect to the number of rungs, the comparable rates of divergence for the two-, three-, and four-legged ladders are respectively α^2 , α'^2 , and α''^2 . We find that the four-legged ladder has a much higher rate of divergence than the two- and three-legged ladders. With respect to the number of spins, for the same set of ladders, the comparable rates are α^6 , α'^4 , and α''^3 , respectively, such that the number of spins to compare at each step are equal, i.e., $2 \times 6 = 3 \times 4 = 4 \times 3$. Again, the four-legged ladder has a much higher rate of divergence than the two-legged ladder, with the three-legged ladder having the lowest rate.

Using a similar approach to counting the number of dimers across the $\tilde{L}:N-\tilde{L}$ rung boundary in the N -rung four-legged RVB ladder, the expression for the valence bond entropy is given by

$$\begin{aligned}
S_{\tilde{L}} &= \frac{1}{Z_N} (10 Z_{\tilde{L}-1} \times Z_{N-\tilde{L}-1} \\
&\quad + 2 \sum_{i=1}^{N-\tilde{L}-3} Z_{\tilde{L}-1} \times Z_{N-\tilde{L}-3-i}) \ln 2,
\end{aligned} \tag{3.17}$$

where the contributions to valence bond entanglement entropy only arise from the $|\bar{4}\rangle$ and $|\xi_i\rangle$ terms in Eq. (3.8). The variation of $S_{\tilde{L}}$ with the increase of block size of rungs \tilde{L} is given in Fig. 3.3. There is no significant change of the pattern of the

increase of $S_{\tilde{L}}$ or area law of the system compared to the two-legged and three-legged cases. Interestingly, in this case, one can see that the value of the saturation entropy, S_{sat} , exceeds the value obtained for the two-legged case. However, it is lower than that of the value of S_{sat} , for three-legged undoped ladder. This is due to the fact that unlike the three-legged case, here the number of dimer coverings those contribute to valence bond entanglement entropy are less in number due to the difference in odd-even RVB state recursion. As before, one can see that with increasing number of legs, among all terms contributing to $S_{\tilde{L}}$, only the first term in Eq. (3.17) dominates, and hence the saturated value of $S_{\tilde{L}}$ can be written in terms of the diverging rate as $\frac{10p''}{\alpha'^{p''}} \ln 2$, where $p'' = \frac{Z_{N/2}}{\alpha'^{N/2}}$, at large N .

Figure 3.3 shows the valence bond entanglement entropy for the undoped RVB ladders with two, three, and four legs and $N = 100$ rungs. The plots differ at their take-off points and neighborhoods of the same when considered in terms of the number of spins (instead of the number of rungs), but soon become similar to the ones depicted in Fig. 3.3. The valence bond entanglement entropy is computable once the generalized sequence $\{Z_N\}$ and the corresponding divergence rate is estimated. We observe that the valence bond entanglement entropy in all multi-legged RVB ladders follow the area law, and saturate with high \tilde{L} , which is consistent with the behavior of entanglement entropy and the exponential decay of quantum correlations in RVB ladders [180, 181]. In the succeeding section, we look at the possibility of extending the analysis to RVB ladders when dopants (holes or defects) are introduced. This considerably increases the inherent complexity in the system, due to the new dimer-monomer arrangement in the bipartite lattice.

3.4 Doped RVB ladders

The doped quantum spin ladder is a strongly-correlated electron system with an extremely rich phase structure. Many physical properties of spin lattices undergo significant changes when some doping or impurity is added to the system. In recent times, attempts have been made to establish fundamental connections between high- T_c superconductivity and quantum spin fluctuations in underdoped cuprates [183–185]. This also helped to draw attention of the community towards the study of the properties of doped RVB states [186, 187]. However, presence of dopants in the system, increases the computational complexity to levels far higher than the undoped cases,

leading to fast growth of the number of coverings. Computation of quantities such as entanglement entropy becomes extremely hard even in comparatively smaller systems as compared to the undoped dimer covered states. Therefore, estimating the valence bond entropy in terms of some generalized sequence of $\{Z_N\}$, as done for undoped ladders, is important and will provide valuable inputs to understand the critical behavior of doped RVB ladders.

To maintain consistency with the undoped case, we investigate the generalized series and the valence bond entanglement entropy for doped RVB ladders with two, three and four legs, for different doping percentage or concentrations. To accommodate the doping in the system, we adopt a slightly different notation to represent the ladder states. We denote the doped RVB ladder with NN dimers as $|N, k\rangle$, where N be the number of rungs as before, and k is the number of dimers or singlets present in the system that forms a complete covering. The remaining sites are vacant or are holes in the spin lattice. The doping concentration is then given by, $n_h = 1 - n_e = 1 - \frac{2k}{l \times N}$, where n_e is the singlet density, and l is the number of legs. The valence bond basis now consists of complete dimer coverings and holes in all possible dimer-monomer arrangements in the ladder lattice, such that $|\phi_i^{N,k}\rangle = ([e_1, e_2] \otimes [e_3, e_4] \otimes \dots [e_{2k-1}, e_{2k}] \otimes |0\rangle^{\otimes h})_i$, where $|0\rangle$ is the hole or dopant present in h vacant sites. The arrangement of k singlets and h holes leads to the basis states, $\{|\phi_i^{N,k}\rangle\}$, and the RVB ladder is then given by $|N, k\rangle = \sum_{i=1}^{Z_{N,k}} W'_i |\phi_i^{N,k}\rangle$.

Let us start with the doped two-leg RVB state and build upon the derivations for the undoped case.

Two-legged doped ladder– Due to presence of holes at some of the lattice sites, in addition to the terms in the Eq. (3.2), one can have various other terms in the recursion. For a two-legged, N -rung RVB ladder with k dimers, the recursion relation reads as

$$\begin{aligned} |N, k\rangle &= |N-1, k-1\rangle|0, 1\rangle + |N-2, k-2\rangle|\bar{2}\rangle \\ &+ |N-1, k\rangle|1, 0\rangle + \sum_{i=1}^k |N-i-1, k-i\rangle|\chi_i\rangle, \end{aligned} \tag{3.18}$$

Here the term $|1, 0\rangle$ denotes a single rung with holes at all of its lattice sites, $|\chi_i\rangle$'s can be obtained from the terms $|\bar{2}\rangle$ by inserting hole pairs. All other terms have

the same meanings as in Eq. (3.2). Using this we find that the number of dimer coverings in $|N, k\rangle$ is given by

$$\begin{aligned}
Z_{N,k} &= Z_{N-1,k-1}Z_{1,1} + Z_{N-2,k-2}Z_2 + Z_{N-1,k}Z_{1,0} \\
&+ \sum_i Z_{N-i-1,k-i}Z_{\chi_i} \\
&= Z_{N-1,k-1} + Z_{N-2,k-2} + Z_{N-1,k} \\
&+ 2 \sum_i Z_{N-i-1,k-i} \\
&= 2Z_{N-1,k-1} + Z_{N-1,k} + Z_{N-2,k-1} - Z_{N-3,k-3},
\end{aligned} \tag{3.19}$$

where we have plugged the terms $Z_{1,1} = 1$, $Z_2 = 1$ and $Z_{\chi_i} = 2$, and rearranged the terms in the sum. Thus we obtain a recursion relation to generate the series $\{Z_{N,k}\}$. From Eq. (3.19), it is clear that the number of dimer coverings has a dependence on the hole concentration (n_h). Similarly, the rate of divergence ($\alpha_{N,k}$) is a function of n_h , and though a closed analytical form is cumbersome to present, the function can be numerically estimated using the recursion with relative ease. In Fig. 3.5, we plot $\alpha_{N,k} = \frac{Z_{N,k}}{Z_{N-1,k}}$, for varying hole concentration (n_h) (solid black circles), where $k' = k - Nh$. We observe that the effect of doping in the two-legged RVB ladder causes $\alpha_{N,k}$ to deviate from golden ratio. Starting off from the golden ratio at $n_h = 0$, for low hole concentration, the quantity $\alpha_{N,k}$ increases with n_h and reaches its maximum value at $n_{h_c} \approx 0.44$. Further increase of hole concentration reduces the rate of divergence.

The valence bond entanglement entropy for the doped two-legged RVB ladder, for a fixed n_h , is given by

$$\begin{aligned}
S_{\tilde{L}} &= \frac{1}{Z_{N,k}} \times \left(2 \sum_{i=0}^{k-2} Z_{\tilde{L}-1,k-2-i} Z_{N-\tilde{L}-1,i} \right. \\
&\quad \left. + 2 \sum_{i=1}^{N-\tilde{L}} \sum_{j=0}^{k-i} Z_{N-\tilde{L}-i,k-i-j} Z_{\tilde{L}-1,j} \right) \ln 2.
\end{aligned} \tag{3.20}$$

Figure 3.6, exhibits the plots for valence bond entanglement entropy in the doped two-legged RVB ladder, for different values of the n_h . We observe that the valence bond entanglement entropy across the lattice boundary, $\tilde{L}:N-\tilde{L}$ rungs, saturates with increasing \tilde{L} and thus follows the area law. This holds for all hole concentrations. However, the saturated values of $S_{\tilde{L}}$ decreases with increasing n_h , as increasing holes

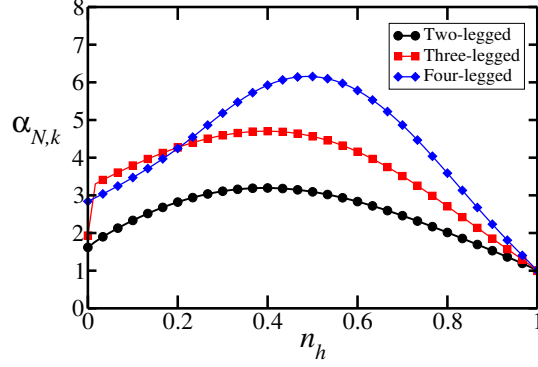


Figure 3.5: The changing face of the generalized Fibonacci sequences with increase in dopants. We exhibit here the rate of increase of the number of coverings $Z_{N,k}$, given by $\alpha_{N,k}$, for different hole concentration n_h . For each doped RVB ladder, with a different number of legs, there is a critical value of hole concentration, n_{hc} , where $\alpha_{N,k}$ is maximum. All quantities are dimensionless.

or dopants reduce the average number of dimers shared at the boundary.

Three-legged doped ladder– For the three-legged ladder, the doped RVB state with a large number of lattice sites, can be constructed from smaller system sizes, following the recursion

$$\begin{aligned}
 |N, k\rangle &= |N-1, k\rangle|1, 1\rangle + |N-1, k\rangle|1, 0\rangle \\
 &+ \sum_{i=1}^{N-1} \sum_{j=0}^{i+2} |N-i+1, k-i-j\rangle |\eta_i^j\rangle,
 \end{aligned} \tag{3.21}$$

where $|\eta_i^j\rangle$'s can be derived directly from the terms $|\eta_i\rangle$ in Eq. (3.9) by introducing pair of holes. Hence, the number of dimer coverings follows the relation

$$\begin{aligned}
 Z_{N,k} &= Z_{N-1,k-1}Z_{1,1} + Z_{N-1,k}Z_{1,0} \\
 &+ \sum_{i=1}^{N-1} \sum_{j=0}^{i+2} Z_{N-i+1,k-i-j}Z_{\eta_i^j}, \\
 &= 2Z_{N-1,k-1} + Z_{N-1,k} + \sum_{i=1}^{N-1} \sum_{j=0}^{i+2} Z_{N-i+1,k-i-j},
 \end{aligned} \tag{3.22}$$

where we have used, $Z_{1,1} = 2$, $Z_{1,0} = 1$ and $Z_{\eta_i^j} = 3$. For the three-legged doped

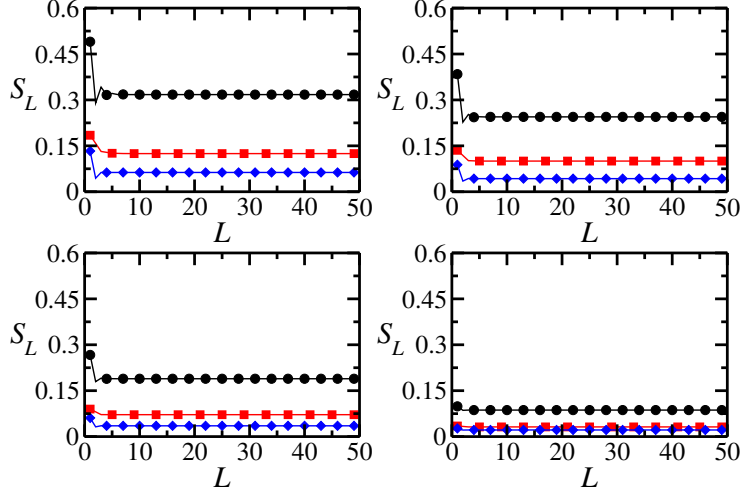


Figure 3.6: Valence bond entanglement entropy in doped RVB ladders. We plot here the variation of the valence bond entanglement entropy, S_L , with increasing block size of L rungs, for two- (black circles), three- (red squares) and four- (blue diamonds) legged doped RVB ladders. The four subfigures correspond to different doping concentrations, with $n_h = 0.1$ (top-left), $n_h = 0.3$ (top-right), $n_h = 0.5$ (bottom-left), and $n_h = 0.8$ (bottom-right). The horizontal axes are dimensionless while the vertical axes are in ebits.

RVB ladder, the rate of divergence $\alpha_{N,k}$ varies with the hole concentration (n_h) in a similar fashion to that observed in case of the doped two-legged ladder (see the red squares in Fig. 3.5). However, here $\alpha_{N,k}$ reaches its maximum value at a lower hole density ($n_{h_c} \approx 0.38$). In addition to this, for an arbitrary doping concentration, the value of the function $\alpha_{N,k}$ remains higher than that of the value obtained for the two-legged case. The valence bond entanglement entropy is then given by

$$\begin{aligned}
S_{\tilde{L}} &= \frac{1}{Z_{N,k}} \times \left(\sum_{j=1}^3 j \sum_{i=0}^{k-j} Z_{\tilde{L}-1, k-j-i} Z_{N-1-\tilde{L}, i} \right. \\
&\quad \left. + 4 \sum_{i=1}^{N/4} \sum_{j=0}^{6i-3} Z_{N-4i-\tilde{L}-1, k-6i-j} Z_{\tilde{L}-1, j} \right) \ln 2,
\end{aligned} \tag{3.23}$$

which is plotted for different n_h in Fig. 3.6. We observe that valence bond entanglement entropy, $S_{\tilde{L}}$, follows the area law as in the undoped case. However, due to the presence of holes or dopants, the saturated value for higher legs decreases in contrast to the undoped ladders.

Four-legged doped ladder– We now derive the recursion relation for a doped four-legged RVB ladder for arbitrary number of rungs (N) and arbitrary hole concentration (n_h). The recursion relation for a four-legged N -rung ladder is given by

$$\begin{aligned} |N, k\rangle &= Z_{N-1, k-2} Z_{1,2} + |N-1, k-1\rangle |1, 1\rangle + |N-1, k\rangle \\ &\times |1, 0\rangle + \sum_{i=1}^{N-1} \sum_{j=0}^{i+2} |N-i-1, k-i-j\rangle |\xi_j^i\rangle, \end{aligned} \quad (3.24)$$

where $|\xi_j^i\rangle$ can directly be derived from the terms $|\xi_i\rangle$ given in Eq. (3.15) by introducing pair of holes. Hence, the number of dimer coverings follow the recursion

$$\begin{aligned} Z_{N,k} &= Z_{N-1, k-2} Z_{1,2} + Z_{N-1, k-1} Z_{1,1} + Z_{N-1, k} Z_{1,0} \\ &+ \sum_{i=1}^{N-1} \sum_{j=0}^{i+2} Z_{N-i-1, k-i-j} Z_{\xi_j^i}, \\ &= Z_{N-1, k-2} + 3Z_{N-1, k-1} + Z_{N-1, k} \\ &+ 2 \sum_{i=1}^{N-1} \sum_{j=0}^{i+2} Z_{N-i-1, k-i-j}. \end{aligned} \quad (3.25)$$

with $Z_{1,2} = 1$, $Z_{1,1} = 3$, $Z_{1,0} = 1$ and $Z_{\xi_j^i} = 2$, which gives us the sequence $\{Z_{N,k}\}$. The rate of divergence, $\alpha_{N,k}$, as a function of n_h , is plotted in Fig. 3.5. In this case, for $0 < n_h \lesssim 0.247$, the quantity $\alpha_{N,k}$ has a value intermediate between the two- and three-legged doped ladders. Moreover, $\alpha_{N,k}$ reaches its maximum value, at a hole concentration ($n_h \approx 0.5$), which is much higher than that of the previous cases for doped ladders. Further increase of the hole concentration leads to reduction of the diverging rate.

The valence bond entanglement entropy for the four-legged RVB ladder is given by,

$$\begin{aligned} S_{\tilde{L}} &= \frac{1}{Z_{N,k}} \times \left(\sum_{j=1}^4 j \sum_{i=0}^{k-j} Z_{\tilde{L}-1, k-j-i} Z_{N-1-\tilde{L}, i} \right. \\ &\quad \left. + 6 \sum_{i=1}^{N/4} \sum_{j=0}^{8i-3} Z_{N-4i-\tilde{L}-1, k-8i+j} Z_{\tilde{L}-1, j} \right) \ln 2. \end{aligned} \quad (3.26)$$

Figure 3.6 shows the plots for valence bond entanglement entropy in doped RVB ladders, with two, three and four legs, and $N = 100$ rungs.

3.5 Summary

The calculation of the valence bond entanglement entropy in dimer-covered systems can be obtained as a direct consequence of derivation of the sequence for the number of possible valence bond coverings in the system. These numbers can in turn be obtained from recursion relations that can be derived for the state of ladder systems. The recursion relations differ with the number of legs in ladder, and whether or not there are dopants in the system. For the two-legged undoped ladder, the sequence so generated is the well-known Fibonacci sequence, with the golden ratio as the rate of divergence. For higher-legged ladders, the sequences deviate from the Fibonacci sequence and have their independent rates of divergence.

Figure 3.3, shows the scaling of valence bond entanglement entropy ($S_{\tilde{L}}$) in undoped RVB ladders, along different bipartitions of $\tilde{L}:N-\tilde{L}$ rungs, where the total number of rungs (N) has been fixed to 100. The calculations can be readily extended to a higher number of rungs. We observe that $S_{\tilde{L}}$ saturates for large \tilde{L} , which is typical of the behavior of entanglement entropy in noncritical systems where the area law is maintained. Some essential properties of the valence bond entanglement entropy in these undoped RVB ladders is also observed. In particular, the rate of increase of Z_N , the number of dimer coverings, is higher with increasing number of legs, if we consider the rate with respect to change in number of rungs. Moreover, the odd-even dichotomy observed in RVB ladders surfaces in the fact that the three-legged ladder has a higher saturation value of valence bond entanglement entropy compared to the even-legged ladders. This indicates that the saturated value of valence bond entanglement entropy (S_{sat}) has independent growth profiles for odd and even ladders, as can also be expected from the very different recursion relations for the respective states.

An interesting extension of the technique developed for undoped ladders, using Fibonacci-type sequences, is to consider doped ladders. The analysis is significantly more complicated, but has certain similarities with the undoped case. In Fig. 3.6, we observe the scaling of valence bond entanglement entropy in doped RVB ladders. The effect of doping on the scaling is shown in the four subfigures, with different values of the n_h , the doping concentration. We once more observe that the scaling of $S_{\tilde{L}}$ follows the area law for all values of n_h , but the value of valence bond entanglement entropy decrease with increasing n_h , as the average number of singlets

reduces with increased doping. An important outcome is that the scaling of valence bond entropy is not affected by increased doping. Although, the rate of divergence of $Z_{N,k}$, the number of dimer-monomer coverings, is dependent on n_h , as shown in Fig. 3.5, and can vary for different number of legs.

The presence of such generalized sequences to obtain the total number of dimer or dimer-monomer coverings in a spin lattice may also prove to be useful in more general settings. Apart from investigating critical phenomena in more complicated structures, it could be possible to estimate other important physical quantities in these systems, including entanglement and other information-theoretic and computationally useful system characteristics.

The results of this Chapter are based on the following paper:

- **Sudipto Singha Roy**, Himadri Shekhar Dhar, Aditi Sen(De), and Ujjwal Sen, *Fibonacci sequence and valence bond entanglement entropy in doped quantum spin ladders*, arXiv:1712.02726 [quant-ph].

Multipartite entanglement in undoped quantum spin ladders

4.0.1 Introduction

From the perspective of quantum many-body physics, the ground state of the Heisenberg ladder [188–190] is an important physical system with a rich topological order. The significance of these quantum spin ladders lie in their nontrivial intermediate properties between one-dimensional (1D) and two-dimensional (2D) spin lattices. For example, specific characteristics of Heisenberg ladders do not extrapolate trivially from the 1D Heisenberg chain to the 2D square lattice. This is due to the fact that odd and even Heisenberg ladders show different physical properties: Even-legged ladders are spin-gapped and have exponentially decaying correlation lengths while odd-legged ladders are gapless with power-law decay [188–192]. In recent years, quantum entanglement [23, 193] have been used as a tool to detect co-operative phenomena and topological order in the ground states of Heisenberg ladders [37, 43, 47, 64, 145, 146, 194–200]. Interestingly, there have been studies to understand the even-odd disparity in terms of entropy area law [151, 201], Rényi entropy [202], entanglement spectra [140], etc. However investigating the odd-even dichotomy via the scaling of co-operative multisite properties in large Heisenberg ladders remains an elusive proposition, primarily due to the unavailability of suitable analytical and numerical tools.

In this Chapter, we investigate the variation in ground state properties of even versus odd Heisenberg ladders by analyzing its genuine multisite entanglement. To characterize the quantity in the ladder states, we use generalized geometric measure

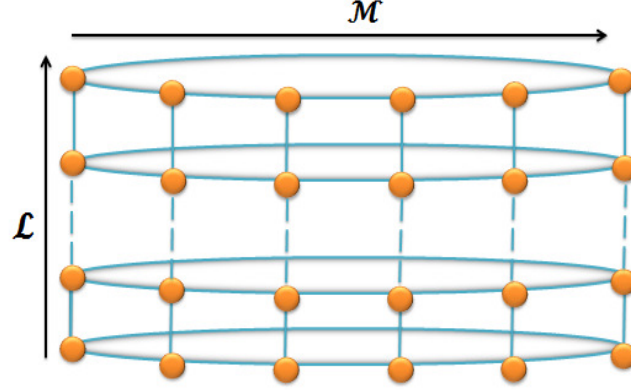


Figure 4.1: Schematic diagram of an \mathcal{L} -legged and \mathcal{M} -rung ladder, with $M (= \mathcal{M})$ and $L (= \mathcal{L})$ number of spin sites along the legs and rungs, respectively. The boundary condition is shown by a solid line that connects the first and last sites on a specific leg.

(GGM) [64, 162] (cf. [163–171], which has already been introduced in Chapter 2. The ground state of the Heisenberg ladder Hamiltonian is obtained using exact diagonalization algorithms [203, 204] for moderate system size. We observe that the genuine multisite entanglement behaves in qualitatively different ways for the ground states of the odd- and even-legged Heisenberg ladders – thus, detecting the odd-even dichotomy present in the system. In particular, the GGM increases with increasing number of ladder “rungs” for odd ladders while it decreases for even ladders. We subsequently observe that in terms of the behavior of GGM, the ground states of these ladder Hamiltonians are qualitatively similar to the ground states obtained from the resonating valence bond (RVB) state ansatz. Simulating the ground state of the Heisenberg ladders using RVB states allows us to analyze the finite-size scaling of genuine multisite entanglement in relatively large spin lattices by employing recursion methods [131, 140, 141, 205]. We observe that although the behavior of the GGMs for odd and even RVB ladders are qualitatively different, they converge to a single value in the asymptotic limit. Therefore, for ladders with large number of rungs, as the number of ladder “legs” are increased, the odd versus even demarcation in terms of GGM vanishes. However, evaluation of the finite size scaling exponent of multisite entanglement for large lattices reveals that the scaling exponents tend to *diverge* for odd and even ladders, as the number of legs are increased, even though the amount of genuine multisite entanglement *converges* in the asymptotic limit.

This Chapter is arranged as follows. In Sec. 4.1, we characterize and compute the genuine multisite entanglement in ground states of the Heisenberg ladder. We introduce the RVB ladder states in Sec. 4.2 and discuss the density matrix recursion method to obtain reduced density matrices. In Sec. 4.3, we compute GGM and study its behavior for short-ranged RVB ladder states. Subsequently, in Sec. 4.4 we study the diverging scaling and converging multisite entanglement property of the multi-legged quantum ladders. We present a summary in Sec. 4.5.

4.1 Characterization of genuine multisite entanglement in Heisenberg ladders

In many-body physics, the dichotomy between the physical properties of odd and even quantum Heisenberg ladders is well known [188–192]. It may now be asked whether one can identify a physical quantity that would have different limiting values depending on whether odd- or even-legged ladders are followed to reach the infinite 2D square lattice. In this section, we answer this question affirmatively by identifying a quantum information theoretic quantity that does the job. In particular, we searched for the answer of the following question, *we know that the sequences of both odd and even numbers mathematically reach the same infinity. The question is whether limits of functions of odd and even numbers reach the same limiting function as the respective sequences tend to infinity.*

To answer the above question, we start with the behavior of the GGM of the ground state of spin-1/2 Heisenberg ladders, which have been intensively studied in strongly-correlated physics in order to investigate exotic quantum phenomena, like high- T_c superconductivity [188], chiral Mott insulators [206–208] etc. Such studies are also interesting in view of the fact that Heisenberg models have been implemented using several experimental settings, ranging from optical lattices to nuclear magnetic resonance [87, 209–216]. The Hamiltonian of a quantum spin-1/2 Heisenberg model, with nearest-neighbor (NN) interactions, can be written as

$$H_{int} = \frac{J}{4} \sum_{|i-j|=1} \vec{\sigma}_i \cdot \vec{\sigma}_j, \quad (4.1)$$

where $J(J > 0)$ represents the NN antiferromagnetic (AFM) coupling constant. The indices, i and j , denote the sites of an arbitrary \mathcal{L} -legged ladder, and $\vec{\sigma}_i (= \sigma_i^x i + \sigma_i^y j + \sigma_i^z k)$ are the Pauli operators acting on the i^{th} site. The notation $|i - j|$ indicates that the corresponding summation is over NN sites. Figure 4.1, shows an \mathcal{L} -legged ladder, with \mathcal{M} rungs. The model can not be analytically approached beyond 1D [217]. Though various approximate techniques such as density matrix renormalization group [76, 218], quantum Monte-Carlo [219], and RVB theory [102, 112, 132, 220] have been used to compute certain correlation and bipartite entanglement properties, the characterization of genuine multisite entanglement in large spin systems remains an extremely challenging task.

Under these restrictions, we limit our exact-diagonalization study to moderate-sized Heisenberg ladders, upto 24 quantum spin-1/2 particles, and examine the GGM for the one-, two-, and three-legged ladders. We apply numerical algorithms, within the Lanczos method [203, 204], in order to obtain the ground state of the ladder Hamiltonian, and compute the GGM. The odd- and even-legged Heisenberg ladders show qualitatively distinct features if one considers correlation length, energy gap etc. [190]. We will now see whether such contrast in behavior can be seen by multipartite entanglement measure.

4.1.1 Odd-legged ladders

We now consider the GGM of the one- and three-legged ($\mathcal{L} = 1$ and 3) quantum spin-1/2 Heisenberg ladders as a function of number of rungs, \mathcal{M} . Fig. 4.2 displays the GGM, \mathcal{G} , as a function of number of rungs. \mathcal{G} exhibits alternating behavior based on whether the number of rungs, \mathcal{M} , is odd or even. This feature can not be observed in the result obtained via recursion technique of the RVB theory, described later in this Chapter, as the RVB ansatz naturally requires an even number of rungs. From Fig. 4.2, it is evident that for both the ladders \mathcal{G} increases with increasing \mathcal{M} . As the number of rungs increases, the rate of increment for \mathcal{G} slows down rapidly. Interestingly note that the fluctuations of \mathcal{G} between odd and even rungs reduces if one increases number of legs which can be observed by comparing the red lines ($\mathcal{L} = 1$) with the blue ones ($\mathcal{L} = 3$) in Fig. 4.2.

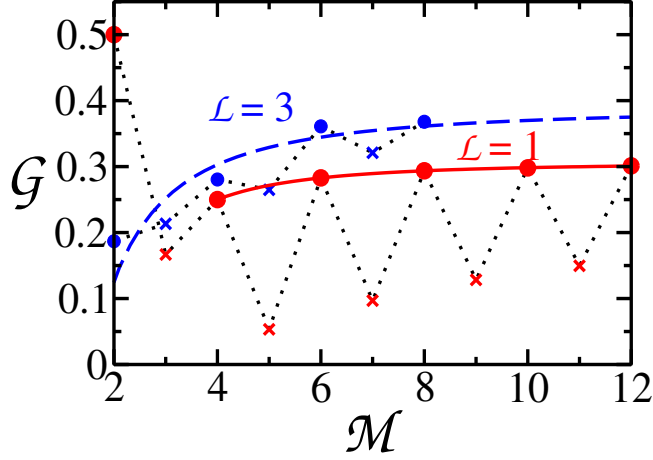


Figure 4.2: The behavior of GGM (\mathcal{G}), with increasing even number of rungs (\mathcal{M}) for odd \mathcal{L} -legged ladders, in ground states obtained by exact diagonalization of the Heisenberg Hamiltonian. The red and blue circles represent the behavior obtained for $\mathcal{L} = 1$ and $\mathcal{L} = 3$ legs, respectively. The solid lines show fits to the data values using Eq. (4.24). The dashed line serves as a guide to the eye. From the plots one can conclude that with even rungs, \mathcal{G} increases for odd-legged ladders while decreases for even ones. All quantities are dimensionless.

4.1.2 Even-legged ladders

Similarly, we also consider the GGM of the two-legged ladder ($\mathcal{L} = 2$), as a function of number of rungs, \mathcal{M} (see Fig. 4.3). We observe, \mathcal{G} decreases with the increase in \mathcal{M} for even rungs, while for odd rungs, it increases. However, as seen from Fig. 4.3, the difference of GGM between even and odd rungs decreases with the increase of rungs, and for relatively high values of \mathcal{M} , they both correspond to a single line following the same pattern. The same feature is obtained for $\mathcal{L} = 1$ and $\mathcal{L} = 3$ in Fig. 4.2. Therefore, we conclude that with even rungs, \mathcal{G} increases for odd legged ladders while decreases for even ones.

At this point, a question that arises is whether the distinct qualitative features obtained for the GGM using exact numerical simulations of the Heisenberg model can be modeled by using the RVB ansatz [102, 132]. This is motivated by the fact that several studies have observed the odd-even dichotomy in Heisenberg ladders using the RVB ground states [191]. It has been noticed that frustrated quantum Heisenberg spin models normally possesses short-range dimer states as their ground states. In particular, the ground states of the J_1 - J_2 model both in 1D and 2D

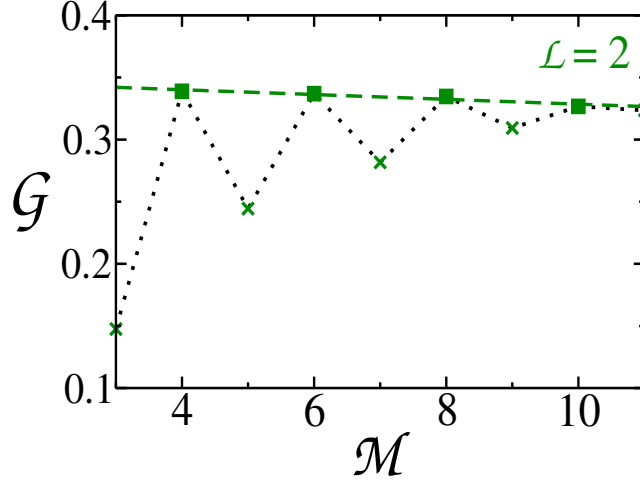


Figure 4.3: The behavior of GGM (\mathcal{G}), with increasing even number of rungs (\mathcal{M}) for odd \mathcal{L} -legged ladders, in ground states obtained by exact diagonalization of the Heisenberg Hamiltonian. The solid lines show fits to the data values using Eq. (4.24). The dashed line serves as a guide to the eye. From the plots one can conclude that with even rungs, \mathcal{G} increases for even-legged ladders while decreases for even ones. All quantities are dimensionless.

[121, 221, 222], the J_1 - J_2 - J_3 AFM Heisenberg model [223, 224], and the frustrated AFM on the 1/5-depleted square lattice [225], in certain parameter regimes, are the RVB states. Parallely, a family of rotationally invariant spin-1/2 Klein Hamiltonians exhibiting ground-state manifolds covered by NN valence bond states have also been proposed [226]. In this direction, a more systematic approach was proposed in which dimer models in different two-dimensional lattices like square, hexagonal, kagomé, are introduced whose exact ground states are valence bond states [127, 227–229]. Further supporting evidence for RVBs being ground states of Heisenberg ladders are provided in Refs. [173, 192, 230–232]. Recent results in the tensor-network formalism reveal that RVB states can be used efficiently to simulate the ground state properties of kagomé [124, 126] and the J_1 - J_2 square Heisenberg models [233–235].

In our work, we assume short-range RVB states, with NN dimer coverings, as the possible ground state of spin-1/2 Heisenberg ladders. Numerical investigation of the ground state from exact diagonalization and the RVB theory, for spin ladders upto 16 spins, provides considerable support for the RVB ansatz from the evaluation of the fidelity (\mathcal{F}) and the normalized relative difference in average energy (ΔE) [236]

between the exact ground states and the RVB states. For example, for both the two-legged and three-legged quantum spin ladders, upto 16-spins, \mathcal{F} as high as 0.9 and ΔE as low as 0.04 are obtained. These numerical findings gives us a good motivation for investigating the genuine multisite entanglement properties of the spin-1/2 Heisenberg ladder using the RVB ansatz.

Let us also mention here that RVB theory has been also popularized as a possible theoretical tool to understand high- T_c superconductivity [107,188] and are important in investigating co-operative phenomena in quantum many-body systems [37,47,138], and related to fault-tolerant quantum computation [237].

In the upcoming section, we will derive the recursion relation for the undoped RVB ladders and compute its few-site reduced density matrices.

4.2 Density matrix recursion method (DMRM)

In this section, we start with a quantum spin-1/2 ladder, with \mathcal{L} “legs” and \mathcal{M} “rungs” on a bipartite lattice (A, B) , comprised of $M(= \mathcal{M})$ sites along the horizontal side and $L(= \mathcal{L})$ sites the vertical side. The total number of spins, $n(= M.N)$, is always even, to allow for complete dimer coverings. Now if the interactions between the spins are restricted to be short-ranged and isotropic, we assume that only NN dimer coverings are allowed. The equal weight superposition of all such possible dimer coverings on the lattice would give us the so-called RVB state, given by

$$|\psi\rangle = \sum_{\mathcal{C}} \left[|A_1, B_1\rangle \otimes |A_2, B_2\rangle \otimes \dots |A_N, B_N\rangle \right]_{\mathcal{C}}, \quad (4.2)$$

where \mathcal{C} refers to a complete dimer covering of the lattice with the summation running over all the coverings, and $|A_i, B_j\rangle$ refers to the dimer

$$|\psi^-\rangle = \frac{1}{\sqrt{2}}(|\uparrow_i\rangle|\downarrow_j\rangle - |\downarrow_i\rangle|\uparrow_j\rangle), \quad (4.3)$$

formed between spins at sites i and j , on the sublattices A and B , respectively. The RVB state $|\psi\rangle$ is rotationally invariant and is always genuinely multisite entangled state in the asymptotic limit [141]. Below we present the proof in detail.

Theorem 1. *The undoped RVB ladder state, $|\psi\rangle$, with n lattice sites, containing all possible coverings of k ($k \neq 0$) spin dimers, is always genuinely multipartite entangled for all ladder topologies that are periodic or infinite along the rails.*

Proof. The RVB state defined in Eq. (4.2), is a pure state. In order to prove that this superposed state is genuinely multisite entangled, we need to prove that the reduced density matrices of the state across any bipartition cannot be pure. Towards that aim, we first divide the proof into three cases (a) Odd bipartitions, (b) Even bipartitions and (c) Other bipartitions.

4.2.0.1 (a) Odd bipartitions:

Using the invariance of $|\psi\rangle$ under the action of $U^{\otimes n}$, one can show that all p -qubit reduced systems, $\rho^{(p)} = \text{Tr}_{\bar{p}}[|\psi\rangle\langle\psi|]$, obtained by tracing over all but p sites, is always invariant under $U^{\otimes p}$, where U is the local unitary acting on each lattice site. For an odd numbers of spin- $\frac{1}{2}$ particles, there is no pure quantum state that is rotationally invariant. Therefore, one can conclude that any odd bipartition of the system is always entangled to the rest of the system. For instance, if one considers any single-site density matrix obeying the rotational invariance property mentioned above, it would have following mathematical expression,

$$\rho^1 = \frac{\mathbb{I}_2}{2}, \quad (4.4)$$

where \mathbb{I}_2 is the identity matrix in \mathbb{C}^2 .

4.2.0.2 (b) Even bipartitions:

Similarly, using the rotational invariance property of the RVB state defined above, one can show that the nearest neighbor two-site density matrix has the form,

$$\rho^{(2)} = q|\psi^-\rangle\langle\psi^-| + (1-q)\mathbb{I}_4/4, \quad (4.5)$$

where $|\psi^-\rangle$ has been defined earlier and \mathbb{I}_4 is the identity matrix on $\mathbb{C}^2 \otimes \mathbb{C}^2$ with $-\frac{1}{3} \leq q \leq 1$. For any nonzero value of the parameter q , $\rho^{(2)}$ is always mixed and hence $|\psi\rangle$ is always entangled across any 2:rest bipartitions.

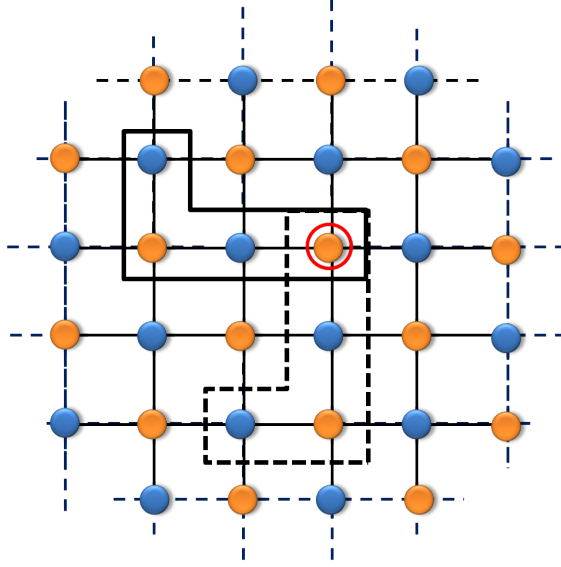


Figure 4.4: Schematic diagram of two possible bipartitions of a multi-legged quantum spin ladder (one denoted by solid lines and the other one by broken lines), sharing a common node and comprised of same number of sites.

4.2.0.3 (c) Other bipartitions:

However, we want to show that all possible bipartitions, irrespective of the number of sites, are always mixed. To prove this let us assume now that an arbitrary r -site density matrix ($\rho^{(r)}$) is pure, which implies that $|\psi\rangle$ is separable along that r : $n - r$. Let $r = r_1 + j$, where $j=1$ or 2 such that $|j| < |r_1|$ ($|\cdot|$ is the cardinality of the argument).

For the periodic or infinite ladder, one can always find another equivalent pure density matrix, $\rho^{(s)}$, such that $s = s_1 + j$ and $|r| = |s|$, where j -sites overlap. Fig. 4.4 shows one such example of two possible bipartitions with a common node. We started with the assumption that, both $\rho^{(r)}$ and $\rho^{(s)}$ are pure. Using strong subadditivity of von Neumann entropy [238],

$$S(\sigma) = -\text{tr}(\sigma \log_2 \sigma), \quad (4.6)$$

one can eventually show that

$$S(\rho^{(r_1)}) + S(\rho^{(s_1)}) \leq S(\rho^{(r_1+j)}) + S(\rho^{(s_1+j)}). \quad (4.7)$$

Since $\rho^{(r)}$ and $\rho^{(s)}$ are pure, this implies

$$S(\rho^{(r_1+j)}) = S(\rho^{(s_1+j)}) = 0. \quad (4.8)$$

Moreover, as $S \geq 0$, we have $S(\rho^{(r_1)}) = S(\rho^{(s_1)}) = 0$, and therefore $S(\rho^{(j)}) = 0$ implying $\rho^{(j)}$ is pure, which is not true as we have shown above. Hence, the contradiction implies that all reduced density matrices, $\rho^{(r)}$ are mixed and all r : $n - r$ bipartitions of the given quantum state, $|\psi\rangle$, are entangled.

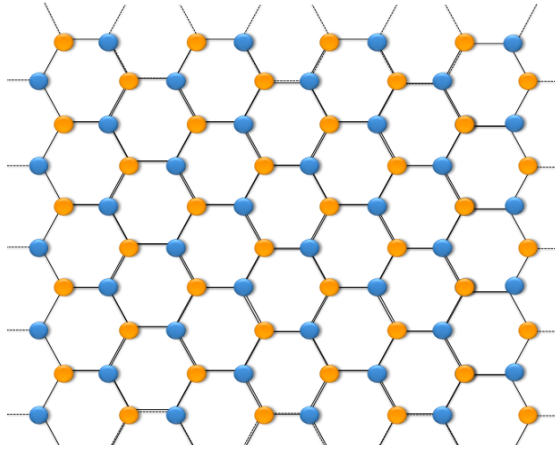


Figure 4.5: A two-dimensional bipartite lattice, with sublattices A (blue-circles) and B (yellow-circles).

We note that the above proof does not include the r : $n - r$ bipartitions where no equivalent $\rho^{(r)}$ with overlap is feasible, such as the bipartition between the two legs of the ladder. However, in such cases, the theorem can be proved using a different argument. We assume that the legs, L_i and L'_i of $|\psi\rangle$ are pure and thus the entire state is separable along that N : N . For the above condition to be satisfied, all reduced states along the rungs, $\rho_{(L_k, L'_k)}^{(2)}$, $\forall k$, must be separable. However, as can be shown by using recursive method, such nearest-neighbor $\rho^{(2)}$ states are always entangled. Hence, the undoped RVB state is genuinely multipartite entangled. ■

The RVB state in Eq. (4.2) is unique. This is done by defining the RVB state on a bipartite lattice (A, B) . A bipartite lattice is formulated by dividing the spin lattice into two sublattices A and B , such that a spin in sublattice A has spins in sublattice B as its nearest neighbours, and vice-versa. See Fig. 4.5 for schematic representation

of a two-dimensional lattice with sublattices A (blue-circles) and B (yellow-circles). In our formalism, we require that all NN dimer states are directed from spins on sublattice A to spins on sublattice B, which removes possible ambiguity in the sign of the ground state, and ensures that the defined RVB state is unique.

In Chapter 3, we have derived the recursion relations for multi-legged doped and undoped quantum spin ladders, considering open boundary condition only. In this section, for completeness, we first start with the same recursion relation for the undoped two-legged quantum ladders and subsequently generalize it for periodic systems. Let the RVB state, defined in Eq. (4.2), for a quantum spin ladder be denoted by $|\mathcal{M}, \mathcal{L}\rangle$, with \mathcal{L} legs and \mathcal{M} rungs. Now, let us consider the system containing $M = \mathcal{M} + 2$ spins along the rungs, and $L = \mathcal{L}$ number of spins along the legs. For even \mathcal{L} , the state with open boundary condition can be generated recursively as [130, 131, 140, 141, 205]

$$\begin{aligned} |\mathcal{M} + 2, \mathcal{L}\rangle &= |\mathcal{M} + 1, \mathcal{L}\rangle |1\rangle_{m+2} + |\mathcal{M}, \mathcal{L}\rangle |\bar{2}\rangle_{m+1, m+2} \\ &= |\mathcal{M}, \mathcal{L}\rangle |2\rangle_{m+1, m+2} + |\mathcal{M} - 1, \mathcal{L}\rangle \\ &\times |\bar{2}\rangle_{m, m+1} |1\rangle_{m+2}, \end{aligned} \quad (4.9)$$

where $|2\rangle_{m+1, m+2}$ and $|1\rangle_{m+2}$ correspond to the RVB ladder states, $|2, \mathcal{L}\rangle$ and $|1, \mathcal{L}\rangle$, respectively, and

$$|\bar{2}\rangle_{m+1, m+2} = |2\rangle_{m+1, m+2} - |1\rangle_{m+1} |1\rangle_{m+2}, \quad (4.10)$$

(see Fig. 4.6). Here, the subscripts denote the rung index. Since, for an \mathcal{L} -legged ladder, the index \mathcal{L} is constant in the recursion relations, without loss of generality, we can remove it in the state description, so that the RVB state is denoted by $|\mathcal{M}\rangle$. Incorporation of the periodic boundary condition leads to the following extension of Eq. (4.9) [140, 141] (see Fig. 4.7):

$$|\mathcal{M} + 2\rangle^{\mathcal{P}} = |\mathcal{M} + 2\rangle_{1, m+2} + |\mathcal{M}\rangle_{2, m+1} |\bar{2}\rangle_{m+2, 1}, \quad (4.11)$$

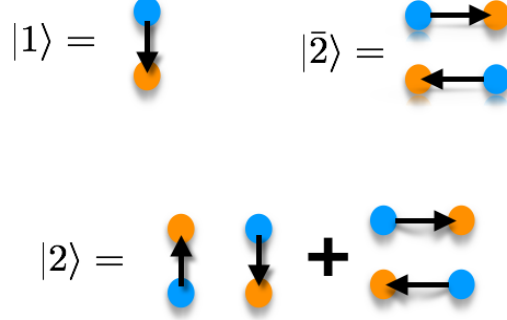


Figure 4.6: The dimer coverings in the state $|1\rangle$, $|\bar{2}\rangle$ and $|2\rangle$. The sites on different bipartite lattices, A and B, have been distinguished using two different colors.

where all the terms on the right can be calculated by using Eq. (4.9) for RVB states with open boundary condition. Hence, and hereafter, the superscript \mathcal{P} will indicate that periodic boundary condition has been used for the corresponding state. Using the recursive relation given in Eq. (4.11) we obtain the density matrix characterizing the periodic RVB ladder system, which is given by

$$\begin{aligned} \rho_{(\mathcal{M}+2)}^{\mathcal{P}} &= \rho_{(\mathcal{M}+2)} + |\mathcal{M}\rangle\langle\mathcal{M}|_{2,m+1} \otimes |\bar{2}\rangle\langle\bar{2}|_{1,m+2} \\ &+ (|\mathcal{M}+2\rangle\langle\mathcal{M}|_{2,m+1} \langle\bar{2}|_{m+2,1} + \text{h.c.}), \end{aligned} \quad (4.12)$$

where, the term $\rho_{(\mathcal{M}+2)}$ corresponds to the density matrix of the non-periodic RVB ladder, computed using Eq. (4.9). We call this as density matrix recursion method (DMRM).

As mentioned earlier, our main interest lies in the multisite entanglement properties of these RVB ladders. In order to explore this, we first need to have expressions for all possible reduced density matrices of the system. The maximal Schmidt coefficients obtained from these reduced density matrices allow us to compute the GGM of the RVB ladder. As the number of spins in the RVB ladder increases, there is a rapid growth of the number of possible reduced density matrices. However, the symmetry of a periodic RVB state can be exploited to obtain the maximal Schmidt coefficient, which is required to compute GGM without considering all possible reduced states. For example, extensive numerical studies upto 16 spins confirm that for

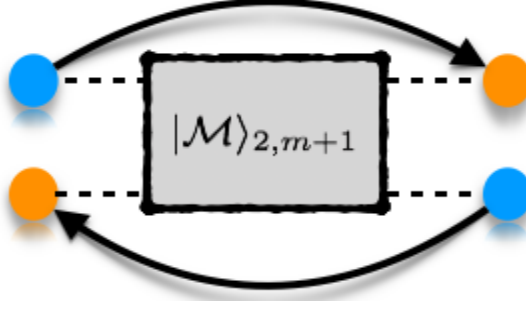


Figure 4.7: Schematic diagram of the additional term $|\mathcal{M}\rangle_{2,m+1}|\bar{2}\rangle$ appeared in Eq. (4.11), due to periodic boundary condition. The sites on different bipartite lattices, A and B, have been distinguished using two different colors.

an $|\mathcal{M}, \mathcal{L}\rangle$ ladder, optimization over the restricted set of all reduced density matrices contained within a reduced $2 \times \mathcal{L}$ block, say at sites $m+1$ and $m+2$, is sufficient to obtain the maximum Schmidt coefficient for calculating the GGM. The symmetry and periodicity of the RVB ladder ensures that all reduced $2 \times \mathcal{L}$ block, between any adjacent pair of sites in the lattice, are topologically equivalent. This reduces the computational difficulty in calculating the genuine multisite entanglement as the optimization over all reduced states is now limited to a $2 \times \mathcal{L}$ block, which can be analytically derived using a recursion method as discussed in the following segments.

For an RVB ladder with open boundary, the reduced density matrix of a $2 \times \mathcal{L}$ block is obtained by tracing out all the spins except those at the rungs $m+1$ and $m+2$, as given by

$$\begin{aligned} \rho_{(m+1,m+2)} &= \mathcal{N}_{\mathcal{M}} |2\rangle\langle 2|_{(m+1,m+2)} + \mathcal{N}_{\mathcal{M}-1} \bar{\rho}_{m+1} \\ &\otimes |1\rangle\langle 1|_{(m+2)} + (|2\rangle_{m+1,m+2}\langle 1|_{m+2} \langle \chi_{\mathcal{M}}|_{m+1} + \text{h.c.}), \end{aligned} \quad (4.13)$$

where $\mathcal{N}_{\mathcal{M}} = \langle \mathcal{M} | \mathcal{M} \rangle$ and

$$\bar{\rho}_{m+1} = \text{tr}_m(|\bar{2}\rangle\langle \bar{2}|_{m,m+1}), \quad \text{and} \quad (4.14)$$

$$\langle \chi_{\mathcal{M}} |_{m+1} = \langle \bar{2} |_{m,m+1} \langle \mathcal{M} - 1 | \mathcal{M} \rangle. \quad (4.15)$$

By using Eq. (4.13) we obtain the reduced density matrix for the $2 \times \mathcal{L}$ block at

rungs $m+1$ and $m+2$, for the periodic RVB ladder state, $\rho_{(\mathcal{M}+2)}^{\mathcal{P}}$, given by Eq. (4.12). The reduced density matrix is given by

$$\begin{aligned}\rho_{(m+1,m+2)}^{\mathcal{P}} &= \rho_{m+1,m+2} + \text{tr}_{1\dots m} \left[|\mathcal{M}\rangle \langle \mathcal{M}|_{2,m+1} |\bar{2}\rangle \langle \bar{2}|_{1,m+2} \right] \\ &+ (|\mathcal{M}\rangle_{2,m+1} |\bar{2}\rangle_{1,m+2} |\langle \mathcal{M}+2| + \text{h.c.}), \\ &= \rho_{m+1,m+2} + \xi_{m+1,m+2}^1 + (\xi_{m+1,m+2}^2 + \text{h.c.}),\end{aligned}\quad (4.16)$$

where

$$\begin{aligned}\xi_{m+1,m+2}^1 &= \mathcal{N}_{\mathcal{M}-1} |1\rangle \langle 1|_{m+1} \otimes \bar{\rho}_{m+2} + \mathcal{N}_{\mathcal{M}-2} \bar{\rho}_{m+1} \\ &\otimes \bar{\rho}_{m+2} + (|1\rangle \langle \chi_{\mathcal{M}-1}|_{m+1}) \otimes \bar{\rho}_{m+2} + \text{h.c.}), \\ \xi_{m+1,m+2}^2 &= |2\rangle_{m+1,m+2} \langle 1|_{m+1} \langle \chi_{\mathcal{M}}|_{m+2} + |2\rangle_{m+1,m+2} \\ &\times \sum_1^{\mathcal{M}} \langle \mathcal{K}_i|_{m+2} \langle \chi_{\mathcal{M}-i}|_{m+1} + \bar{\rho}_{m+1} \otimes |1\rangle_{m+2} \\ &\times \langle \chi_{\mathcal{M}}|_{m+2} + 1/\mathcal{N}_1 (|\mathcal{K}_1\rangle_{m+1} |1\rangle_{m+2}) \\ &\times \langle 1|_{m+1} \sum_{i=1}^{\mathcal{M}} \langle \mathcal{K}|_{m+2} \mathcal{J}_{\mathcal{M}-1}^1.\end{aligned}\quad (4.17)$$

Here $\mathcal{J}_{\mathcal{M}}^1 = \langle \mathcal{M}|\mathcal{M}-1\rangle$ and $\langle \mathcal{K}_i|_{m+1} = {}_{m,m+1} \langle \bar{2}|\mathcal{K}_{i-1}\rangle_m$ with $|\mathcal{K}_0\rangle_m = |1\rangle_m$. The recursion relation for the inner product $\langle \mathcal{M}|\mathcal{M}\rangle$ can now be expressed as

$$\mathcal{N}_{\mathcal{M}} = \mathcal{N}_1 \mathcal{N}_{\mathcal{M}-1} + \mathcal{N}'_2 \mathcal{N}_{\mathcal{M}-2} + 2(-1)^{m-1} \sum_i \gamma_i^1 \mathcal{J}_{\mathcal{M}-1}, \quad (4.18)$$

where $\mathcal{N}'_2 = \langle \bar{2}|\bar{2}\rangle$ and all the γ_i 's can be calculated using the linear equation

$$\langle \gamma_i|\bar{2}\rangle_{m,m+1} = (-1)^{m-1} \sum_{j=1}^{j_2} \gamma_j |\gamma_j\rangle_{m+1}, \quad (4.19)$$

where $|\gamma_j\rangle$ form an independent set of vectors consisting of certain singlet combinations of an $(1, \mathcal{N}+2)$ spin system, e.g $|\gamma_1\rangle = |1\rangle$.

For odd \mathcal{L} , the recursion relations are much simpler as the number of possible coverings is lower. The recursion relation for the RVB ladder with periodic boundary conditions is given by

$$\begin{aligned} |\mathcal{M} + 2, \mathcal{L}\rangle_{\mathcal{P}} &= |\mathcal{M}, \mathcal{L}\rangle_{1,m} |2\rangle_{m+1,m+2} \\ &+ |\mathcal{M}, \mathcal{L}\rangle_{2,m+1} |2\rangle_{m+2,1}. \end{aligned} \quad (4.20)$$

The reduced density matrix for the $2 \times \mathcal{L}$ block, at sites $m+1$ and $m+2$, corresponding to the above state is given by

$$\begin{aligned} \rho_{(m+1,m+2)}^{\mathcal{P}} &= \mathcal{N}_{\mathcal{M}} |2\rangle \langle 2|_{m+1,m+2} + \mathcal{N}_{\mathcal{M}-2} \rho_{m+1} \otimes \rho_{m+2} \\ &+ \left(|2\rangle_{m+1,m+2} \langle \xi^3|_{m+1,m+2} + \text{h.c.} \right), \end{aligned} \quad (4.21)$$

where

$$\langle \xi^3|_{m+1,m+2} = \langle 2|_{1,m+2} \langle \mathcal{M}|_{2,m+1} |\mathcal{M}\rangle_{1,m}, \quad \text{and} \quad (4.22)$$

$$\rho_{m+1} = \text{tr}_m(|2\rangle \langle 2|_{m,m+1}). \quad (4.23)$$

Hence, using Eqs. (4.16) and (4.21) for even- and odd-legged RVB ladders, respectively, one can obtain the reduced density matrices for the $2 \times \mathcal{L}$ block necessary to compute the generalized geometric measure. We note that the maximal Schmidt coefficient is obtained by considering the reduced states within the $2 \times \mathcal{L}$ block. It is observed that the maximum Schmidt coefficients are typically obtained from the 2 : rest or the 4 : rest bipartitions where the reduced spins are nearest neighbors, though there does not seem to be any distinctive pattern that can systematically differentiate between the typical bipartitions in odd and even ladders. Moreover, no systematic pattern is observed in which topologically inequivalent reduced states provide the same maximum Schmidt coefficient.

We subsequently compare the GGM of the RVB state with that of the ground state of the Heisenberg ladder obtained by exact diagonalization. Note here that although we use the above method for calculating the GGM, the same recursion can be used to calculate other system properties like magnetization, susceptibility, classical correlators, bipartite entanglement and other quantum correlations, etc. A

more developed exposition and formalism for the density matrix recursion method can be obtained in Refs. [140, 141].

4.3 Characterization of genuine multisite entanglement in RVB ladders

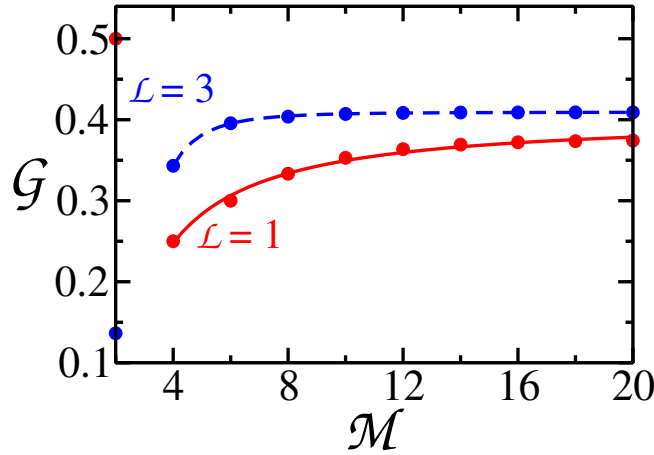


Figure 4.8: The behavior of GGM (\mathcal{G}), with increasing number of rungs (\mathcal{M}) in one- and three-legged ladders, using short-range RVB states. The solid lines show fits to the data values using the equation given in Eq. (4.24). The dashed line serves as a guide to the eye. The “two-rung” case for the one-legged ladder is just a singlet—instead of superpositions over several coverings of singlets, and also correspondingly provides a value that is drastically different from the higher-rung cases of the same ladder. We therefore ignore this case from the one-legged ladder case.

Applying the recursion technique, we can investigate the behavior of genuine multisite entanglement of the RVB state in large quantum spin lattices. For example, one can study the finite-size scaling of GGM in \mathcal{L} -legged ladders with large number of rungs and investigate the odd-even dichotomy in the asymptotic limit. For odd-legged RVB ladders, the GGM initially increases with increasing number of even rungs, \mathcal{M} , before approaching a constant value at large \mathcal{M} (see Fig. 4.8), while for even-legged ladders, the GGM decreases with increasing \mathcal{M} , before flattening to a constant for larger number of rungs as shown in Fig. 4.9. Note that the DMRM approach is not possible to access an odd number of rungs. Importantly,

we find that the behavior of genuine multisite entanglement of the ground state of the Heisenberg ladder with even- and odd-legged ladders is qualitatively similar to results obtained with the RVB ansatz. This is clearly seen by comparing Fig. 4.2 with 4.8, and Fig. 4.3 with Fig. 4.9.

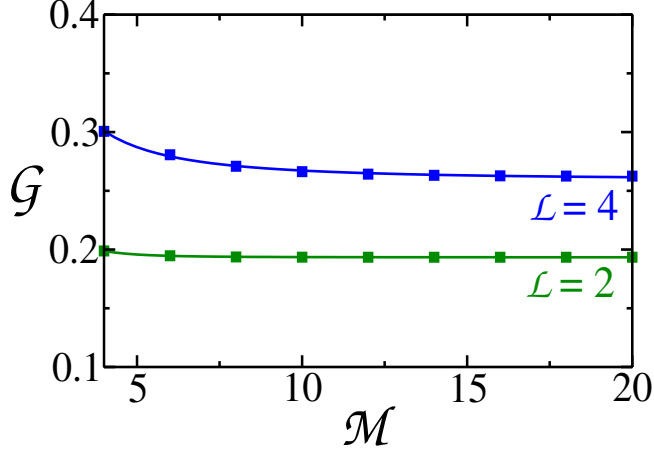


Figure 4.9: The behavior of GGM (\mathcal{G}), with increasing number of rungs (\mathcal{M}) in two- and four-legged ladders using short-range RVB states. The solid lines show fits to the data values using the equation given in Eq. (4.24). The dashed line serves as a guide to the eye.

The similarity between the two methods, viz. exact diagonalization of the Heisenberg ladder and RVB ansatz on the same lattice, motivates us to perform finite-size scaling analysis of GGM, by using RVB theory, wherein we can handle large lattice sizes. The analysis would shed light on the finite-size behavior of multiparty entanglement of the original Heisenberg ladder.

4.4 Diverging scaling with converging multisite entanglement

The finite-size scaling of GGM in a pure quantum spin ground state, $|\psi\rangle$, can be analyzed through the scaling relation, $\mathcal{G}(|\psi\rangle) \approx \mathcal{G}_c(|\psi\rangle) \pm kn^{-x}$, where, n is the total number of spins, \mathcal{G}_c is an estimated value of GGM at high n , and x is the “scaling exponent” with which the GGM approaches its asymptote at large n . For

an \mathcal{L} -legged RVB ladder, written as $|\mathcal{L}, \mathcal{M}\rangle$, the finite-size scaling is given by the relation,

$$\mathcal{G}(|\mathcal{L}, \mathcal{M}\rangle) \approx \mathcal{G}_c(\mathcal{L}) \pm kn^{-x(\mathcal{L})}. \quad (4.24)$$

Using the DMRM method, we have computed the GGM for RVB ladders upto $\mathcal{L} < 8$, with $\mathcal{M} = 20$. One can easily extend the computation for higher values of \mathcal{M} .

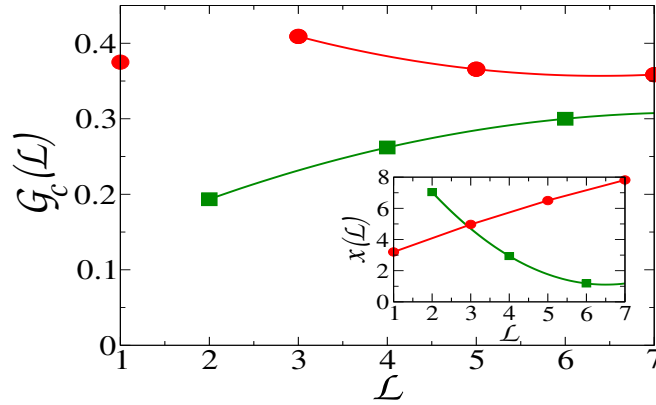


Figure 4.10: Diverging scaling with converging multisite entanglement. The behavior of the asymptotic GGM ($\mathcal{G}_c(\mathcal{L})$) and the scaling exponent ($x(\mathcal{L})$) with increasing \mathcal{L} . We observe that even though, the $\mathcal{G}_c(\mathcal{L})$ for odd- and even-legged ladders, converge with increasing \mathcal{L} , the scaling $x(\mathcal{L})$ diverge. All axes are dimensionless. The data point corresponding to the case of only two “rungs” on the one-legged ladder is not considered for the fitting. Please see the caption of Fig 4.8 in this regard.

Fig. 4.10 shows the values of $\mathcal{G}_c(\mathcal{L})$ and $x(\mathcal{L})$, for different values of \mathcal{L} , where the GGM is scaled upto $\mathcal{M} = 20$ rungs for an RVB ladder of \mathcal{L} legs. We observe that as \mathcal{L} increases, the $\mathcal{G}_c(\mathcal{L})$ for the odd- ladders converges to that for the even ones. This is consistent since the pseudo-2D spin ladders slowly approaches the square-2D lattice, and in the asymptotic limit, one cannot distinguish whether the system was originally generated by increasing \mathcal{L} in an odd- or even-legged ladder. However, we find that the scaling exponent, $x(\mathcal{L})$, for odd and even ladders, converges to *different* values with increase of \mathcal{L} (see inset of Fig. 4.10). We therefore have a diverging scaling exponent for odd- and even-legged ladders, even though the corresponding multisite entanglement converge. The diverging $x(\mathcal{L})$, therefore, shows that the finite-size scaling of GGM for RVB ladders can highlight the odd-even dichotomy at

large \mathcal{L} . The results show that the GGM for odd RVB ladders converges slower than that for even ladders at low \mathcal{L} , which is reversed as \mathcal{L} is increased and holds even at large \mathcal{L} , where $\mathcal{G}_c(\mathcal{L})$ for odd and even RVB ladders are indistinguishable.

Therefore, we observe that although the value of genuine multisite entanglement can not distinguish the odd-legged ladders from the even-legged ones for large lattice size, the corresponding finite-size scaling exponents are capable of detecting the difference.

4.5 Summary

To summarize, in this Chapter, we investigate the behavior of genuine multipartite entanglement in the ground state of odd- and even- Heisenberg ladders. Even though such models have immense fundamental and practical importance, owing in particular to the dissimilarities on the two sides of the odd-versus-even divide, they are not analytically accessible. In this work, we began our investigation through exact diagonalization techniques to find that the genuine multisite entanglement, as quantified by the GGM, of the ground state obtained from the odd-legged ladder, increases with the number of rungs. The opposite is true in the even-legged ladder. This feature is in good qualitative agreement with the assumption that ground states of odd and even Heisenberg ladders are RVB states. We perform scaling analyses of the RVB states on ladders of large system sizes by employing the DMRG, and find that while the GGM of the RVB states on large ladders converges to a single value independent of the odd-even parity of the ladders, their scaling exponents diverge from each other. While the study reported is for the isotropic Heisenberg model, we have carried out parallel studies for the quantum XXZ model. We observed qualitative similarity of the results obtained for values of the zz vs. xx anisotropy up to approximately 1.4.

The results of this Chapter are based on the following paper:

- **Sudipto Singha Roy**, Himadri Shekhar Dhar, Debraj Rakshit, Aditi Sen(De), and Ujjwal Sen, *Diverging scaling with converging multisite entanglement in odd and even quantum Heisenberg ladders*, New J. Phys. **18**, 023025 (2016).

Multipartite entanglement in doped quantum spin ladders

5.1 Introduction

An important yet demanding task in the study of complex quantum system is to characterize how quantum correlations, in particular multiparty entanglement, are distributed among the subparts of a strongly correlated systems. This is motivated, on one hand, by the fact that study of multisite physical quantities in many-body quantum systems often provide deeper insights into the co-operative phenomena they exhibit [37, 47]. On the other hand, such investigation can play an important role for implementation of quantum information processing tasks in the laboratory. However, estimation of the same remains a challenging task, primarily due to the exponential growth of the Hilbert space with increasing system size. This is especially true if we try to obtain analytical expressions or bounds of multisite physical properties such as entanglement. Therefore, obtaining a general method to characterize entanglement in multipartite states is crucial to investigate physical phenomena of a complex system.

In the previous Chapter, we considered one such important many-body system, e.g. undoped multi-legged quantum spin ladders and studied its multiparty entanglement characteristics. In this Chapter, we will consider a more general scenario, where along with the dimers, one needs to consider holes in the remaining lattice sites. One of the best framework to study strongly-correlated doped quantum spin ladders is the t - J model, which is obtained in the limit of large on-site interaction

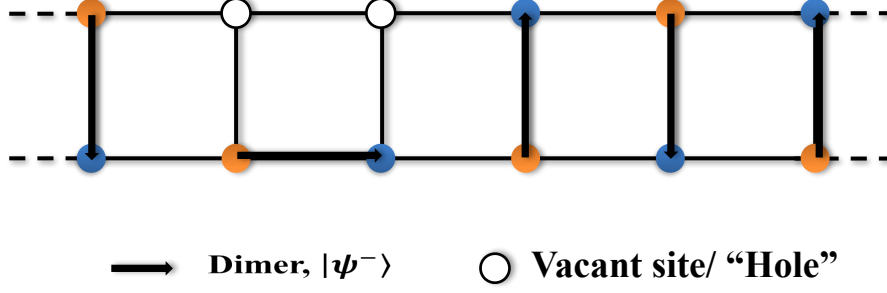


Figure 5.1: Schematic diagram of a two-legged doped quantum ladder. The sites on different bipartite lattice A and B , have been distinguished using two different colors.

from the Hubbard model [239–244]. At half-filling, without doping, the system reduces to a Heisenberg ladder with a spin liquid ground state (GS) [188, 192, 245]. Upon doping the spin ladder, studies based on mean-field theory using Gutzwiller renormalization show that the spin gap is persistent [246–249] which is a tell-tale sign of strong superconducting fluctuations [188, 192, 245–251]. The t - J model, under finite doping, exhibits a rich phase diagram, which has been extensively studied for low-dimensional antiferromagnets (AFM) [252–259]. In particular, in 1D and ladder configurations, the system possess exotic correlation properties that are characterized by the Luttinger liquid theory [260–262], as confirmed using exact diagonalization calculations, and exhibits a rich superconducting (SC) phase for a specific range of values of J/t and electron density, n_{el} [252–255, 257–259, 263, 264]. Moreover, the superconducting states of the quantum spin ladder can be represented using the short-range resonating valence bond (RVB) ansatz [102–105, 110, 111] which were introduced to describe Mott-insulators.

In this work, we consider short-range doped resonating valence bond (RVB) states, and for finite values of the electron density (n_{el}), using the symmetry properties of the RVB state [2, 138, 141, 142], we prove that the doped RVB ladder is always genuinely multipartite entangled. To quantify the genuine multipartite entanglement in large spin ladders, we introduce an analytical recursion method to build the doped RVB state. The novelty of this recursion method stems from the fact that in a large spin network with arbitrary electron density (n_{el}), one can analytically compute the reduced density matrices of the superposition state, thus allowing an exact estimation of the genuine multipartite entanglement using the generalized geometric measure (\mathcal{G}) [162] (cf. Refs. [64, 166, 195, 196, 265]). Using the proposed recursion method, we observe that in the thermodynamic limit, \mathcal{G} increases with n_{el} , reaching a maximum at $n_c \approx 0.56$, before decreasing for higher n_{el} (cf. [139]).

Interestingly, we further show that the qualitative multipartite features of doped RVB states are closely mimicked by ground states (GSs) of doped t - J ladders obtained through exact diagonalization for moderate-sized lattices. In particular, we present a representative case with $J/t \approx 0.6$, where we observe that genuine multipartite entanglement of the GS of the t - J ladder emulates the same of the doped RVB state. The maximum \mathcal{G} occurs at $n_c \approx 0.65$, close to that obtained using the doped RVB ansatz. The discrepancy in the values of electron densities need to account for finite size effect. Hence, using the analytical recursion method, one can show that within the considered parameter range, the trend of genuine multipartite entanglement of the former state qualitatively matches with that of the GS of the latter model. We note that although we use the recursion method to study multipartite entanglement, the method can also be employed to investigate other properties like single-site, two-site physical quantities of the doped RVB ladders for systems with an arbitrary number of sites. In our calculations, we have considered up to 300 sites, and though a higher number of sites are accessible through our method, the physical quantities of interest converge much earlier.

This Chapter is organized as follows. In Sec. 5.2, we present the recursion method that generates the doped RVB state corresponding to arbitrary electron density. Thereafter, in Sec. 5.3, we propose the recursion relation for density matrices of multiple sites, considering both periodic as well as open boundary conditions. In Sec. 5.4, we provide analytical results on genuine multipartite entanglement in the doped RVB state. In Sec. 5.5, we introduce the t - J model and subsequently compare

the behavior of \mathcal{G} obtained using the doped RVB state ansatz to that obtained via exact diagonalization of the t - J model. We present a brief summary in Sec. 5.6.

5.2 Recursion method to generate doped RVB states

We begin by considering the doped RVB state containing $2N$ lattice sites, on a ladder configuration, with $2k$ spin-1/2 particles and $2(N - k)$ holes or vacant lattice sites, expressed using a *bipartite lattice*, consisting of sublattices A and B .

The corresponding (unnormalized) wavefunction, with electron density $n_{el} = k/N$, is given by

$$|\Psi\rangle_{k,N-k} = \sum_i r_i |(a_{n_1} b_{n_1})(a_{n_2} b_{n_2}) \cdots (a_{n_k} b_{n_k})\rangle_i \otimes |h_{m_{2k+1}} h_{m_{2k+2}} \cdots h_{m_{2N}}\rangle_i, \quad (5.1)$$

where $|(a_{n_j} b_{n_j})\rangle = \frac{1}{\sqrt{2}}(|01\rangle - |10\rangle)_{n_j}$ represents a dimer, with $a_j \in A$ and $b_j \in B$. $|\{(a_{n_j} b_{n_j})\}\rangle_i$ (where $\{\}$ represents tensor product over the sites ' j ') represents a complete dimer covering at occupied sites n_j . The holes, $|h_{m_j}\rangle = |2\rangle_{m_j}$, are at sites m_j , such that

$$\sum_{j=1}^k 2n_j + \sum_{j=2k+1}^{2N} m_j = 2N \cdot r_i = 1, \forall i. \quad (5.2)$$

In general, while considering the RVB ansatz for the ground state of a moderate-sized doped quantum spin ladder, as described in Eq. (5.1), the number of dimer coverings in the state increases exponentially with the increase of the electron density [266, 267]. For example, in a small spin ladder with 5 spins on each leg, the number of dimer coverings at electron density $n_{el} = 0.33$ is 94, and at $n_{el} = 0.66$, it is equal to 294. Hence, even for small ladders, a direct construction of the RVB ground state is computationally expensive. Moreover, the Hilbert space also increases rapidly with increase in the number of spins. This makes the analytical recursion method proposed for studying physical properties of doped RVB states on large quantum spin ladders, a very important part of our results. We recur-

sively [2, 130, 140, 205] construct the state $|\psi\rangle_{k,N-k}$, defined in Eq. (5.1) and generate its reduced states. Though earlier attempts have been made to obtain recursion relations for physical observables such as the ground state energy [205], the novelty of our approach lies in the fact that the proposed method recursively constructs the reduced density matrices of the doped RVB state, which allows us to study quantum and classical properties, in particular, multipartite entanglement, which in turn are used to characterize the system. In Chapter 3, we introduced the recursion relation for the doped two-legged quantum ladders with open boundary condition. In this Chapter, we first explain the steps to derive the same recursion relation, explicitly. Thereafter, we generalize the recursion relations considering open boundary condition.

In order to generate the analytical recursion method, let us begin with an open $2N$ -site ladder lattice with all vacant sites (holes), which is successively filled with dimers. We use the notation, $|N-k, k\rangle$ to denote the N -rung ladder, $|\psi\rangle_{k,N-k}$, containing $2k$ spins filled with dimers and $2(N-k)$ holes. The state $|N-k, k\rangle$ is achieved by successively filling k dimers in the $|N, 0\rangle$ state, i.e.,

$$|N, 0\rangle \xrightarrow{k} |N-k, k\rangle. \quad (5.3)$$

As an example, consider an initial configuration with 8 site RVB ladder, doped with 4 holes. Now the state $|2, 2\rangle$ mentioned above, can be generated in the following way:

$$|4, 0\rangle \xrightarrow{k=1} |3, 1\rangle \xrightarrow{k=1} |2, 2\rangle,$$

where $|4, 0\rangle$ is the initial lattice with all holes, and $|2, 2\rangle$ is the final state, for an 8 site RVB ladder, with 2 dimers and 2 pairs of holes.

For an analytical method which allows us to build the superpositions in an arbitrary $|N-k, k\rangle$, we propose the generator

$$\begin{aligned} |N-k, k\rangle &= \mathcal{U}^{\otimes k'=1} |N-k+1, k-1\rangle \\ &+ |N-k-1, 0\rangle |\chi_{k+1}\rangle + |N-k-2, 0\rangle |\chi_{k+1}\rangle |1, 0\rangle, \end{aligned} \quad (5.4)$$

where $\mathcal{U}^{\otimes k'}$ is the operator to add k' dimers. The methodology to derive the above recursion relation and the description of $|\chi_{k+1}\rangle$ are given below.

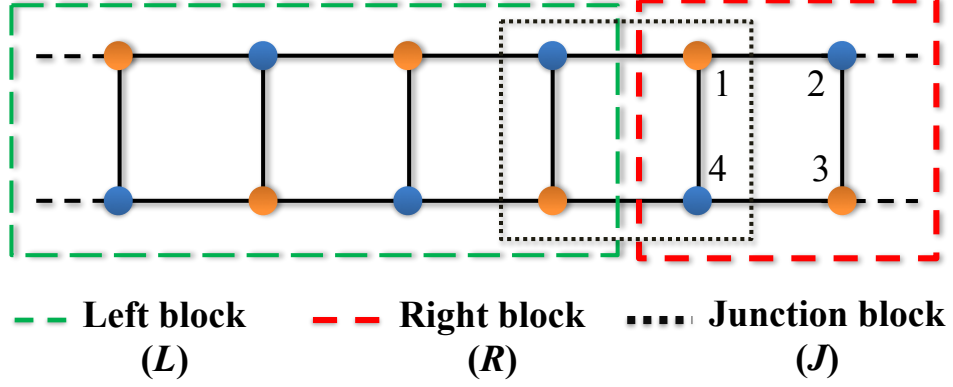


Figure 5.2: Schematic diagram of the blocks L , R , and J in the spin lattice. To compute \mathcal{G} , we obtain the reduced density matrix (ρ_{red}) corresponding to the sites 1-4 in the R block. The rest of the lattice is traced out. Numerical studies show that the reduced state ρ_{red} is sufficient to compute \mathcal{G} in doped RVB states.

To facilitate our calculations, we divide the $2N$ ladder lattice into specific regions that can be filled with dimers. We start by splitting the initial state $|N, 0\rangle$ into two regions, denoted by left (L) and right (R) block, such that

$$|N, 0\rangle = |N - 2, 0\rangle_L \otimes |2, 0\rangle_R. \quad (5.5)$$

This is explicitly shown in Fig. 5.2. An important region is the junction (J) block between L and R blocks, which is shown in Fig. 5.2 using a black-dotted square. The blocks, excluding overlapping region, can be written as:

$$|N - 3, 0\rangle_{L'} \otimes |2, 0\rangle_J \otimes |1, 0\rangle_{R'},$$

where L' (R') implies the region $L - L \cap J$ ($R - R \cap J$).

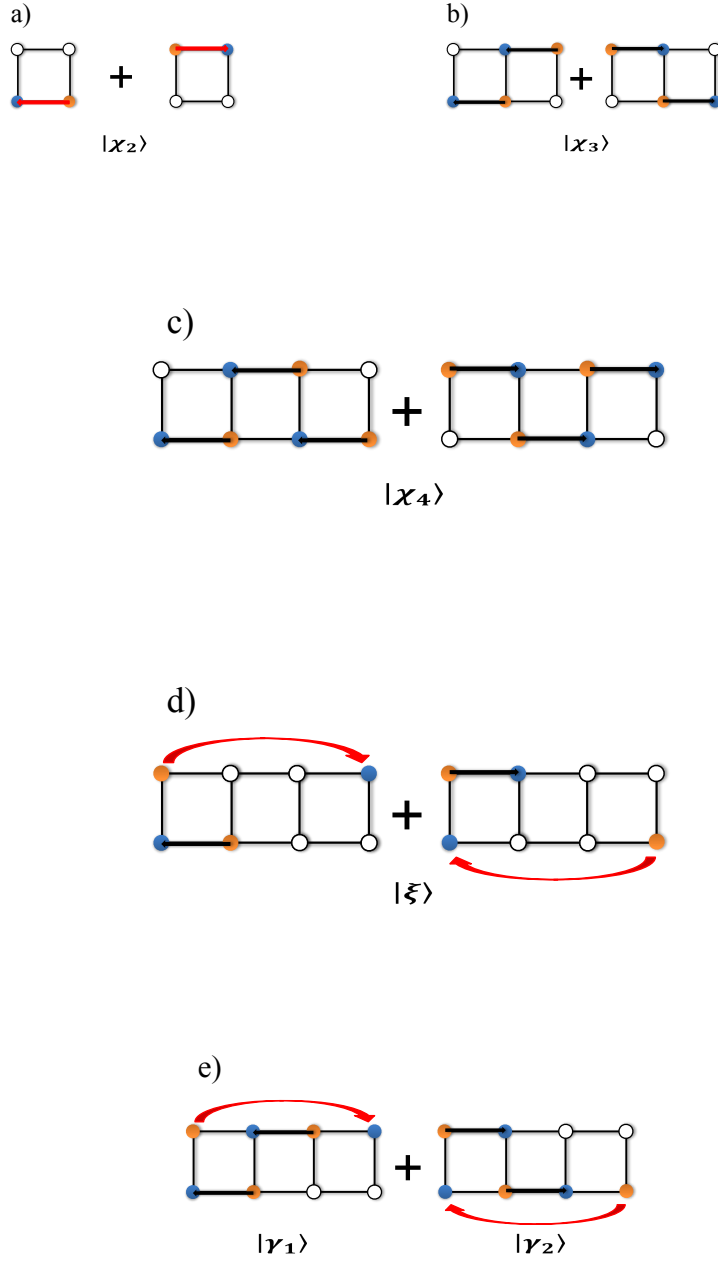


Figure 5.3: Schematic diagram of the states: a) $|\chi_2\rangle$, b) $|\chi_3\rangle$, c) $|\chi_4\rangle$, and the periodic terms: d) $|\xi\rangle$, and e) $|\gamma_1\rangle$ and $|\gamma_2\rangle$, used in the recursion relations.

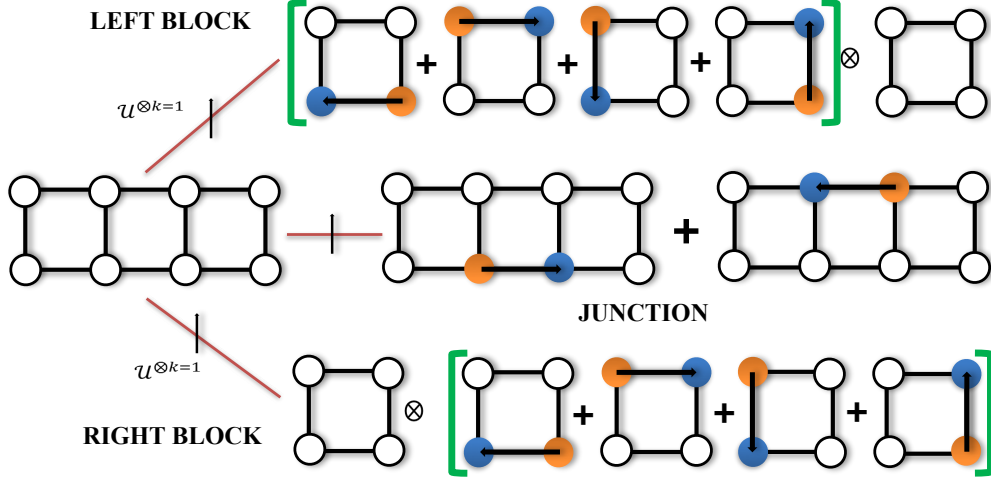


Figure 5.4: Schematic diagram of the scheme to build a doped-RVB state from a lattice filled with holes, for an 8 site RVB ladder, as given by the process: $|4, 0\rangle \xrightarrow{k=1} |3, 1\rangle$, described in Eq. (5.4).

Now starting from an initial configuration $|N, 0\rangle$, our aim is to reach the final state $|N - k, k\rangle$ by systematically introducing k numbers of dimers in the different blocks of the lattice. The first dimer is introduced in the initial hole configuration through the following possible ways:

1. *Update the left block:* In this step, a dimer is introduced into the L block and the updated state is

$$|N - 2, 0\rangle_L |2, 0\rangle_R \xrightarrow{k=1} |N - 3, 1\rangle_L |2, 0\rangle_R. \quad (5.6)$$

2. *Update the right block:* Similarly, in the next step, a dimer is injected into the

R block. The updated state looks like

$$|N-2, 0\rangle_L |2, 0\rangle_R \xrightarrow{k=1} |N-2, 0\rangle_L |1, 1\rangle_R. \quad (5.7)$$

3. *Update of the junction block:* In this step a dimer is introduced in the junction of the L and R blocks, i.e., the J block. The updated state turns out to be

$$|N-2, 0\rangle_L |2, 0\rangle_R \xrightarrow{k=1} |N-1, 0\rangle |\chi_2\rangle |1, 0\rangle, \quad (5.8)$$

where the state $|\chi_2\rangle$ is depicted in Fig. 5.3(a). Now combining the above three steps, the final state after introduction of a single dimer in the lattice is given by

$$\begin{aligned} |N, 0\rangle &\xrightarrow{k=1} |N-1, 1\rangle \\ &\equiv |N-3, 1\rangle_L |2, 0\rangle_R + |N-2, 0\rangle_L |1, 1\rangle_R \\ &+ |N-1, 0\rangle |\chi_2\rangle |1, 1\rangle. \end{aligned} \quad (5.9)$$

For example, consider the initial state $|4, 0\rangle$ in Eq. (5.4). We have, $|4, 0\rangle = |2, 0\rangle_L |2, 0\rangle_R$. Then the state, after introduction of one dimer, would be (see Fig. 5.4 for an illustration of the three update paths)

$$\begin{aligned} |4, 0\rangle &\xrightarrow{k=1} |3, 1\rangle = |1, 1\rangle |2, 0\rangle + |2, 0\rangle |1, 1\rangle \\ &+ |1, 0\rangle |\chi_2\rangle |1, 0\rangle, \end{aligned} \quad (5.10)$$

where the first two terms are the contributions from the blocks L and R , and the third term comes from the update of the junction, J . Now after completion of the first step, we need to introduce one more dimer into the present configuration in order to continue the iteration process. It can be done following a path similar to the one described above, i.e., a direct update of the L and R blocks, which is basically updating all the terms of the state by introducing dimers into the left and right blocks, and an update, which consists of injecting a dimer at the junction block. The above scheme can be repeated k times so that the final state contains k dimers and $2(N-k)$ holes in the lattice. In general, by updating the L , J , and R blocks, with $k' = 1$ singlets, we obtain the recursive generator expressed in Eq. (5.4).

As mentioned before, here $\mathcal{U}^{\otimes k'}$ is the direct update operator to inject k' dimers in the L and R blocks of the state, $|N-k+1, k-1\rangle$. Subsequently, the second and

the third terms in Eq. (5.4) correspond to the indirect update of the J block. For example, the first two terms in Eq. (5.10), $|1, 1\rangle |2, 0\rangle$ and $|2, 0\rangle |1, 1\rangle$, is generated from the direct update of the state $|4, 0\rangle$ and the third term $|1, 0\rangle |\chi_2\rangle |1, 0\rangle$ emerges from the indirect update of the junction sites. Note that, there may arise similar terms due to the update process of the L , R , and the J block. In those cases we need to carefully include such terms only once in the recursion, so that overcounting of the terms can be avoided. In Eq. (5.4), we note that the term $|\chi_{k+1}\rangle$ can be generated recursively from $|\chi_k\rangle$ by introducing an additional rung to the left and assigning a dimer along the horizontal direction, as demonstrated in Fig. 5.3, for $|\chi_2\rangle$, $|\chi_3\rangle$ and $|\chi_4\rangle$.

In the succeeding section, we present a detailed discussion on how reduced density matrices for a block of lattice sites can be obtained from the recursion method. For the purposes of our study, a block of four sites, in two nearest neighbor (NN) rungs of the ladder, is sufficient.

5.3 Recursion relation for reduced density matrices

In order to calculate the \mathcal{G} of the doped RVB state, we required to derive expressions for the reduced density matrices, using the generator expressed in Eq. (5.4). Let us consider the cases for open and periodic ladders separately.

5.3.1 Open ladder

The primary method to build the recursive relations is to divide the lattice into blocks and junctions. The advantage lies in the fact that these blocks do not overlap, and hence can be independently traced to obtain ρ_{red} needed to calculate the \mathcal{G} . Hence, from the non-periodic ladder state, $|N - k, k\rangle$, by tracing all sites apart from rungs $m - 1$ and m , we get the reduced state, $\rho_{red}^{\mathcal{NP}}$, of 4-sites, given by

$$\begin{aligned}
\rho_{red}^{\mathcal{NP}} &= \sum_{i=0}^2 \mathcal{Z}_{(k-i)}^{(S-1+i)} |2-i, i\rangle \langle 2-i, i| + \sum_{k_1=2}^{k+1} \mathcal{Z}_{(k-k_1+1)}^{(S-1)} \text{tr}(|\chi_{k_1}\rangle \langle \chi_{k_1}|) |1'\rangle \langle 1'| \\
&+ \sum_{k_2=2}^k \mathcal{Z}_{(k-k_2)}^{(S)} \text{tr}(|\chi_{k_2}\rangle \langle \chi_{k_2}|) |1\rangle \langle 1| + \sum_{i=0}^1 \mathcal{Z}_{(k-2-i)}^{(S+i)} \text{tr}(|\bar{2}\rangle \langle \bar{2}|) |1-i, i\rangle \langle 1-i, i| \\
&+ \sum_{k_3=3}^{k+1} \mathcal{Z}_{(k-k_3+1)}^{(S)} (\text{tr}(|\chi_{k_3}\rangle \langle \chi_{k_3}|)) + \sum_{k_4=2}^k \mathcal{Z}_{(k-k_4)}^{(S)} (\text{tr}(|\chi_{k_4+1}\rangle \langle \chi_{k_4}| \langle 1|) + \text{h.c.}) \\
&+ \sum_{i=0, j=0}^{i=1, j=k-2-i} \mathcal{Z}_{(k-2-i-j)}^{(S+i)} (1/2)^{j+1} (|1\rangle |1-j, j\rangle \langle 1-j, j+1| + \text{h.c.}), \tag{5.11}
\end{aligned}$$

where $S = N - k - 1$, and

$$\mathcal{Z}_k^{N-k} = \langle N-k, k | N-k, k \rangle, \tag{5.12}$$

and $|\bar{2}\rangle = |0, 2\rangle - |0, 1\rangle |1, 0\rangle$.

Numerical studies for a moderate N , suggest that obtaining the reduced state of a square block of 4 sites for large ladders, which is symmetric for the ladder, is sufficient for the computation of \mathcal{G} . Hence, we use the recursion method to obtain the 4-site reduced state (ρ_{red}) at rungs $m-1$ and m .

The main advantage in formulating the recursion relation for the entire state, as expressed in Eq. (5.4), can be seen when one needs to obtain the reduced density matrix, ρ_{red} . This is because the terms which correspond to the blocks R and L are mutually orthogonal to those belong to the junction block J . As a result, in the expression for ρ_{red} , one would never get any contribution from the terms that emanate from $|\bullet\rangle_{L(R)} \langle \bullet|_J$. Now if one starts from the L and R blocks coverings and traces out all but the sites of last two rungs (sites (1-4) in Fig. 5.2), then there would be the following three possibilities,

- i) The reduced block contains holes only.
- ii) The reduced block contains one singlet and one pair of hole.

iii) The reduced block contains singlet coverings only.

The first term in Eq. (5.11),

$$\sum_{i=0}^2 \mathcal{Z}_{(k-i)}^{(S-1+i)} |(2-i), (i)\rangle \langle (2-i), (i)|$$

basically corresponds to the above possibilities. As an example, consider an initial eight-site doped RVB state which includes only one singlet and 3 hole-pairs. The contribution from the L block and R block would lead to the following terms in the expression of the doped RVB state, $|1, 1\rangle_L \otimes |2, 0\rangle_R + |2, 0\rangle_L \otimes |1, 1\rangle_R$. Therefore, the reduced state would contain following terms,

$$a_1 |2, 0\rangle \langle 2, 0| + a_2 |1, 1\rangle \langle 1, 1|, \quad (5.13)$$

where $a_1 = \mathcal{Z}_1^1$, and $a_2 = \mathcal{Z}_0^2$, which can be obtained from Eq. (5.11).

Subsequently, the junction J would generate additional terms in the expression of the reduced state. As an example, first consider terms which has only one singlet at the junction block (see Fig. 5.3). Mathematically, those can be expressed as $|\bullet\rangle \otimes |\chi_k\rangle \otimes |\bullet\rangle$, where $|\chi_2\rangle$ and $|\chi_3\rangle$ are depicted in Fig. 5.3. Now the contributions from the overlap of those terms are given by second, third, and fourth terms in Eq. (5.11). Considering, once more, the previous example of an eight-site doped RVB state containing only one singlet, we can write the contributing term from the junction as $|1, 0\rangle \otimes |\chi_2\rangle \otimes |1, 0\rangle$. Hence after tracing out all but the sites those are at the last two-rungs, we get

$$\begin{aligned} \rho_{red}^{\mathcal{NP}} = & a_1 |2, 0\rangle \langle 2, 0| + a_2 |1, 1\rangle \langle 1, 1| \\ & + a_3 \text{tr} |\chi_2\rangle \langle \chi_2| \otimes |1, 0\rangle \langle 1, 0|, \end{aligned} \quad (5.14)$$

where $a_3 = \mathcal{Z}_0^1$ is again evaluated using Eq. (5.11).

Additionally, there may be terms which would contain two horizontal singlets at the junctions such as $|\bullet\rangle \otimes |\bar{2}\rangle \otimes |\bullet\rangle$. Those would certainly have non-zero overlap

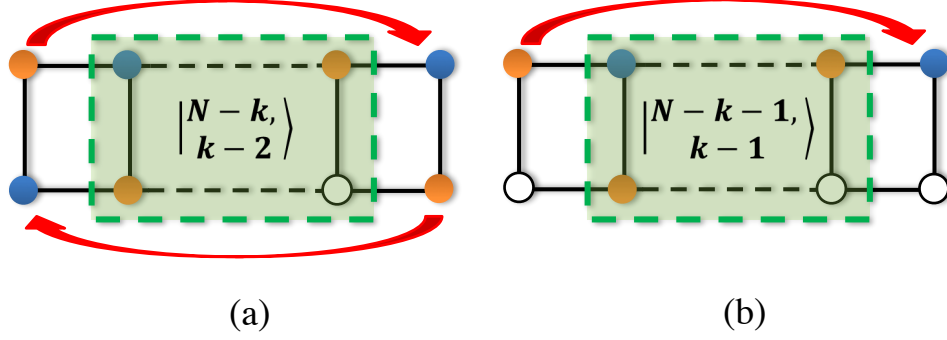


Figure 5.5: Schematic diagram of the blocks L , R , and J in the spin lattice with periodic boundary condition.

with the L and R block terms. The fifth and sixth terms of Eq. (5.11) correspond to contribution from these terms. As an example, instead of inserting one singlet if we now introduce two singlets in the eight-site doped RVB state i.e. $|2, 2\rangle$, we would have terms in the doped RVB state such as $|1, 0\rangle \otimes |\bar{2}\rangle \otimes |1, 0\rangle$. Hence the reduced density matrix would have following terms,

$$a_4 \text{tr} |\bar{2}\rangle\langle\bar{2}| \otimes |1, 0\rangle\langle 1, 0| + a_5/2 |0, 1\rangle\langle 1, 0| \langle H|,$$

where a_4 and a_5 are given by \mathcal{Z}_0^1 which can be obtained from Eq. (5.11), for $N = 4$ and $k = 2$.

5.3.2 Periodic ladder

Incorporation of periodic boundary condition, $N + 1 \equiv N$, leads to additional terms in the state $|N - k, k\rangle$. Consequently, we find that the number of terms in the expression of the recursively generated reduced density matrix, $\rho_{red}^{\mathcal{P}}$, increases, due to overlap of different states. These extra terms in $\rho_{red}^{\mathcal{P}}$ can be redeemed by analyzing two separate situations, say \mathcal{P}_1 and \mathcal{P}_2 , corresponding to different boundary terms:

- I) \mathcal{P}_1 – the end sites of both the legs share a singlet (see Fig. 5.5(a)).
- II) \mathcal{P}_2 – the end sites of only one of the leg share a singlet and the end site of the other leg contains holes (see Figs. 5.5(b) and (c)).

Therefore, in the expression of the reduced density matrix, there would be additional terms due to the overlap of the states in I with itself, and the L and R blocks ($\rho_{red}^{\mathcal{P}_1}$) (see Eq. (5.15)) and similarly, the overlap of states in II with itself, and L and R blocks ($\rho_{red}^{\mathcal{P}_2}$) (see Eq. (5.16) for $N - k = 1$ and Eq. (5.17) for $N - k = 2$).

$$\begin{aligned}
\rho_{red}^{\mathcal{P}_1} = & \text{tr} (|\zeta\rangle\langle\zeta|) + \frac{1}{2} \sum_{i=0, j=0}^{i=1, j=k-2-i} \mathcal{Z}_{(k-2-i-j)}^{(\mathcal{S}+i)} \left(\frac{1}{2}\right)^j |1-i, i\rangle\langle 1-i-1, i+1| \\
& + \frac{1}{2} \sum_{j=0}^{j=k-4} \mathcal{Z}_{(k-4-j)}^{(\mathcal{S}+1)} \left(\frac{1}{2}\right)^j \text{tr} (|\bar{2}\rangle\langle\bar{2}|) |1\rangle\langle 1| + \left(\frac{1}{2}\right)^j \sum_{k_6=2, j=0}^{k_6=k-1, j=k-k_6-1} \mathcal{Z}_{(k-k_6-1-j)}^{(\mathcal{S})} \left(\frac{1}{2}\right)^j \\
& \text{tr} (|\chi_{k_6}\rangle\langle\chi_{k_6}| |1\rangle\langle 1| + |\chi_{k_6}\rangle\langle 1| \langle\chi_{k_6+1}|) + \frac{1}{2} \sum_{i=0, j=0}^{j=k-4-i} \mathcal{Z}_{(k-4-(i+j))}^{(\mathcal{S}+1)} \left(\frac{1}{2}\right)^{i+j} \\
& \times \text{tr} (|\bar{2}\rangle\langle 1| \langle 1| \langle 2|) + \frac{1}{2} \sum_{i=0, j=0, l=0}^{i=1, j=k-3-i, l=k-3-(i+j)} \mathcal{Z}_{(k-3-(i+j+l))}^{(\mathcal{S}+i)} \left(\frac{1}{2}\right)^{j+l} \text{tr} (|1\rangle\langle 1-i, i| |1\rangle\langle \bar{2}| \langle 1-i, i|), \\
& \text{where } \mathcal{S} = N - k - 1,
\end{aligned} \tag{5.15}$$

$$\begin{aligned}
\rho_{red}^{\mathcal{P}_2} = & |\gamma_1\rangle\langle\gamma_1| + |\gamma_2\rangle\langle\gamma_2| + \left(\frac{1}{2}\right)^{k-3} (|\gamma_1\rangle\langle\gamma_2| + |\gamma_2\rangle\langle\gamma_1|) + [(|\gamma_1\rangle + |\gamma_2\rangle)(\mathcal{D}_{k-2}\langle 1| \langle \bar{2}| \langle 1| \\
& + \mathcal{D}_{k-1}\langle H|) + h.c.] (-1)^{k+1/2}, \text{ where } N - k = 1,
\end{aligned} \tag{5.16}$$

$$\rho_{red}^{\mathcal{P}_2} = (|\xi\rangle\langle\xi| + |\xi\rangle\langle\chi_2|\langle 1'|)(-1)^{k/2-1}\mathcal{D}_{k-1}, \text{ where } N - k = 2. \quad (5.17)$$

The terms $|\xi\rangle$, $|\gamma_1\rangle$, $|\gamma_2\rangle$, and $|\zeta\rangle$, along with an illustrative description of the recursion method is provided in the Figs. 5.3 and 5.5. \mathcal{D}_k can recursively be generated using

$$\mathcal{D}_x = \mathcal{D}_{x-1} + 2\mathcal{D}_{x-2} \quad (5.18)$$

with the initial condition $\mathcal{D}_0 = \mathcal{D}_1 = 1$. Now if $N - k = 1$, periodic states corresponding to the two types, \mathcal{P}_1 and \mathcal{P}_2 , would overlap with each other and lead to the following additional terms in the expression of the total reduced density matrix of 4-sites given by,

$$\rho_{red}^{\mathcal{P}_{12}} = 1/2^{(k-3)}(-1)^{(k+1)/2}(|\gamma\rangle(\langle\gamma_1| + \langle\gamma_2|) + h.c.)\mathcal{D}_{k-3}, \quad (5.19)$$

where

$$|\gamma\rangle = |\bar{2}\rangle_{1,N}|N - k - 2, k - 2\rangle_{2,N-1}. \quad (5.20)$$

Hence considering all possible periodic boundary terms, the expression of the reduced density matrix for the system is given by

$$\rho_{red}^{\mathcal{P}} = \rho_{red}^{\mathcal{NP}} + \rho_{red}^{\mathcal{P}_1} + \rho_{red}^{\mathcal{P}_2} + \rho_{red}^{\mathcal{P}_{12}}. \quad (5.21)$$

Fig. 5.6 shows the \mathcal{G} of a periodic doped RVB state calculated using the recursion method for upto 300 lattice sites.

The expression of the reduced density matrices obtained using the recursion method can be applied to compute various bipartite as well as multipartite physical quantities that characterize the ground state properties of the system, even for large lattice size. In the following section, we will look at the genuine multipartite entanglement properties of the doped RVB ladder, which can be efficiently obtained using this technique.

5.4 Genuine multipartite entanglement in quantum ladders

Here we investigate the multipartite entanglement of a doped quantum spin ladder, under the RVB ansatz. Since the study of GS properties of t - J Hamiltonian is limited to numerical simulations and approximate methods, explicit estimation of multipartite entanglement is extremely difficult for large systems. The doped RVB ansatz for the GS of the t - J model provides a viable alternative to study such quantities. It is known that the RVB liquid state with no holes, $|\Psi\rangle_{N,0}$, is rotationally invariant under the unitary $U^{\otimes 2N}$, where U is a local unitary acting on a single qubit [138, 141, 142]. In the composite dimer-hole qutrit space, the doped RVB state, $|\Psi\rangle_{k,N-k}$, is invariant under unitary operations of the form

$$\tilde{U}^{\otimes 2N} = (U \oplus \mathbb{I})^{\otimes 2N}, \quad (5.22)$$

where \oplus is the direct sum, \mathbb{I} is the scalar 1 and U is an arbitrary single qubit unitary. This invariance property of doped RVB ladders is important in investigating its multipartite entanglement as shown below.

Theorem 2. *The doped RVB ladder state, $|\Psi\rangle_{k,N-k}$, with $2N$ lattice sites, containing all possible coverings of k ($k \neq 0$) spin dimers interspersed with $2(N-k)$ holes, is always genuinely multipartite entangled for all ladder topologies that are periodic or infinite along the rails.*

Proof. To prove that $|\Psi\rangle_{k,N-k}$ is genuinely multisite entangled, we need to show that the state is entangled across every possible bipartition or alternatively, we have to prove that all reduced density matrices of the system are mixed. Using the invariance of $|\Psi\rangle_{k,N-k}$ under the action of $\tilde{U}^{\otimes 2N}$, one can show that all p -qutrit reduced systems,

$$\rho^{(p)} = \text{Tr}_{\bar{p}}[|\Psi\rangle\langle\Psi|_{k,N-k}], \quad (5.23)$$

obtained by tracing over all but p (\bar{p}) sites, is always invariant under $\tilde{U}^{\otimes p}$. Hence, a single qutrit reduced state must have the form,

$$\rho^{(1)} = p|2\rangle\langle 2| + (1-p)/2 \mathbb{I}_2, \quad (5.24)$$

where $\mathbb{I}_2 = |0\rangle\langle 0| + |1\rangle\langle 1|$ and p is fixed by the number of holes in the system. The relation shows that $\rho^{(1)}$ is always mixed for $p \neq 1$. Since all $\rho^{(1)}$ are equivalent, the condition $p = 1$ is satisfied *iff* all $2N$ sites contain holes. Similarly, the nearest neighbor two-site density matrix has the form,

$$\rho^{(2)} = p_1|22\rangle\langle 22| + p_2/9 \mathbb{I}_9 + p_3 W_2(q), \quad (5.25)$$

where \mathbb{I}_9 is the identity matrix on $\mathbb{C}^3 \otimes \mathbb{C}^3$ and

$$W_2(q) = q|\psi^-\rangle\langle\psi^-| + (1-q)\mathbb{I}_4/4 \quad (5.26)$$

is the Werner state [143] with \mathbb{I}_4 being the identity operator on the 4-dimensional space defined in the projected two-qubit spin basis. Now, $\rho^{(2)}$ is pure when $p_1 = p_2 = 0$ and $q = 1$. Which implies that it is pure *iff* the entire lattice is either filled with holes or is a single dimer covering, and these options are disallowed by the premise. Therefore, $\rho^{(1)}$ and $\rho^{(2)}$ are always mixed and $|\Psi\rangle_{k,N-k}$ is always entangled across these bipartitions.

However, we want to show that all possible bipartitions, irrespective of the number of sites, are always mixed. To prove this let us assume now that an arbitrary p -site density matrix ($\rho^{(p)}$) is pure, which implies that $|\Psi\rangle_{k,N-k}$ is separable along that p : $2N - p$. Let $p = p_1 + j$, where $j=1$ or 2 such that $|j| < |p_1|$ ($|\cdot|$ is the cardinality of the argument). For the periodic or infinite ladder, one can always find another equivalent pure density matrix, $\rho^{(q)}$, such that $q = q_1 + j$ and $|p| = |q|$, where j -sites overlap. By assumption, both $\rho^{(p)}$ and $\rho^{(q)}$ are pure. Using strong subadditivity of von Neumann entropy, $S(\sigma) = -\text{tr}(\sigma \log_2 \sigma)$, [238] we obtain

$$S(\rho^{(p_1)}) + S(\rho^{(q_1)}) \leq S(\rho^{(p_1+j)}) + S(\rho^{(q_1+j)}). \quad (5.27)$$

Now

$$S(\rho^{(p_1+j)}) = S(\rho^{(q_1+j)}) = 0, \quad (5.28)$$

since $\rho^{(p)}$ and $\rho^{(q)}$ are pure. Since $S \geq 0$, we have $S(\rho^{(p_1)}) = S(\rho^{(q_1)}) = 0$, and therefore $S(\rho^{(j)}) = 0$ implying $\rho^{(j)}$ is pure, which is not true since all $\rho^{(1)}$ and $\rho^{(2)}$ are mixed under finite doping. The contradiction implies that all reduced density matrices, $\rho^{(p)}$ are mixed and all $p: 2N - p$ are entangled.

We note that the above proof does not include the $p: 2N - p$ bipartitions where no equivalent $\rho^{(q)}$ with overlap is feasible, such as the bipartition between the two legs of the ladder. In that case, we assume that the legs, L_i and L'_i of $|\Psi\rangle_{k,N-k}$ are pure and thus the entire state is separable along that $N: N$. For the above condition to be satisfied, all reduced states along the rungs, $\rho^{(2)}_{(L_k, L'_k)}$, $\forall k$, must be separable. However, as can be shown by using recursive method, such nearest-neighbor $\rho^{(2)}$ states are always entangled. Hence, the doped RVB state is genuinely multipartite entangled. \blacksquare

The next step is to quantify the genuine multipartite entanglement in doped RVB ladders and characterize its variation with the electron density. Towards that aim, we use the computable measure of genuine multiparty entanglement, generalized geometric measure (GGM) [162] (cf. [64]), introduced in Chapter 2. Genuine multipartite entanglement is a well understood physical property in entanglement theory (see Ref. [23]), which essentially captures the presence of entanglement between every constituent of a many-body system. In contrast, measures such as entanglement entropy and entanglement of formation are essentially bipartite entanglement measure, which do not necessarily say anything about the global entanglement properties of a many-body state. Although entanglement entropy is important in studying the decay of quantum correlations and co-operative phenomena such as area laws, it is not adequate to study the multipartite entanglement properties of many-body systems.

Presence of multipartite entanglement may give rise to interesting co-operative properties that are not necessarily exhibited by restricting to bipartite entanglement. An obvious advantage of using GGM, is that it can be efficiently calculated through the reduced density matrices of a many-body quantum state. Here we would like to reiterate that in order to characterize genuine multiparty entanglement, it is not

sufficient to use measures such as entanglement entropy, which captures the entanglement between two blocks of the system. In comparison, GGM allows us to characterize the entanglement between all possible partitions of the system into two, three, four, ... blocks, which provides insight about the co-operative properties of the ground state, beyond correlation decay or area laws [163–171]. In the upcoming section we will make a comparative study of the behavior of GGM (\mathcal{G}) present in the ground state of the t - J ladder with that obtained using the doped RVB ansatz.

5.5 Trends of genuine multisite entanglement: GS of t - J ladder vs doped RVB state

We now consider a quantum spin-1/2 ladder model, consisting of an arbitrary numbers of holes and spin particles, and consider the short-ranged RVB state as a framework to study its GS multiparty entanglement properties. The model can be derived using second order perturbation theory from the Hubbard model in the limit of large on-site interaction [239–244]. The t - J Hamiltonian on a ladder can be written as

$$\mathcal{H} = -t \sum_{\langle i,j \rangle, \sigma} \mathcal{P}_G (c_{i\sigma}^\dagger c_{j\sigma} + \text{h.c.}) \mathcal{P}_G + J \sum_{\langle i,j \rangle} \vec{S}_i \cdot \vec{S}_j, \quad (5.29)$$

where $c_{i\sigma}$ ($c_{i\sigma}^\dagger$) is the fermionic annihilation (creation) operator of spin σ ($= \{\uparrow, \downarrow\}$), and \vec{S}_i is the triad of spin-1/2 operators, at site i . The Heisenberg exchange coupling (J) is isotropic along the rungs and legs while t represents the transfer energy and the expression $\langle i, j \rangle$ denotes that the sum is taken over nearest neighbor (NN) sites. \mathcal{P}_G is the Gutzwiller projector $\Pi_i(1 - n_{i\uparrow}n_{i\downarrow})$ which enforces at most single occupancy at each lattice site. This ensures that the undoped state physically represents a Mott insulator. The t - J model, under finite doping, exhibits a rich phase diagram [252–262]. Note that these models can potentially be realized in fermionic ultracold gases at high energy scales [268]. For moderate sized t - J ladders, at half-filling, the Hamiltonian in Eq. (5.29) can be exactly diagonalized, provided certain properties of the system are invoked. For example, the spin number Hamiltonian,

$$\hat{N} = \sum_i (|0\rangle\langle 0| + |1\rangle\langle 1|)_i, \quad (5.30)$$

and the total spin along the z-axis, $\hat{S}^z = \sum_i S_i^z$ commute with the Hamiltonian, \mathcal{H} . Hence, the Hamiltonian can be block-diagonalized in the $(\mathbb{C}^3)^{\otimes 2N}$ Hilbert space basis for different total spin \hat{S}^z and electron density $n_{el} = \langle \hat{N} \rangle / 2N$. For our case, we assume that the spins form an initial insulating phase with $\hat{S}^z = 0$, and with n_{el} varying from 0 to 1. Note that $n_{el} = 0$ and 1, correspond to a completely vacant and occupied lattice, respectively. For $n_{el} = 1$, the state is an insulating RVB spin liquid. The doping concentration is denoted by $x = 1 - n_{el}$. In our work, we have developed a numerical algorithm [269] based on the Lanczos method, [203] to exactly solve the composite hole-dimer qutrit system. By dividing the Hilbert space in different subspaces, according to the hole concentration x and total \hat{S}^z , exact ground state of the t - J Hamiltonian can be obtained for upto 14 qutrits, with even number of holes.

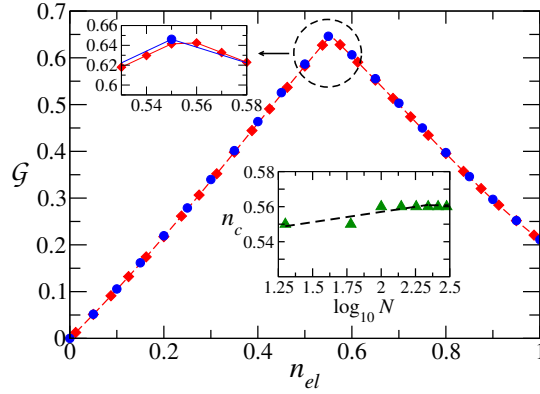


Figure 5.6: Genuine multisite entanglement in doped RVB ladder. Variation of \mathcal{G} with n_{el} in doped RVB ladder states, for $2N = 40$ (blue circles) and 200 (red diamonds) lattice sites. The top inset magnifies the encircled region in the plot. The bottom inset shows the scaling of n_c with the $\log_{10} N$. The inset shows that as N increases (plotted up to 300 sites), n_c converges to 0.56 . This is to be compared to the result for the systems described by the t - J model in the superconducting regime, in Fig. 5.7.

Although we have shown that the doped RVB state is always genuinely multipartite entangled, a quantitative analysis of \mathcal{G} requires its computation for large systems. Using the analytical recursion method proposed in the work, one can recursively build the doped RVB state and subsequently obtain its relevant reduced density matrices which is necessary to estimate \mathcal{G} . Figure 5.6 shows the behavior of the \mathcal{G} with increasing n_{el} . We observe that at $n_{el} = 0$, \mathcal{G} vanishes as expected since it corresponds to a product state, containing only holes. The maximum \mathcal{G} is achieved at a

critical density, $n_{el} = n_c \approx 0.56$. Interestingly, we find that this critical value of n_c with respect to \mathcal{G} corresponds to that of the superconducting phase of the t - J model.

We now consider the behavior of genuine multisite entanglement in the GS of the periodic t - J ladder, obtained through exact diagonalization. Figure 5.7, shows the variation of \mathcal{G} with n_{el} for different moderately-sized systems. We observe that the behavior of \mathcal{G} is qualitatively equivalent to those corresponding to doped RVB states (see Fig. 5.6). Below a certain critical density (n_c), i.e., in the region where $n_{el} < n_c$, \mathcal{G} scales linearly with n_{el} , independent of J/t . This is due to the fact that \mathcal{G} is obtained from the 1:rest bipartition, where the single-site density matrix is diagonal in the computational basis, with elements

$$\rho^1 = [1 - n_{el}, n_{el}/2, n_{el}/2]. \quad (5.31)$$

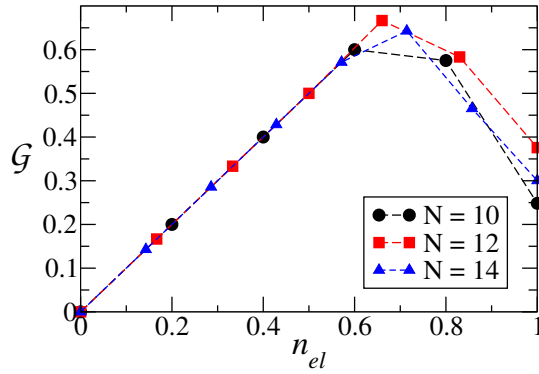


Figure 5.7: Genuine multisite entanglement in the t - J ladder. Variation of \mathcal{G} with n_{el} for the exact GS of the t - J ladder Hamiltonian, given in Eq. (5.29), for $N = 10, 12$, and 14 . \mathcal{G} reaches its maximum value at $n_c \approx 0.65$. Here $J/t = 0.66$. All quantities plotted are dimensionless.

When $1 \geq n_{el} \geq n_c$, the \mathcal{G} is a function of both n_{el} and J/t . For the t - J ladders, the maximum \mathcal{G} is achieved at a critical density, $n_c \approx 0.65$ which is close to that obtained using the doped RVB state ansatz. However, the small discrepancy in the exact values of the electron densities need to account for finite size effect. Moreover, we infer that this critical density mark the onset of a superconducting phase in the two-legged t - J ladder. For example in t - J ladder with $J/t \approx 0.6$, the superconducting phase has been predicted to occur for relatively high values of n_{el} [257], which is close to the critical density corresponding to the \mathcal{G} , as obtained from our analyses. Even though the microscopic theory behind high- T_c supercon-

ductivity [108, 109, 263, 264, 270, 271] remains unresolved [272–274], t - J ladder stands out as an important framework for understanding this novel phenomena. [107, 275] Furthermore, the short-range RVB ansatz has been pitched to describe the superconducting states of the t - J ladder [102–105, 110, 111].

The RVB state is a possible GS of the half-filled t - J ladder [189] and, upon finite doping, provides a simple mechanism to describe high- T_c superconductivity. In this respect, our work indicates that \mathcal{G} bears the signature of the t - J ladder entering into the superconducting phase and even the minimalistically designed doped RVB state considered in this work supports this feature, at least at the level of multiparty entanglement. Based on the behavior of both doped RVB states and exact GS of the t - J Hamiltonian, one can hypothesize that the trend of \mathcal{G} can detect the superconducting phase boundary, irrespective the size of the ladder. Note, however that we do not claim to detect a superconducting phase by using the genuine multiparty entanglement as an order parameter for the high- T_c superconducting phase. This is also not the primary intention of our work, which is to construct an efficient recursive method for evaluating multiparty observables in large doped RVB states. As an useful spin-off to our main results, we are able to show that for some parameter ranges, \mathcal{G} may serve as an indicator to whether the system has entered into the SC phase or not. It is plausible that one would require further physical properties along with the GGM to identify all the phases. Since there exists, as yet, no order parameter that can uniquely identify all the relevant phases of the ground states of doped Hubbard or t - J model, [43] the applicability of \mathcal{G} as a suitable order parameter requires further investigation.

An important point in our work is the use of a non-variational RVB state as the GS of the doped quantum spin ladder. It is clear that a variational RVB (vRVB) state, which lends possible support to d -wave pairing, is a more suitable state to study the doped ladder. However, vRVB states will, in general, not possess a recursive form that allows computation of reduced states with high efficiency in large systems, as the number of parameters to optimize increases exponentially. However, our results show that by omitting the variation in RVB, we obtain significant advantage in computation power, which allows us to compute \mathcal{G} in large doped ladders. Comparison with exact GS of the t - J ladder shows that the non-variational RVB state, quite accurately simulates the behavior of \mathcal{G} . But we do think that efficient recursions for the certain variational RVB states is an important problem for future

tasks.

5.6 Summary

In this Chapter, we adopted two techniques for studying multisite entanglement in doped quantum spin ladders. Firstly, we consider the doped RVB states as possible ground states of the t - J Hamiltonian, which we have shown to be always genuinely multiparty entangled. To overcome the limitations of exact diagonalization, we introduced a recursion method to generate the doped RVB state and to compute its reduced density matrices. By using the iterative method, we find that we can compute the genuine multiparty entanglement of doped RVB ladders, for large systems under finite doping of the ladder. We found that the maximum value occurs at doping concentration $n_{el} = 0.56$. Secondly, we use an exact diagonalization method for the t - J Hamiltonian, for upto 14 sites and observe that the GS of the Hamiltonian is also genuinely multipartite entangled, with maximum entanglement occurring at the superconducting phase boundary, where the electron density $n_{el} \approx 0.65$.

We note that the primary outcome of our work is an analytical recursion method to evaluate the genuine multipartite entanglement in RVB ladders with finite doping. An immediate offshoot of our results is the connection between maximal entanglement in doped RVB states and the high- T_c superconducting phases of the t - J Hamiltonian. In this regard, we would like to mention that even though GGM may apparently be useful in signalling the onset of the high- T_c superconducting phase, it is possible that the different phases of the Hubbard or the t - J model can not be completely characterized by just using entanglement. Recently, using the behavior of multiparty entanglement, attempts have been made to get more accurate insight about the phase boundaries which emerge in the ground state configuration of XXZ quantum spin ladders [62, 63]. However, it has been shown that there are regions in the parameter space at which multiparty entanglement alone fails to provide a conclusive phase diagram and one needs to study the behavior of other ground state properties such as magnetization and spin correlation functions in order to obtain a complete picture of the different phase boundaries [63].

In a similar vein, for the case of doped ladders, it is plausible that one would require further physical properties along with the GGM, to characterize different

phases of the t - J Hamiltonian. This requires further investigations on the model which are planned in forthcoming works. Apart from this, there has also been attempt to quantify the bipartite entanglement of certain multipartite pure states, like the Bardeen-Cooper-Schrieffer (BCS) state of superconducting compounds [276] which shed light on the relation of entanglement to that of the superconducting order parameter. We believe that the extension of such investigations to the case of high- T_c cuprates may uncover interesting underlying microscopic properties.

In the forthcoming Chapter, we move further and consider physical systems in higher dimensional lattices viz. the two-dimensional isotropic quantum network and study the effects of doping on its bipartite as well as multipartite entanglement characteristics.

The results of this Chapter are based on the following paper:

- **Sudipto Singha Roy**, Himadri Shekhar Dhar, Debraj Rakshit, Aditi Sen(De), and Ujjwal Sen, *Analytical recursive method to ascertain multisite entanglement in doped quantum spin ladders*, Phys. Rev. B **96**, 075143 (2017).

Isotropic quantum spin networks in two-dimensions

6.1 Introduction

A critical aspect in the study of quantum networks [7, 9, 277, 278] is the distribution of entanglement [23] between the nodes [23, 37, 38, 279–294]. For implementation of quantum protocols such as information transmission [281, 282], long-range quantum teleportation in spin chains [283, 284], and measurement-based quantum computation [285, 286], engineered generation and modulation of entanglement between the spins on the lattice is a necessary prerequisite. In several hybrid quantum networks designed using superconducting or optomechanical cavities [295–299], entanglement is the key resource enabling the fidelity and speed of information transfer [300, 301] within the network. In this regard, robustness of entanglement in the presence of defects is an important requirement in the design of scalable information and computation models.

In our work, we investigate the effect of particle loss or *defects* on the entanglement properties of a quantum spin network with a fixed number of lattice sites. Such defects may destroy physical properties including entanglement in a system, and hence can adversely affect its computational and communication abilities [302–316]. We consider a quantum spin network consisting of spin-1/2 particles on a *bipartite* lattice, with an isotropic topology and of arbitrary dimensions. The interaction between the spins is such that the wave function of the spin network consists of superpositions of all short-range dimer coverings on the lattice [141]. We show,

using information-theoretic properties such as quantum telecloning [317] and the strong-subadditivity of von Neumann entropy [238] that even in the presence of a finite fraction of defects, the spin network sustains a considerable amount of genuine multisite entanglement. Moreover, the defects may also generate small but finite bipartite entanglement between two moderately distant sites. We also discuss potential applications of such spin networks in quantum computation.

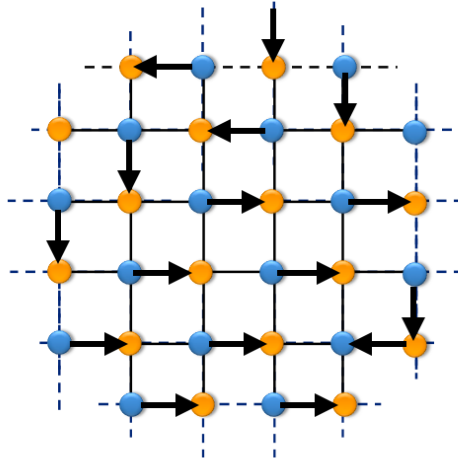


Figure 6.1: Schematic diagram of a two-dimensional quantum lattice with dimer coverings.

This Chapter is organized as follows. In Sec. 6.2, we introduce the isotropic network we have considered in our work. Thereafter, in Sec. 6.3, we derive the forms of the singlet- two-site reduced density matrices. In Sec. 6.4, we provide bounds on the bipartite entanglement that the network can sustain. In Sec. 6.5, we prove that the multiparty quantum state characterizing the quantum network is genuinely multiparty entangled. We present a brief summary in Sec. 6.6.

6.2 Isotropic spin network

Let us consider a quantum network consisting of \mathcal{N} (even) lattice sites shared between the two sublattices of a bipartite lattice, say \mathcal{A} and \mathcal{B} (see Fig. 6.1). Each site is occupied by a spin-1/2 particle such that a spin on sublattice \mathcal{A} is surrounded

by \mathcal{R} nearest neighbor (NN) spins on sublattice \mathcal{B} , and vice-versa. The network is isotropic, which implies that the lattice appears the same from the perspective of any lattice site. Moreover, the quantum state of the network is invariant, upto a global phase, under identical local unitaries, i.e., the spin state is *rotationally invariant*. Such a spin network is in principle equivalent to the spin liquid phases of certain antiferromagnetic strongly-correlated systems [107, 138, 140, 142], such that the state consists of equal-weight superposition of all possible dimer coverings. A dimer between any two NN spin-1/2 particles on a bipartite lattice is given by

$$|\psi\rangle_{ij} = \frac{1}{\sqrt{2}}(|\uparrow_i\downarrow_j\rangle - |\downarrow_i\uparrow_j\rangle), \quad (6.1)$$

where $i \in \mathcal{A}$ and $j \in \mathcal{B}$. The state of the \mathcal{N} -spin quantum network can then be defined as

$$\Psi_{\mathcal{N}} = \sum_k \{ \prod_{i \in \mathcal{A}, j \in \mathcal{B}}^{\otimes} |\psi\rangle_{ij} \}_k, \quad (6.2)$$

where $\{\cdot\}_k$ is the k^{th} (defect-free) unique dimer covering, which is the product of $\mathcal{N}/2$ dimers across the bipartite lattice. Since $|\psi\rangle_{ij}$ is rotationally invariant under operations of the form $\mathcal{U} \otimes \mathcal{U}$, where \mathcal{U} is a unitary acting on a single spin-1/2 particle, the entire state, $|\Psi\rangle_{\mathcal{N}}$, is rotationally invariant under the local operation, $\mathcal{U}^{\otimes \mathcal{N}}$ [138]. In presence of defects, description of the state can be mapped to a three-level basis or the qutrit Hilbert space [3], such that each node of the network is represented by $\{|\nu_0\rangle, |\nu_1\rangle\}$, where $|\nu_0\rangle$ denotes a node with no spin particle (a defect). The occupied node is $|\nu_1\rangle$, representing the spin-1/2 particle with the two-level basis $\{|\uparrow\rangle, |\downarrow\rangle\}$. Hence, the overall state of the network can be expressed by the joint three-level basis, $\{|\nu_0\rangle, |\nu_1\rangle|\uparrow\rangle, |\nu_1\rangle|\downarrow\rangle\} \rightarrow \{|\zeta_0\rangle, |\zeta'_1\rangle, |\zeta'_2\rangle\}$. In this new basis, a dimer between two NN spins is defined as

$$|\psi\rangle_{ij} = \frac{1}{\sqrt{2}}(|\zeta'_1\rangle_i |\zeta'_2\rangle_j - |\zeta'_2\rangle_i |\zeta'_1\rangle_j), \quad (6.3)$$

and a defect at node l is written as $|\zeta_0\rangle_l$. We note that the (un)primed elements of the basis represent the spin (un)occupied sites, corresponding to $(|\nu_0\rangle)|\nu_1\rangle$. An important property of the spin network is its rotational invariance, which is preserved by considering the distribution of the defects to be such that the remaining spin

occupied sites always form a complete dimer covering. This is supported by the fact that in strongly-correlated systems such coverings are known to be energetically favorable as compared to states where dimer pairs break to form free spins [318,319]. Hence, for an \mathcal{N} -spin network containing \mathcal{P} nodes with defects, the overall state can be written as

$$\bar{\Psi}_{\mathcal{N}}^{\mathcal{P}} = \sum_k \left(\prod_{i \in \mathcal{A}, j \in \mathcal{B}}^{\otimes} |\psi\rangle_{ij} \otimes \{\phi_l\}_k \right), \quad (6.4)$$

where $\{\phi_l\} = |\zeta_0\rangle_{l_1} |\zeta_0\rangle_{l_2} \cdots |\zeta_0\rangle_{l_{\mathcal{P}}}$ and l_i are the nodes containing the \mathcal{P} defects,

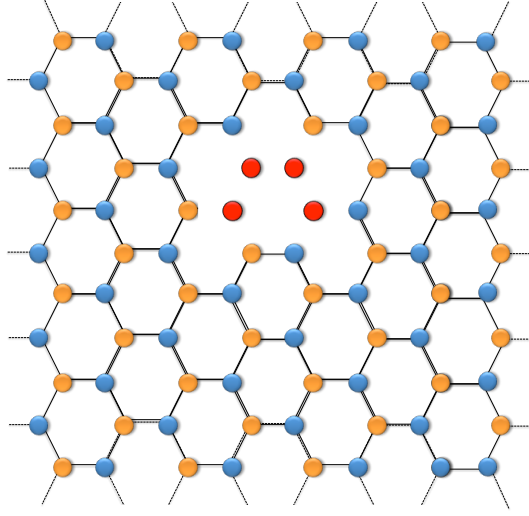


Figure 6.2: A two-dimensional bipartite honeycomb lattice, with defects (red-circles) in the network. The nodes in sublattice \mathcal{A} (blue-circles) and \mathcal{B} (yellow-circles), are occupied by spin-1/2 particles.

equally distributed between sublattices \mathcal{A} and \mathcal{B} , such that the sites i and j ($i \in \mathcal{A}$ and $j \in \mathcal{B}$) are occupied by $\mathcal{N} - \mathcal{P}$ spins which form a complete dimer covering. $\mathcal{D} = \mathcal{P}/\mathcal{N}$ gives us the defect density of the network.

6.3 Single- and two-node Reduced states of the spin network

An important aspect in studying the bipartite and multipartite entanglement properties in spin networks with defects is to derive the reduced density matrix for arbitrary

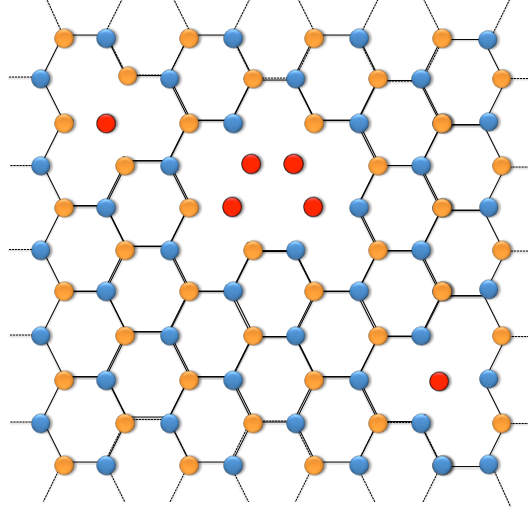


Figure 6.3: Another instance of a two-dimensional bipartite honeycomb lattice, with defects (red-circles) spread in the network.

single and two nodes. This would allow us to estimate the entanglement between two nodes in the network, as well as understand the local, single node properties of the spin network. The state of the quantum network with finite defects, $\bar{\Psi}_{\mathcal{N}}^{\mathcal{P}}$, is invariant under the three-level local unitary operation

$$\tilde{\mathcal{U}}^{\otimes \mathcal{N}} = (1 \oplus \mathcal{U})^{\otimes \mathcal{N}} = \begin{pmatrix} 1 & 0 \\ 0 & \mathcal{U} \end{pmatrix}^{\otimes \mathcal{N}}, \quad (6.5)$$

where \mathcal{U} is a 2×2 unitary operator acting on the spin space $\{|\zeta'_1\rangle, |\zeta'_2\rangle\}$, and each node of any term of $\bar{\Psi}_{\mathcal{N}}^{\mathcal{P}}$ contains either a defect or is part of a dimer. The invariance of $\bar{\Psi}_{\mathcal{N}}^{\mathcal{P}}$ is significant in analysing the entanglement properties of the quantum network, and it can be shown that the reduced state, $\rho^{(x)}$, for any x nodes, obtained by tracing over all but x (say, \bar{x}) nodes from the state $\bar{\Psi}_{\mathcal{N}}^{\mathcal{P}}$, is also invariant under the action of $\tilde{\mathcal{U}}^{\otimes x}$. To elaborate, $\rho^{(x)} = \text{Tr}_{\bar{x}}[|\bar{\Psi}\rangle\langle\bar{\Psi}|] = \sum_{\bar{x}} |\langle\phi_{\bar{x}}|\bar{\Psi}\rangle|^2$, where $\{|\phi_{\bar{x}}\rangle\}$ forms a complete basis over the system of \bar{x} sites. Now,

$$\rho^{(x)} = \sum_{\bar{x}} |\langle\phi_{\bar{x}}|\tilde{\mathcal{U}}^{\otimes \mathcal{N}}|\bar{\Psi}\rangle|^2, \quad (6.6)$$

due to the invariance property of $|\bar{\Psi}\rangle\langle\bar{\Psi}|$. Therefore,

$$\rho^{(x)} = \sum_{\bar{x}} |\langle\phi_{\bar{x}}|\tilde{\mathcal{U}}^{\otimes\bar{x}}\tilde{\mathcal{U}}^{\otimes x}|\bar{\Psi}\rangle|^2 = \tilde{\mathcal{U}}^{\otimes x} \left(\sum_{\bar{x}} |\langle\tilde{\phi}_{\bar{x}}|\bar{\Psi}\rangle|^2 \right) \tilde{\mathcal{U}}^{\otimes x\dagger}, \quad (6.7)$$

where $|\tilde{\phi}_{\bar{x}}\rangle = \tilde{\mathcal{U}}^{\otimes\bar{x}\dagger}|\phi_{\bar{x}}\rangle$ forms another basis of the system of \bar{x} nodes. The invariance of $\rho^{(x)}$ allows us to obtain the expressions for the reduced states of single and two nodes.

For instance, let $\rho^{(1)}$ be a single node reduced state, such that it satisfies

$$\tilde{\mathcal{U}}\rho^{(1)}\tilde{\mathcal{U}}^\dagger = \rho^{(1)}. \quad (6.8)$$

Let us denote, $\rho^{(1)} = \rho_{ij}^{(1)}$ and $\tilde{\mathcal{U}} = u_{ij}$, where $\{i, j\} = \{1, 2, 3\}$. Now from definition of $\tilde{\mathcal{U}}$, $u_{1j} = u_{j1} = \delta_{1j} \forall j$, and the unitarity of \mathcal{U} in the spin space demands, $u_{kl}u_{lk'}^* = \delta_{kk'}$, for $\{k, k', l\} = \{2, 3\}$. This gives us

$$(\tilde{\mathcal{U}}\rho^{(1)}\tilde{\mathcal{U}}^\dagger)_{ij} = \sum_{j'k} u_{ij'}\rho_{j'k}^{(1)}u_{kj}^*, \quad (6.9)$$

and the invariance is satisfied if

$$\rho_{ij}^{(1)} = u_{ij'}\rho_{j'k}^{(1)}u_{kj}^*\delta_{ij'}\delta_{kj} = u_{ii}\rho_{ij}^{(1)}u_{jj}^*. \quad (6.10)$$

For $\tilde{\mathcal{U}}$, it is known that $u_{ii}u_{ii}^* = 1$, for $i = \{1, 2, 3\}$. Hence, for all single-node reduced states, the invariance holds if and only if $\rho_{ij}^{(1)}$ is diagonal, i.e., $\rho_{ij}^{(1)} = p_i \delta_{ij}$, such that $\sum_i p_i = 1$, and $p_2 = p_3$. Therefore, the single site reduced density matrix at site a is given by

$$\rho_a^{(1)} = \text{diag}\{p_1, p_2/2, p_2/2\} = p_1|\zeta_0\rangle\langle\zeta_0|_a + p_2\frac{\mathbb{I}_2}{2}, \quad (6.11)$$

where $\mathbb{I}_2 = (0 \oplus I_2)$, with I_2 being the identity matrix in the spin space $\{|\zeta'_1\rangle_a, |\zeta'_2\rangle_a\}$. Note that the single-site density matrix in the absence of defects is just $\mathbb{I}_2/2$.

Let us illustrative the approach to determining the reduced state $\rho^{(1)}$. From Figs. 6.4(a)-(b), one observes that the a single-node state may either contain a

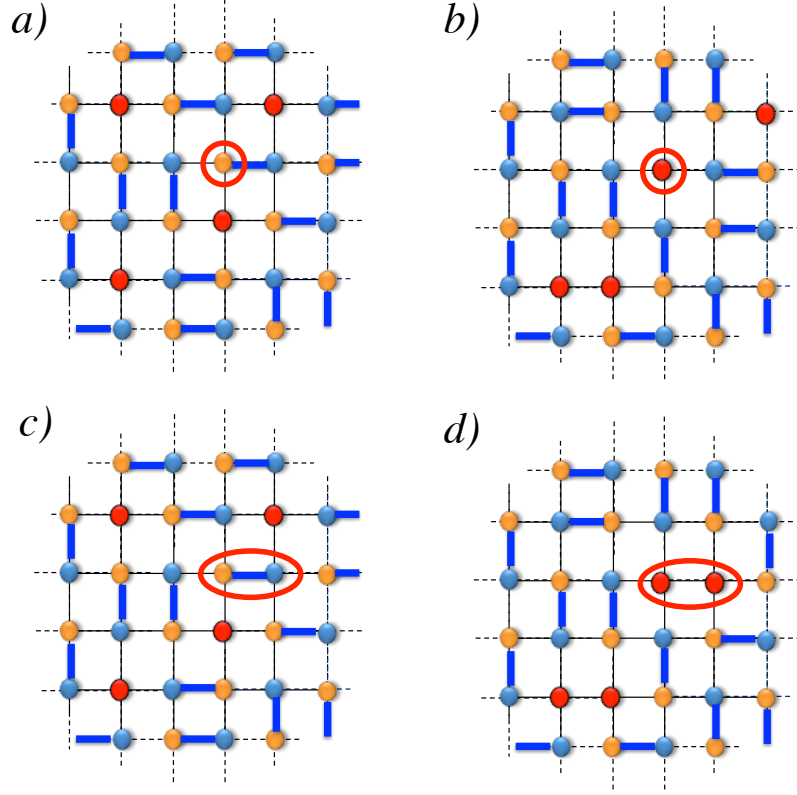


Figure 6.4: (Color online). a) Single node containing a spin-1/2 belonging to a dimer, b) Single node containing a defect, c) A NN two-node containing a dimer, and d) A NN two-node containing a pair of defects.

spin-1/2 particle, which is a part of a dimer, or a defect. The first arrangement has several possibilities depending on the orientation of the dimer. However, the two arrangements do not overlap or produce cross terms as basis formed by the remaining sites in each case are orthogonal to each other. This is due to the fact that the distribution in Fig. 6.4(a), contains $\mathcal{P} = 4$, holes in the remaining sites, whereas the arrangement in Fig. 6.4(b), has $\mathcal{P} = 3$, rendering the remaining state orthogonal. All possible distributions of the type (a) lead to $\mathbb{I}_2 = (0 \oplus I_2)$, with I_2 being the identity matrix in the spin space, $\{|\zeta'_1\rangle, |\zeta'_2\rangle\}$, as defined in the main text. The arrangement in (b) leads to the state $|\zeta_0\rangle\langle\zeta_0|$. Hence, the one-node reduced density matrix has the general form,

$$\rho^{(1)} = \text{diag}\{p_1, p_2/2, p_2/2\} = p_1|\zeta_0\rangle\langle\zeta_0| + p_2\frac{\mathbb{I}_2}{2}. \quad (6.12)$$

For very low defect densities, $\mathcal{D} \approx 0$, $p_2 \approx 1 \gg p_1$. Evidently, in the other limit, $\mathcal{D} \approx 1$, $p_1 \approx 1 \gg p_2$. However, in general, estimating the probabilities, p_1 and p_2 , for arbitrary \mathcal{P} and \mathcal{N} is intractable due to the overcomplete defect-dimer basis. Therefore, it is clear that for all values of \mathcal{D} , except the case where all nodes have a defect (no spins) or $\mathcal{D} = 1$, the one-node reduced state is mixed and thus always entangled to the rest of the system. As shown in the main text, this is a crucial point in determining the genuine multipartite entanglement of the spin network.

Similarly, one can obtain the analytical expression for the reduced two-node states invariant under the local unitary operation, $\tilde{\mathcal{U}} \otimes \tilde{\mathcal{U}}$. For an arbitrary pair of nodes a and b , where $a \in \mathcal{A}$ and $b \in \mathcal{B}$, the reduced density matrix is given by

$$\rho_{ab}^{(2)} = p'_1|\zeta_0\zeta_0\rangle\langle\zeta_0\zeta_0|_{ab} + p'_2\mathbb{I}_4/4 + p'_3\mathcal{W}(q), \quad (6.13)$$

where $p'_i \geq 0 \forall i$, and $\sum_i p'_i = 1$. The diagonal matrix

$$\mathbb{I}'_4 = \sum_i |\zeta_0\zeta'_i\rangle\langle\zeta_0\zeta'_i|_{ab} + |\zeta'_i\zeta_0\rangle\langle\zeta'_i\zeta_0|_{ab}. \quad (6.14)$$

$\mathcal{W}(q)$ is the Werner state [143] on $\mathbb{C}^2 \otimes \mathbb{C}^2$, where \mathbb{C}^2 is spanned by $\{|\zeta'_1\rangle, |\zeta'_2\rangle\}$, so that

$$\mathcal{W}(q) = q|\psi\rangle\langle\psi|_{ab} + (1-q)\mathbb{I}_4/4, \quad (6.15)$$

for $-1/3 \leq q \leq 1$, with $|\psi\rangle_{ab} = \frac{1}{\sqrt{2}}(|\zeta'_1\zeta'_2\rangle - |\zeta'_2\zeta'_1\rangle)_{ab}$ being the spin dimer and

$$\mathbb{I}_4 = \sum_{i,j=1}^2 |\zeta'_i\zeta'_j\rangle\langle\zeta'_i\zeta'_j|_{ab}, \quad (6.16)$$

being the identity matrix.

Let us now consider the case for the reduced states of two NN nodes, or two arbitrary nodes, where each node belongs to a different sublattice. In Figs. 6.4(c)-(d),

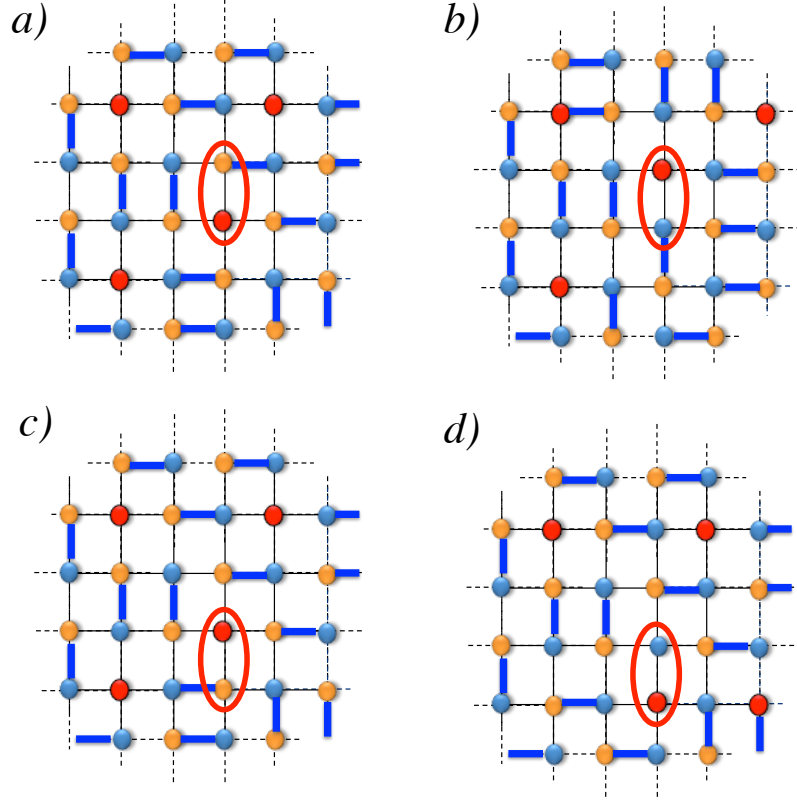


Figure 6.5: (Color online). a) A NN two node containing a spin-1/2 belonging to a dimer in sublattice \mathcal{B} and a defect in sublattice \mathcal{A} , b) same two node now containing a spin-1/2 belonging to a dimer in \mathcal{A} and a defect in \mathcal{B} , c)-d) Another instance of the arrangement a)-b), respectively, at a different pair of nodes.

we present the two quintessential components of the density matrix. The arrangement in (c) shows the case where both nodes have a spin. There are several possible arrangements but two broad possibilities emerge: the nodes share a dimer or the nodes have spins which are part of different dimers. This case is reminiscent of a two-node state in a network with no defects and gives us the Werner state, $\mathcal{W}(q)$, as the rotationally invariant two-node density matrix.

$$\mathcal{W}(q) = q|(i, j)\rangle\langle(i, j)| + (1 - q) \mathbb{I}_4/4, \quad (6.17)$$

where $-1/3 \leq q \leq 1$ and \mathbb{I}_4 is the identity matrix in the two-qubit spin space. The arrangement in (d) contains two defects, and gives the state, $|\zeta_0\zeta_0\rangle\langle\zeta_0\zeta_0|$. We

note once more that this arrangement has no overlap with the former, and hence no cross-terms.

However, other terms will arise for the arrangements shown in Fig. 6.5, where one site has a defect and the other has a part of the spin dimer. This arrangements give rise to state of the form: $|\zeta_0\zeta'_1\rangle\langle\zeta_0\zeta'_1|$, $|\zeta_0\zeta'_2\rangle\langle\zeta_0\zeta'_2|$, $|\zeta'_1\zeta_0\rangle\langle\zeta'_1\zeta_0|$, and $|\zeta'_2\zeta_0\rangle\langle\zeta'_2\zeta_0|$. No cross terms arise due to the distribution of the dimers and defects in the system. To elaborate, cross terms, such as $|\zeta_0\zeta'_1\rangle\langle\zeta_0\zeta'_2|$, do not exist as the reduced single nodes, for occupied nodes, is always I_2 . Moreover, terms such as $|\zeta_0\zeta'_1\rangle\langle\zeta'_1\zeta_0|$, do not occur as there exists no overlap between these states. In Fig. 6.5(a)-(b), and also (c)-(d), one can see that the distribution of defects is such that, the remaining sites in arrangements (a) and (b) (also, (c) and (d)) are orthogonal. This is due to the fact that defects occupy nodes equally distributed between sublattice \mathcal{A} and \mathcal{B} , to allow the remaining spins to form a complete dimer covering. In arrangement (a), where $\mathcal{P} = 4$, there will be two defects in \mathcal{B} and one in \mathcal{A} among the remaining nodes, since the reduced state (red-circle) contains the other defect in \mathcal{A} . However, arrangement (b) will have two defects in \mathcal{A} and one in \mathcal{B} , rendering the basis states for the remaining sites orthogonal to each other. This will always be the case for all \mathcal{N} and \mathcal{P} . The two-node reduced state is thus given by,

$$\rho^{(2)} = p'_1|\zeta_0\zeta_0\rangle\langle\zeta_0\zeta_0| + p'_2 \mathbb{I}'_4/4 + p'_3 \mathcal{W}(q), \quad (6.18)$$

where

$$\mathbb{I}'_4 = |\zeta_0\zeta'_1\rangle\langle\zeta_0\zeta'_1| + |\zeta_0\zeta'_2\rangle\langle\zeta_0\zeta'_2| + |\zeta'_1\zeta_0\rangle\langle\zeta'_1\zeta_0| + |\zeta'_2\zeta_0\rangle\langle\zeta'_2\zeta_0|. \quad (6.19)$$

Once more, it is not possible to estimate the terms p'_1 , p'_2 , p'_3 , and q , for arbitrary isotropic lattice, with any \mathcal{N} and \mathcal{P} . One of the main objectives of the main text is to obtain more information on the these quantities, which allow us to estimate the bipartite entanglement properties of the spin network.

Hence, Eqs. (6.12) and (6.18) give us the analytical expressions for the single- and two-node reduced density matrices of the spin network with finite defects represented by the state $|\bar{\Psi}\rangle_{\mathcal{N}-\mathcal{P}}$. We observe that $\rho_a^{(1)}$ and $\rho_{ab}^{(2)}$ are dependent on the defect density, $\mathcal{D} = \mathcal{P}/\mathcal{N}$. For instance, for $\mathcal{D} = 0$, which corresponds to a spin network with no defects, $p_2 = p'_3 = 1$. For large networks with a small number of defects, $\mathcal{D} \ll 1$, $p_1 \ll p_2$, and $p'_3 \gg \{p'_1, p'_2\}$. However, exact values of p_i 's, p'_i 's, and

q are difficult to compute and are intractable, even for simple 2D lattices. This is due to the fact that the enumeration of arrangements in a defect-dimer covering is known to be *NP-complete* [267]. This makes the estimation of entanglement properties of these spin networks a formidable task. We show that by using concepts from quantum information theory (QIT), such as strong-subadditivity of von Neumann entropy and quantum telecloning, one can unearth substantial details about the bipartite and multipartite entanglement of these quantum spin networks.

6.4 Bound on bipartite entanglement

We begin by investigating the bipartite entanglement properties of the state, given by Eq. (6.18), between any two arbitrary sites ($a \in \mathcal{A}$ and $b \in \mathcal{B}$) of the quantum spin network. The condition of positive partial transposition (PPT) [156, 157] is given by $[p'_3(1 - 3q)]/4 \geq 0$. Therefore, $\rho_{ab}^{(2)}$ has a negative-partial-transpose (NPT), and hence is entangled, iff $q > 1/3$, which is the same criterion as that for the Werner state. To obtain a more specific criteria for the bipartite entanglement properties of the spin network with defects, one needs to estimate the bounds on the parameter q in terms of the defect in the network. To this effect, we use a QIT concept called *quantum telecloning* [317], which combines the concept of quantum teleportation [33] and quantum cloning [320]. While teleportation provides the fidelity with which a quantum state can be transferred to \mathcal{M} parties using shared bipartite entanglement and classical communication, quantum cloning provides the optimal fidelity with which \mathcal{M} copies of a quantum state can be prepared. Consider a site a ($\in \mathcal{A}$) with \mathcal{M} sites surrounding it, given by $\{b_i\}$ ($\in \mathcal{B}$), giving rise to \mathcal{M} reduced states, ρ_{ab_i} . We suppose that an ancillary system in an arbitrary quantum state, $|\alpha\rangle$, is brought near the site a . This can be teleported to the site b_i , using the channel ρ_{ab_i} , with some optimal fidelity, \mathcal{F}_{tele} . If all ρ_{ab_i} 's are the same (a has \mathcal{M} equidistant neighbors b_i in an isotropic state), then the state $|\alpha\rangle$ can be teleported to \mathcal{M} sites with fidelity \mathcal{F}_{tele} . However, using an optimal cloning machine, \mathcal{M} copies of a d -dimensional quantum state, $|\alpha\rangle$, can only be produced with a fidelity,

$$\mathcal{F}_{clo} = \frac{2\mathcal{M} + (d - 1)}{\mathcal{M}(d + 1)}. \quad (6.20)$$

Therefore,

$$\mathcal{F}_{tele} \leq \mathcal{F}_{clo}, \quad (6.21)$$

and we obtain an upper bound on the fidelity with which \mathcal{M} copies of a quantum state can be remotely prepared.

Let us now consider the quantum state of the system under consideration as the required resource for the remote protocol where an unknown qutrit, $|\alpha\rangle$, is brought near site a , and \mathcal{M} copies of it are to be prepared at \mathcal{M} sites, $\{b_i\}$, on the isotropic network. The \mathcal{M} equivalent two-site density matrices, $\rho_{ab_i}^{(2)}$, are of the form given in Eq. (6.18). The fidelity of teleporting $|\alpha\rangle$ from near site a to site b_i , is obtained from the maximal singlet fraction,

$$F = \max \langle \psi^s | \Lambda(\rho_{ab_i}^{(2)}) | \psi^s \rangle, \quad (6.22)$$

where the maximization is over all local operations and classical communication protocols, Λ , and where $|\psi^s\rangle$ is a maximally entangled state on $\mathbb{C}^d \otimes \mathbb{C}^d$. The teleportation fidelity is then given by [320]

$$\mathcal{F}_{tele} = (Fd + 1)/(d + 1), \quad (6.23)$$

where $d = 3$ for the qutrit. For

$$|\psi^s\rangle = \frac{1}{\sqrt{3}}(|\zeta'_1 \zeta'_2\rangle - |\zeta'_1 \zeta'_2\rangle + |\zeta_0 \zeta_0\rangle) \quad (6.24)$$

and for Λ as the identity operation,

$$F' = \langle \psi^s | \rho_{ab_i}^{(2)} | \psi^s \rangle \leq F. \quad (6.25)$$

Using Eq. (6.18), for $\rho_{ab_i}^{(2)}$, we obtain

$$F' = p'_1/3 + (p'_3/3)[(3q + 1)/2]. \quad (6.26)$$

Therefore, for $d = 3$, we obtain

$$\mathcal{F}_{tele} \geq \frac{(F'd + 1)}{(d + 1)} = \frac{p'_1 + p'_3[(3q + 1)/2] + 1}{4}, \text{ and} \quad (6.27)$$

$$\mathcal{F}_{clo} = \frac{2\mathcal{M} + (d - 1)}{\mathcal{M}(d + 1)} = \frac{1}{2} + \frac{1}{2\mathcal{M}}. \quad (6.28)$$

As discussed earlier, $\mathcal{F}_{tele} \leq \mathcal{F}_{clo}$, and using Eqs. (6.27) and (6.28), we obtain an upper bound on the parameter q in $\rho_{ab_i}^{(2)}$, given by

$$q \leq \frac{1}{3} \left(\frac{2}{p'_3} - 1 \right) - \frac{2}{3p'_3} \left(p'_1 - \frac{1}{\mathcal{M}} \right). \quad (6.29)$$

As we know the two-site density matrix is entangled if $q > 1/3$, the above relation provides us important indicators about the bipartite entanglement between two sites of the lattice. For relatively small number of defects in the lattice, $p'_1 \ll p'_3$, such that $p'_1/p'_3 \approx 0$. Hence,

$$q \leq (1/3)(1 + 2/\mathcal{M} + \delta), \quad (6.30)$$

where $\delta = 2/p'_3 - 2$, with $\delta \rightarrow 0$ as $p'_3 \rightarrow 1$. Hence, the upper bound on q decreases as the number of copies, \mathcal{M} , increases. For example, let us consider an isotropic 2D square lattice with a low number of defects. We consider the telecloning of a qutrit from a site to its four NNs ($\mathcal{M} = 4$), so that the bound on q for NN two-party reduced density matrices is given by $q \leq 1/2 + \delta/3$. Hence, the NN state with highest bipartite entanglement for the isotropic 2D square lattice is given by Eq. (6.18), with $q = 1/2 + \delta/3$.

Similarly, let us consider the telecloning of a qutrit to \mathcal{R} nodes ($\{b_1, b_2, \dots, b_{\mathcal{R}}\}$), x edges away from node a , such that $\mathcal{M} = \mathcal{R}$. Alternatively, one may consider \mathcal{R} to be the number of nodes contained in the area formed by concentric circles of radius $r > x$ and $r \leq x + x'$, where $x' \ll x$ (see Figs. 6.6). For large x , all the \mathcal{R} nodes can be considered as equidistant from node a . \mathcal{R} increases with x , and we have

$$q \leq 1/3 + \delta/3. \quad (6.31)$$

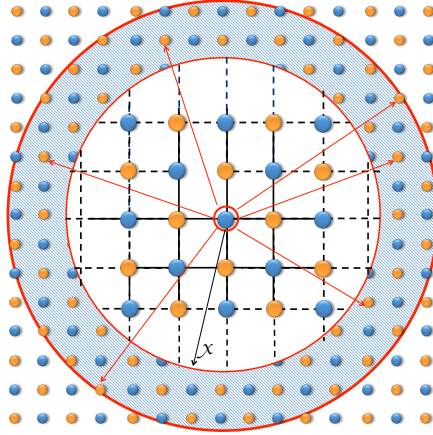


Figure 6.6: Possible two-node reduced states, represented by Eq. (6.18), between a central node (encircled red) and a set of \mathcal{M} distant nodes, separated by approximately x edges. The central node belongs to sublattices \mathcal{A} , with the distant nodes belonging to sublattice \mathcal{B} . These two-node states form the channel for the quantum telecloning protocol discussed in the main text.

We observe that as $\delta \rightarrow 0$, $q \leq 1/3$ and the states $\rho_{ab_i}^{(2)}$ ($i = 1, 2, \dots, \mathcal{R}$) are separable, since $\rho_{ab_i}^{(2)}$ is then a mixture of three unentangled states. Figure 6.7 shows that the permissible upper limit on bipartite entanglement, as quantified by logarithmic negativity [156, 157, 159–161], is finite for any two sites in the isotropic lattice with defects but decreases as the number of equidistant isotropic pairs (\mathcal{M}) increases.

6.5 Genuinely multipartite entanglement

We now show that an \mathcal{N} -spin network with \mathcal{P} defective nodes, given by $|\bar{\Psi}\rangle_{\mathcal{N}}^{\mathcal{P}}$, such that $\mathcal{P} < \mathcal{N}$, is *always* genuine multipartite entangled. For a pure multiparty quantum state to be genuinely multipartite entangled, it must be entangled across all possible bipartitions of the system. This requires that the reduced density matrices across all possible bipartitions must necessarily be mixed. From Eqs. (6.12) and (6.18), for $\mathcal{D} < 1$, we observe that the reduced single- and two-node reduced states are always mixed. Hence, the state $|\bar{\Psi}\rangle_{\mathcal{N}}^{\mathcal{P}}$ is entangled across all *single:rest* and *two:rest* bipartitions. Now we need to show that $|\bar{\Psi}\rangle_{\mathcal{N}}^{\mathcal{P}}$ is entangled across the other possible bipartitions.

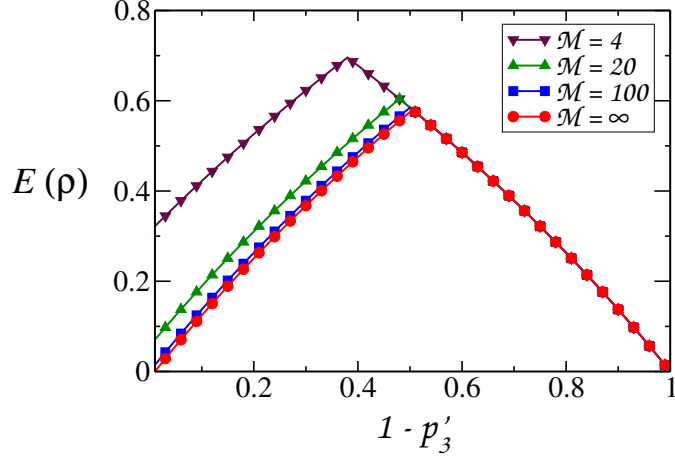


Figure 6.7: Maximum permissible bipartite entanglement. We show the upper bound on entanglement due to quantum telecloning, quantified using logarithmic negativity ($E(\rho)$), for the two-party reduced state $\rho_{AB_i}^{(2)}$, for $\mathcal{M} = 4, 20, 100$, and ∞ , as a function of $1 - p'_3$. The plot shows that the maximum permissible entanglement decreases as \mathcal{M} increases. Interestingly, in the absence of defects ($p'_3 = 1$) no bipartite entanglement is present as $\mathcal{M} \rightarrow \infty$. The vertical axis is in ebits, while the horizontal one is dimensionless.

Consider the reduced state, $\rho^{(x)} = \text{Tr}_{\bar{x}}[(|\Psi\rangle\langle\Psi|)_{\mathcal{N}}^{\mathcal{P}}]$, for any arbitrary but fixed set of x nodes. Let us assume that $\rho^{(x)}$ is pure and thus $|\bar{\Psi}\rangle_{\mathcal{N}}^{\mathcal{P}}$ is separable along the $x : (\mathcal{N} - x)$ bipartition. Let $x = (\tilde{x} \setminus 1) \cup y$, where y is one specific node. Since, the spin network is isotropic, there shall always exist an equivalent but spatially different set of x' nodes, such that both x' and x contain an equal number of nodes and the node y is common to both reduced sets. Hence, $x' = (\tilde{x}' \setminus 1) \cup y$. Now, $\rho^{(x')}$ is also pure, by the symmetry of the isotropic lattice. Applying the strong subadditivity of von Neumann entropy ($S(\cdot)$) [238], we obtain

$$S(\rho^{(\tilde{x} \setminus 1)}) + S(\rho^{(\tilde{x}' \setminus 1)}) \leq S(\rho^{(\tilde{x} \setminus 1) \cup y}) + S(\rho^{(\tilde{x}' \setminus 1) \cup y}). \quad (6.32)$$

As $\rho^{(x)}$ and $\rho^{(x')}$ are pure,

$$S(\rho^{(\tilde{x} \setminus 1) \cup y}) = S(\rho^{(\tilde{x}' \setminus 1) \cup y}) = 0. \quad (6.33)$$

Since $S(\rho)$ is non-negative, $S(\rho^{(\tilde{x} \setminus 1)}) = S(\rho^{(\tilde{x}' \setminus 1)}) = 0$, and this implies that $S(\rho^{(y)}) = 0$ or $\rho^{(y)}$ is pure. However, y is a single node, and from Eq. (6.12) all single node

reduced states are mixed, for $\mathcal{D} < 1$. Hence $\rho^{(y)}$ is mixed and the initial assumption that $\rho^{(x)}$ is pure does not hold. Therefore, $\rho^{(x)}$ must always be mixed and thus $|\bar{\Psi}\rangle_{\mathcal{N}-\mathcal{P}}$ is entangled across all $x : (\mathcal{N} - x)$ bipartitions. This proves that $|\bar{\Psi}\rangle_{\mathcal{N}-\mathcal{P}}$ is genuine multipartite entangled for spin networks with finite defects. The above method can also be extended to prove that infinite spin networks are entangled across infinite line of bipartition. For example, the isotropic spin state, $|\bar{\Psi}\rangle$, defined on an infinite 2D lattice is always entangled across infinite lines on the lattice. This proves that the entire multiparty state of the isotropic spin network is genuinely multiparty entangled, except in the extreme case where all spins are lost ($\mathcal{D} = 1$), so that the state becomes a product of vacuum nodes, given by $|\zeta_0^{(1)}\rangle \otimes |\zeta_0^{(2)}\rangle \cdots \otimes |\zeta_0^{(\mathcal{N})}\rangle$.

6.6 Summary

The single- and two-node reduced states in Eqs. (6.12) and (6.18), respectively, are defined for the quantum spin network with finite defects. Without defects, the network can be mapped to the two-qubit space, spanned by $\{|\zeta'_1\rangle, |\zeta'_2\rangle\}$. The single-node reduced density matrix is then $I_2/2$ ($p_1 = 0, p_2 = 1$ in Eq. (6.12)) and the two-node reduced state is given by the Werner state, $\mathcal{W}(q)$ ($p'_1 = p'_2 = 0, p'_3 = 1$). Since, the single-node state is always mixed, using the approach discussed earlier, but applied to the case of zero defects, it can be shown that the quantum spin network is always genuine multisite entangled. Finite defects in the network do not destroy the multiparty entanglement, but for the extreme case, where all spins are lost ($\mathcal{D} = 1$).

In the absence of defects, the condition of bipartite entanglement between any two arbitrary nodes reduces to $q \leq (1/3)(1 + 2/\mathcal{M})$, since $\delta = 0$. Again, considering the example of an isotropic 2D square lattice, in the limit $\mathcal{M} \rightarrow \infty$, we obtain $q \leq 1/3$, and the upper bound ensures that the system has no long-range bipartite entanglement [37]. However, in the presence of finite defects, the upper bound may allow a small but finite entanglement, as $q \leq (1/3)(1 + \delta)$. Hence, presence of defects in quantum spin networks may not qualitatively affect the presence of genuine multipartite entanglement in the system but, counterintuitively, may permit the presence of finite bipartite entanglement between moderately-distant sites, in contrast to the spin network with no defects.

In summary, our work primarily aims at highlighting the response to defects of

the distribution of entanglement, both bipartite as well as multipartite, in a particular prototype of quantum spin networks. Our results show that presence of finite defects do not affect the presence of multisite entanglement properties of the network, while, interestingly, finite moderate-range bipartite entanglement may emerge. This shows that isotropic spin networks that can be obtained as dimerized ground states of spin Hamiltonians provide a robust model for implementation of quantum protocols in presence of defects.

The spin network considered in our work is a useful tool in realization of solid-state quantum computation protocols, in particular as realistic dimer models for fault tolerant *topological computation* [127, 145, 146, 194, 237, 321–324]. Moreover, the state under study is closely related to interpolations of the projected entangled pair states [325–327], which are valuable resources for *measurement-based quantum computation* [285, 286]. Such spin network states, provide the necessary resource for measurement-based quantum computation [328–335] and may potentially be more accessible in many-body architectures (e.g. in photonic and ultracold gas systems), as they may appear as natural ground states [127, 215, 336–338].

The results of this Chapter are based on the following paper:

- **Sudipto Singha Roy**, Himadri Shekhar Dhar, Debraj Rakshit, Aditi Sen(De), and Ujjwal Sen, *Response to defects in multi- and bipartite entanglement of isotropic quantum spin networks*, arXiv:1607.05195 [quant-ph].

Summary

The quantum mechanical description of nature is radically different from what we require, if we wish to understand and describe most of our experiences in our everyday life. In classical theory, complete information of any physical system can, in general, be obtained via proper characterization of its subparts. On the contrary, for quantum systems, there may be scenarios for which full knowledge about the system may fail to provide complete information about its subparts. A celebrated example is the singlet. The singlet is a maximally entangled state, and for all such states, though a complete characterization of the properties related to the composite system is always possible, one remains totally ignorant about the physical states of the subparts when those are probed locally. In other words, in this case, all the information remain hidden in the shared correlation.

Over the last two decades or so, this non-intuitive property of quantum theory has given rise to the birth of many revolutionary ideas related to computation and information theory. Schemes have been proposed where quantum entanglement have been used as a resource to accomplish tasks which cannot be realized under the realm of classical theory, or are severely less efficient in the latter. Many efficient algorithms have been proposed which surpass the capability of their classical counterparts. Using fundamental concepts related to quantum theory, secure classical communication networks have been proposed, in which any intervention of an eavesdropper, armed with arbitrary quantum devices, can be traced efficiently.

Apart from its applications in information theory and computation, quantum entanglement has turned out to be an efficient tool to detect many important properties related to other interdisciplinary areas of physics as well. One such vibrant area of re-

search is the interface between quantum information and many-body systems. Over the last two decades, many important works have reported where entanglement have been emerged as an efficient detector of quantum phase transition points for various complex quantum systems. It has also been argued that distribution of ground state entanglement sometime may provide a clearer picture about all the phase transition boundaries, when characterized together with the conventional order parameters. In addition to this, many useful techniques have been proposed to simulate complex many-body systems on a large number of lattice sites, in an efficient way.

These theoretical developments were soon brought to fruition, at least to a certain extent via experimental realization in some small-to-moderate scale quantum networks in laboratories. These include quantum networks fabricated by embedding quantum atoms in the optical cavities, where qubits can be represented by long-lived internal atomic and molecular states in electronic ground states, or in metastable excited electronic states, which can be manipulated by optical and microwave fields. The accuracy of neutral atom quantum computing lies on several factors, such as well developed cooling and trapping techniques. These techniques indeed provide an ideal platform to use these networks for large-scale quantum computation. At present, these trapping and cooling techniques are being extended to molecules.

The main goal of these techniques is to implement various theoretical quantum protocols in real physical systems. To this end, one of the main challenges is to protect them from environmental perturbations. As is often the case, quantum correlation, in particular, quantum entanglement, turns out to be fragile to environmental perturbation, and one needs to design the quantum network in a way so that environmental effects can be suppressed to some extent. In addition to this, defects in the quantum system occur unavoidably in real materials and can now also be engineered artificially in, e.g., cold gas experiments. Usually, such defects or disorders play destructive roles by diminishing physical properties like magnetization, classical correlators, and quantum correlations.

Therefore, in order to design a quantum network to accomplish any information processing tasks, one must have proper knowledge about the distribution of quantum entanglement among its various subparts. In this thesis, we have considered one such rich and complex quantum many-body system, viz. the resonating valence bond states, constructed on various lattices geometries and have characterized its various

bipartite as well as multipartite entanglement properties. The physics of resonating bond states have arguably started to become appealing since superconductivity was discovered for some unusual materials. In case of conventional superconductors, the element exhibits superconducting properties via its transition from a metallic state to a superconducting state. On the contrary, for high- T_C superconductivity, the parent system is a Mott insulator which upon doping starts exhibiting superconducting properties. It was argued that in copper oxide lattices, electrons from neighboring copper atoms interact to form a valence bond, which locks them in place. Hence, a plausible description of high- T_c superconductivity can indeed be obtained in terms of a doped resonating valence bond state formalism.

Besides this, notable success has also been achieved for the description of ground state properties of certain higher dimensional lattices using the framework of short-ranged resonating valence bond theory. Efficient analytical techniques to deal with multi-legged ladder systems, based on the variational resonating valence bond state ansatz have also been proposed. In addition to this, various other important properties of resonating valence bond states, which include the presence of topological order, reveals phase properties of many complex quantum systems which remain elusive when studied using the behavior of conventional order parameters.

Over the years, the resonating valence bond technique has turned out to be an efficient technique to provide insight about many useful properties related to various complex quantum systems. In addition to this, using extensive numerical and analytical techniques, a signature of resonating valence bond liquid phases have also been identified for some complex quantum systems. It is therefore natural to explore the possibility of employing resonating valence bond states as potential candidates for designing quantum information and computation networks. One such example is the one-way quantum computation in which resonating valence bond states have turned out to be an appealing candidate. Topological quantum computation is another network which may find resonating valence bond states as a possible substrate. In this Chapter, we present a summary of the main results that we have obtained in this thesis.

In Chapter 1, we have briefly highlighted the importance of characterization of quantum correlations present in states of interacting quantum-many-body systems. In Chapter 2, we have discussed a few measures of bipartite as well as multiparty

quantum entanglement which we have later used in this thesis. Thereafter, in Chapter 3, we derived analytical recursive methods to construct resonating valence bond states in doped and undoped multi-legged spin-1/2 quantum ladders. We found that though for two-legged undoped quantum ladders, the number of dimer coverings with the increase of the number of ladder-rungs, follow the Fibonacci sequence, significant deviations result, if we introduce doping into the system or extend to multi-legged doped and undoped quantum ladders. Using the analytical recursion method, we then investigated the behavior of valence bond entanglement entropy between a contiguous block to the rest of the system with the increase of size of the block. This provides useful information regarding the scaling of entanglement in the ground state configuration of the system. We found that the ground state entanglement follows the area law and this property remains invariant even if finite amount of doping is introduced into the system.

In Chapter 4, we considered the ground state of Heisenberg spin ladders and investigated the odd-even dichotomy of genuine multiparty entanglement. We found that when the size of the system is small, multiparty entanglement measure can capture the odd-even dichotomy present in the system. It turned out that for odd-legged quantum ladders, multiparty entanglement increases with the increase of system size, whereas for the even one, it shows the opposite behavior. However, as the size of the system is increased to a moderately large value, this odd-even dichotomy of multiparty entanglement appears to become elusive. In order to capture the behavior of multiparty entanglement even for large lattices, one needs to look for other “order parameters” to detect the dichotomy. Interestingly, over the years, many properties of these strongly coupled quantum ladders systems have been successfully characterized using the framework of the short-ranged resonating valence bond state ansatz, which emerges as possible ground state of the Heisenberg spin ladders in some parameter range, we derived an analytical recursion method which provided all possible reduced density matrices of the system, even in the limit of large lattice sites. We further showed that those reduced states can indeed be useful to quantify the amount of multiparty entanglement present in the quantum state. By performing a comparison with the result obtained via the exact diagonalization techniques, we found that the behavior of multiparty entanglement obtained using short-ranged resonating valence bond states encapsulates the qualitative features that are obtained for both the ladders, and hence can serve as an efficient tool to capture the behavior in the asymptotic limit. By doing finite-size scaling analysis, we showed that though

multiparty entanglement measure itself fails to capture the odd-even dichotomy, its scaling behavior is capable of distinguishing same, even in the asymptotic limit.

Thereafter, In Chapter 5, we investigate the trends of genuine multipartite entanglement in the ground states of a Hubbard model with large onsite interactions, viz. the t - J model, obtained by exact diagonalization technique. Subsequently, for finite hole doping, the short-range doped resonating valence bond state was considered to be the ground state of the Hubbard model. We prove that doped resonating valence bond ladder states are always genuine multipartite entangled. We then formulated an analytical recursion method for the wave function, which allowed us to efficiently estimate the entanglement as well as other physical quantities in large doped resonating valence bond ladders. From the behavior of multiparty entanglement obtained from the doped resonating valence bond state ansatz, we showed that multiparty entanglement has an explicit dependence on the hole concentration of the system and at high doping scales linearly with the doping concentration. Thereafter, it reaches to a maxima at some finite value of the doping concentration, and decays for further increase of the doping. In order to compare the behavior of multiparty entanglement obtained using the short-ranged resonating valence bond ansatz to that of the exact diagonalization results, we made a comparative study for small systems and found quantitative agreement of both the behavior. Note, however that we did not claim to detect a high T_c superconducting phase by using the genuine multipartite entanglement as an order parameter. This was also not the primary motivation of our work, which was to construct an efficient recursive method for evaluating bipartite as well as multiparty observables in large doped RVB states. As an useful spin-off to our main results, we are able to show that for some parameter ranges, genuine multiparty entanglement may serve as an indicator to whether the system has entered into the superconducting phase or not. It is plausible that one would require further physical properties along with the genuine multiparty entanglement, to identify all the phases. Since there exists, as yet, no order parameter that can uniquely identify all the relevant phases of the ground states of doped Hubbard model, the applicability of genuine multiparty entanglement as a suitable order parameter may merit further investigation.

In Chapter 6, we considered an isotropic quantum network of spin-1/2 particles with a finite fraction of defects, where the corresponding wave function of the network is rotationally invariant under the action of local unitaries. By using quantum

information-theoretic concepts like strong subadditivity of von Neumann entropy and approximate quantum telecloning, we prove analytically that even in the presence of defects, the network sustains genuine multisite entanglement, and at the same time may exhibit finite amount of bipartite entanglement, in contrast to the network with no defects.

We believe that the results obtained will be useful in general for analysis and understanding of resonating valence bond states, and in particular for their utilization in quantum information processing protocols. A large number of questions remain open, including the question of error corrected quantum protocols in resonating valence bond-type systems.

Bibliography

- [1] S. S. Roy, H. S. Dhar, A. Sen(De), and U. Sen, *Fibonacci sequence and valence bond entanglement entropy in quantum spin ladders*, under preparation.
- [2] S. S. Roy, H. S. Dhar, D. Rakshit, A. Sen(De), and U. Sen, *Diverging scaling with converging multisite entanglement in odd and even quantum Heisenberg ladders*, New J. Phys. **18**, 023025 (2016).
- [3] S. S. Roy, H. S. Dhar, D. Rakshit, A. Sen(De), and U. Sen, *Analytical recursive method to ascertain multisite entanglement in doped quantum spin ladders*, Phys. Rev. B **96**, 075143 (2017).
- [4] S. S. Roy, H. S. Dhar, D. Rakshit, A. Sen(De), and U. Sen, *Response to defects in multi- and bipartite entanglement of isotropic quantum spin networks*, arXiv:1607.05195 [quant-ph].
- [5] C. H. Bennet and P. W. Shor, *Quantum Information Theory*, IEEE Trans. Inf. Theory **44**, 2724 (1998).
- [6] J. Preskill, *Lecture Notes for Physics 229: Quantum Information and Computation* (California Institute of Technology, 1998).
- [7] M. A. Nielsen and I. L. Chuang, *Quantum Computation and Quantum Information* (Cambridge University Press, Cambridge, 2000).
- [8] D. Bruß, G. Leuchs, *Lectures on Quantum Information* (Wiley-VCH, Weinheim, 2006).
- [9] M. M. Wilde, *Quantum Information Theory* (Cambridge University Press, Cambridge, 2013).

- [10] R. P. Feynman, *Simulating Physics with Computers*, Int. Jour. Theor. Phys. **21**, 6 (1982).
- [11] D. Deutsch, *Quantum Theory, the Church-Turing Principle and the Universal Quantum Computer*, Proc. R. Soc. A. **400**, 97 (1985).
- [12] D. Deutsch and R. Jozsa, *Rapid solutions of problems by quantum computation*, Proc. R. Soc. A. **439**, 553 (1992).
- [13] P. W. Shor, *Polynomial-Time Algorithms for Prime Factorization and Discrete Logarithms on a Quantum Computer*, SIAM J. Comput. **26**, 1484 (1997).
- [14] L. K. Grover, *A fast quantum mechanical algorithm for database search*, Proce., 28th Ann. ACM Symp. on the Theor. of Comp. **212** (1996).
- [15] R. Cleve, A. Ekert, C. Macchiavello, and M. Mosca, *Quantum algorithms revisited*, Proc. R. Soc. A **454**, 339 (1998).
- [16] C. H. Bennett, *Quantum cryptography using any two nonorthogonal states*, Phys. Rev. Lett. **68**, 3121 (1992).
- [17] C. H. Bennett and G. Brassard, *Quantum cryptography: Public key distribution and coin tossing*, in Proc. IEEE Intl. Conf. on Computers, Systems, and Signal Processing, **175** (1994).
- [18] H. B. Pasquinucci and N. Gisin, *Incoherent and coherent eavesdropping in the six-state protocol of quantum cryptography*, Phys. Rev. A **59**, 4238 (1999).
- [19] N. Gisin, G. Ribordy, W. Tittel, and H. Zbinden, *Quantum cryptography*, Rev. Mod. Phys. **74**, 145 (2002).
- [20] D. Bruss, G. Erdelyi, T. Meyer, T. Riege, J. Rothe, *Quantum Cryptography: A Survey*, ACM Comput. Surv. **39** (2007).
- [21] W. Wootters and W. Zurek, *The no-cloning theorem*, Phys. Today **62**, 76 (2009).
- [22] C. P. Bauer, *Secret History-The Story of Cryptology* (CRC Press, Boca Raton 2013).
- [23] R. Horodecki, P. Horodecki, M. Horodecki, and K. Horodecki, *Quantum entanglement*, Rev. Mod. Phys. **81**, 865 (2009).

- [24] A. Einstein, B. Podolsky, and N. Rosen, *Can Quantum-Mechanical Description of Physical Reality Be Considered Complete?*, Phys. Rev. **47**, 777 (1935).
- [25] E. Schrödinger, *Die gegenwärtige Situation in der Quantenmechanik*, Naturwissenschaften **23**, 807 (1935).
- [26] J. Bell, *On the Einstein Podolsky Rosen paradox*, Physics **1**, 195 (1964).
- [27] J. Bell, *On the problem of hidden variables in quantum mechanics*, Rev. Mod. Phys. **38**, 447 (1966).
- [28] J. F. Clauser, M. A. Horne, A. Shimony, and R. A. Holt, *Proposed Experiment to Test Local Hidden-Variable Theories*, Phys. Rev. Lett. **23**, 880 (1969).
- [29] J. Dalibard and G. Roger, *Experimental Test of Bell's Inequalities Using Time-Varying Analyzers Alain Aspect*, Phys. Rev. Lett. **49**, 1804 (1982).
- [30] G. Weihs, T. Jennewein, C. Simon, H. Weinfurter, and A. Zeilinger, *Violation of Bell's Inequality under Strict Einstein Locality Conditions*, Phys. Rev. Lett. **81**, 5039 (1998).
- [31] D. Kielpinski, A. B. Kish, J. Britton, V. Meyer, M. A. Rowe, C. A. Sackett, W. M. Itano, C. Monroe, and D. J. Wineland, *Recent Results in Trapped-Ion Quantum Computing*, arXiv:0102086 [quant-ph].
- [32] M. Barbieri, F. De Martini, G. Di Nepi, P. Mataloni, G. M. D'Ariano, and C. Macchiavello, *Detection of Entanglement with Polarized Photons: Experimental Realization of an Entanglement Witness*, Phys. Rev. Lett. **91**, 227901 (2003).
- [33] C. H. Bennett, G. Brassard, C. Crépeau, R. Jozsa, A. Peres, and W. K. Wootters, *Teleporting an unknown quantum state via dual classical and Einstein-Podolsky-Rosen channels*, Phys. Rev. Lett. **70**, 1895 (1993).
- [34] C. Bennett, S. Wiesner, *Communication via one- and two-particle operators on Einstein-Podolsky-Rosen states*, Phys. Rev. Lett. **69**, 2881 (1992).
- [35] A. K. Ekert, *Quantum cryptography based on Bell's theorem*, Phys. Rev. Lett. **67**, 661 (1991).
- [36] Y. Shi, *Entanglement in Relativistic Quantum Field Theory*, Phys. Rev. D **70**, 105001 (2004).

- [37] M. Lewenstein, A. Sanpera, V. Ahufinger, B. Damskic, A. Sen(De), and U. Sen, *Ultracold atomic gases in optical lattices: mimicking condensed matter physics and beyond*, Adv. Phys. **56**, 243 (2007).
- [38] L. Amico, R. Fazio, A. Osterloh, and V. Vedral, *Entanglement in many-body systems*, Rev. Mod. Phys. **80**, 517 (2008).
- [39] S. Das, S. Shankaranarayanan, S. Sur, *Black hole entropy from entanglement: A review*, Horizons in World Physics, **268** (2009).
- [40] J. I. Cirac, *Entanglement in many-body quantum systems*, arXiv:1205.3742 [quant-ph].
- [41] M. Lewenstein, A. Sanpera, and V. Ahufinger, *Ultracold Atoms in Optical Lattices: Simulating Quantum Manybody Systems* (Oxford University Press, Oxford, 2012).
- [42] M. V. Raamsdonk, *Lectures on Gravity and Entanglement*, Proc. 2015 Theor. Adv. Stud. Inst. Elem. Part. Phys. (2015).
- [43] S. Sachdev, *Quantum Phase Transitions*, 2nd Ed. (Cambridge University Press, Cambridge, 2011).
- [44] S. L. Sondhi, S. M. Girvin, J. P. Carini, and D. Shahar, *Continuous quantum phase transitions*, Rev. Mod. Phys. **69**, 315 (1997).
- [45] M. Vojta, *Quantum Phase Transitions*, Rep. Prog. Phys. **66**, 2069 (2003).
- [46] V. Coffman, J. Kundu, and W. K. Wootters, *Distributed entanglement*, Phys. Rev. A **61**, 052306 (2000).
- [47] A. Osterloh, L. Amico, G. Falci, and R. Fazio, *Scaling of entanglement close to a quantum phase transition*, Nat. **416**, 608 (2001).
- [48] X. Wang, *Entanglement in the quantum Heisenberg XY model*, Phys. Rev. A **64**, 012313 (2001).
- [49] K. A. Dennison and W. K. Wootters, *Entanglement sharing among qudits*, Phys. Rev. A **65**, 010301 (2001).
- [50] T. J. Osborne and M. A. Nielsen, *Entanglement in a simple quantum phase transition*, Phys. Rev. A **66**, 032110 (2002).

- [51] D. A. Meyer and N. R. Wallach, *Global entanglement in multiparticle systems*, J. Math. Phys. **43**, 4273 (2002).
- [52] W. K. Wootters, *Parallel transport in an entangled ring*, J. Math. Phys. **43**, 4307 (2002).
- [53] P. Zanardi, *Quantum entanglement in fermionic lattices*, Phys. Rev. A **65**, 042101 (2002).
- [54] I. Bose and E. Chattopadhyay, *Macroscopic entanglement jumps in model spin systems*, Phys. Rev. A **66**, 062320 (2002).
- [55] X. Wang, and P. Zanardi, *Quantum entanglement and Bell inequalities in Heisenberg spin chains*, Phys. Lett. A **301**, 1 (2002).
- [56] G. Vidal, J. I. Latorre, E. Rico, and A. Kitaev, *Entanglement in Quantum Critical Phenomena*, Phys. Rev. Lett. **90**, 227902 (2003).
- [57] J. I. Latorre, E. Rico, and G. Vidal, *Ground state entanglement in quantum spin chains*, Quantum Inf. Comput. **4**, 48 (2004).
- [58] F. Verstraete, M. A. M. Delgado, and J. I. Cirac, *Diverging Entanglement Length in Gapped Quantum Spin Systems*, Phys. Rev. Lett. **92**, 087201 (2004).
- [59] J. K. Pachos and M. B. Plenio, *Three-Spin Interactions in Optical Lattices and Criticality in Cluster Hamiltonians*, Phys. Rev. Lett. **93**, 056402 (2004).
- [60] R. W. Chhajlany, P. Tomczak, A. Wójcik, and J. Richter, *Entanglement in the Majumdar-Ghosh model*, Phys. Rev. A **75**, 032340 (2007).
- [61] G. De Chiara, L. Lepori, M. Lewenstein, and A. Sanpera, *Entanglement Spectrum, Critical Exponents, and Order Parameters in Quantum Spin Chains*, Phys. Rev. Lett. **109**, 237208 (2012).
- [62] Y. Chen, P. Zanardi, Z. D. Wang, and F. C. Zhang, *Sublattice entanglement and quantum phase transitions in antiferromagnetic spin chains*, New J. Phys. **8**, 97 (2006).
- [63] S. S. Roy, H. S. Dhar, D. Rakshit, A. Sen(De), and U. Sen, *Detecting phase boundaries of quantum spin-1/2 XXZ ladder via bipartite and multipartite entanglement transitions*, J. Mag. Mag. Mat. **444**, 227 (2017) .

- [64] A. Biswas, R. Prabhu, A. Sen(De), and U. Sen, *Genuine-multipartite-entanglement trends in gapless-to-gapped transitions of quantum spin systems*, Phys. Rev. A **90**, 032301 (2014).
- [65] J. Eisert, M. Cramer, and M. B. Plenio, *Area laws for the entanglement entropy*, Rev. Mod. Phys. **82**, 277 (2010).
- [66] H. S. Dhar, A. K. Pal, D. Rakshit, A. Sen De, and U. Sen, *Monogamy of quantum correlations - a review*, arXiv:1610.01069 [quant-ph].
- [67] L. Cincio, J. Dziarmaga, M. M. Rams, and W. H. Zurek, *Entropy of entanglement and correlations induced by a quench: Dynamics of a quantum phase transition in the quantum Ising model*, Phys. Rev. A **75**, 052321 (2007).
- [68] A. M. Läuchli and C. Kollath, *Spreading of correlations and entanglement after a quench in the one-dimensional Bose-Hubbard model*, J. Stat. Mech. P05018 (2008).
- [69] K. Sengupta and D. Sen, *Entanglement production due to quench dynamics of an anisotropic XY chain in a transverse field*, Phys. Rev. A **80**, 032304 (2009).
- [70] A. Polkovnikov, K. Sengupta, A. Silva, and M. Vengalattore, *Colloquium: Nonequilibrium dynamics of closed interacting quantum systems*, Rev. Mod. Phys. **83**, 863 (2011).
- [71] A. Sen(De), U. Sen, and M. Lewenstein, *Nonergodicity of entanglement and its complementary behavior to magnetization in an infinite spin chain*, Phys. Rev. A **70**, 060304(R) (2004).
- [72] A. Sen(De), U. Sen, and M. Lewenstein, *Dynamical phase transitions and temperature-induced quantum correlations in an infinite spin chain*, Phys. Rev. A **72**, 05231 (2005).
- [73] E. Plekhanov, A. Avella, and F. Mancini, *Nonergodic dynamics of the extended anisotropic Heisenberg chain*, Phys. Rev. B **74**, 115120 (2006).
- [74] R. Prabhu, A. Sen(De), and U. Sen, *Dual quantum correlation paradigms exhibit opposite statistical-mechanical properties*, Phys. Rev. A **86**, 012336 (2012).
- [75] U. Mishra, R. Prabhu, A. Sen(De), and U. Sen, *Tuning interaction strength leads to ergodic nonergodic transition of quantum correlations in anisotropic Heisenberg spin model*, Phys. Rev. A **87**, 052318 (2013).

- [76] S. R. White, *Density matrix formulation for quantum renormalization groups*, Phys. Rev. Lett. **69**, 2863 (1992).
- [77] G. Vidal, *Efficient simulation of one-dimensional quantum many-body systems*, Phys. Rev. Lett. **93**, 040502 (2004).
- [78] F. Verstraete, V. Murg, and J. I. Cirac, *Matrix product states, projected entangled pair states, and variational renormalization group methods for quantum spin systems*, Adv. Phys. **57**, 143 (2008).
- [79] J. I. Cirac and F. Verstraete, *Renormalization and tensor product states in spin chains and lattices*, J. Phys. A **42**, 504004 (2009).
- [80] J. Eisert, *Entanglement and tensor network states*, Model. Simul. **3**, 520 (2013).
- [81] R. Órus, *A Practical Introduction to Tensor Networks: Matrix Product States and Projected Entangled Pair States*, Ann. Phys. **349**, 117 (2014).
- [82] A. Zeilinger, *Experiment and the foundations of quantum physics*, Rev. Mod. Phys. **71**, S288 (1999).
- [83] X. S. Ma, S. Zotter, J. Kofler, R. Ursin, T. Jennewein, C. Brukner, and A. Zeilinger, *Experimental delayed-choice entanglement swapping*, Nat. Phys. **8**, 479 (1999).
- [84] J. W. Pan, D. Bouwmeester, M. Daniell, H. Weinfurter, and A. Zeilinger, *Experimental delayed-choice entanglement swapping*, Nat. **403**, 51 (2000).
- [85] P. Walther, K. J. Resch, T. Rudolph, E. Schenck, H. Weinfurter, V. Vedral, M. Aspelmeyer, and A. Zeilinger, *Experimental one-way quantum computing*, Nat. **434**, 16 (2005).
- [86] J. A. Jones, *Quantum Computing and Nuclear Magnetic Resonance*, Phys. Chem. Comm. **11** (2001).
- [87] L. M. Vandersypen and I. L. Chuang, *NMR techniques for quantum control and computation*, Rev. Mod. Phys. **76**, 1037 (2005).
- [88] G. Misguich and C. Lhuillier, *Frustrated Spin Systems*, edited by H. T. Diep (World-Scientific, Singapore, 2005).
- [89] A. Aharony, *Spin-flop multicritical points in systems with random fields and in spin glasses*, Phys. Rev. B **18**, 3328 (1978).

- [90] B. J. Minchau and R. A. Pelcovits, *Two-dimensional XY model in a random uniaxial field*, Phys. Rev. B **32**, 3081 (1985).
- [91] C. L. Henley, *Ordering due to disorder in a frustrated vector antiferromagnet*, Phys. Rev. Lett. **62**, 2056 (1989).
- [92] A. Moreo, E. Dagotto, T. Jolicoeur, and J. Riera, *Incommensurate correlations in the t - J and frustrated spin-1/2 Heisenberg models*, Phys. Rev. B **42**, 6283 (1990).
- [93] D. A. Abanin, P. A. Lee, and L. S. Levitov, *Randomness-Induced XY Ordering in a Graphene Quantum Hall Ferromagnet*, Phys. Rev. Lett. **98**, 156801 (2007).
- [94] L. Adamska, M. B. S. Neto, and C. M. Smith, *Competing impurities and reentrant magnetism in $\text{La}_{2-x}\text{Sr}_x\text{Cu}_{1-z}\text{Zn}_z\text{O}_4$: Role of Dzyaloshinskii-Moriya and XY anisotropies*, Phys. Rev. B **75**, 134507 (2007).
- [95] A. Niederberger, T. Schulte, J. Wehr, M. Lewenstein, L. S. Palencia, and K. Sacha, *Disorder-Induced Order in Two-Component Bose-Einstein Condensates*, Phys. Rev. Lett. **100**, 030403 (2008).
- [96] A. Niederberger, J. Wehr, M. Lewenstein, and K. Sacha, *Disorder-induced phase control in superfluid Fermi-Bose mixtures*, Euro. Phys. Letts. **86**, 26004 (2009).
- [97] T. Yu and J. H. Eberly, *Sudden Death of Entanglement*, Science **323**, 598 (2009).
- [98] Z. Y. Xu and M. Feng, *Sudden death and birth of entanglement beyond the Markovian approximation*, Phys. Lett. A **373**, 1906 (2009).
- [99] X. Qin and F. M. Fa, *Entanglement Dynamics of the Double Intensity-Dependent Coupling Jaynes-Cummings Models*, Int. J. Theor. Phys. **51**, 778 (2012).
- [100] M. Pandit, S. Das, S. S. Roy, H. S. Dhar, and U. Sen, *Effects of cavity-cavity interaction on the entanglement dynamics of a generalized double Jaynes-Cummings model*, arXiv:1612.01165 [quant-ph].
- [101] L. Pauling, *Nature of the interatomic forces in metals*, Phys. Rev. **54**, 899 (1938).
- [102] P. W. Anderson, *Resonating valence bonds: A new kind of insulator?*, Mater. Res. Bull. **8**, 153 (1973).

- [103] P. Fazekas and P. W. Anderson, *On the ground state properties of the anisotropic triangular antiferromagnet*, Philos. Mag. **30**, 23 (1974).
- [104] G. Baskaran, Z. Zou, P. W. Anderson, *The resonating valence bond state and high- T_c superconductivity—A mean field theory*, Solid State Commun. **63**, 973 (1987).
- [105] P. W. Anderson, G. Baskaran, Z. Zou, and T. Hsu, *Resonating-valence-bond theory of phase transitions and superconductivity in La_2CuO_4 -based compounds*, Phy. Rev. Lett. **58**, 2790 (1987).
- [106] *Possible high T_c superconductivity in the Ba-La-Cu-O system*, Zeitschrift für Physik B, **64**, 189 (1986).
- [107] P. W. Anderson, *The Resonating Valence Bond State in La_2CuO_4 and Superconductivity*, Science **235**, 1196 (1987).
- [108] P. W. Anderson, *The Theory of Superconductivity in the High- T_c Cuprate Superconductors*, Princeton University Press, Princeton (1997).
- [109] P. Anderson, P. Lee, M. Randeria, T. M. Rice, N. Trivedi, and F. Zhang, *The physics behind high-temperature superconducting cuprates: the ‘plain vanilla’ version of RVB*, J. Phys. Condens. Matter **16**, 755 (2004).
- [110] G. Baskaran, *Resonating Valence Bond States in 2 and 3D: Brief History and Recent Examples*, Indian J. Phys. **89**, 583 (2006).
- [111] G. Baskaran and P. W. Anderson, *Gauge theory of high-temperature superconductors and strongly correlated Fermi systems*, Phys. Rev. B **37**, 580(R) (1988).
- [112] S. Liang, B. Doucot, and P. W. Anderson, *Some New Variational Resonating-Valence-Bond-Type Wave Functions for the Spin-1/2 Antiferromagnetic Heisenberg Model on a Square Lattice*, Phys. Rev. Lett. **61**, 365 (1988).
- [113] P. W. Anderson, *An Approximate Quantum Theory of the Antiferromagnetic Ground State*, Phys. Rev. **86**, 694 (1952).
- [114] J. Oitmaa and D. D. Betts, *The ground state of two quantum models of magnetism*, Canad. Jour. Phys. **56**, 897 (1978).
- [115] M. Kohmoto, *Resonating-valence-bond state: Comments on the antiferromagnetic ordering of the two-dimensional Heisenberg model*, Phys. Rev. B **37**, 3812(R) (1988).

- [116] J. T. Chayes, L. Chayes, and S. A. Kivelson, *Valence bond ground states in a frustrated two-dimensional spin-1/2 Heisenberg antiferromagnet*, Comm. Math. Phys. **123**, 53 (1989).
- [117] T. K. Lee and S. Feng, *Resonating-valence-bond wave function for the two-dimensional Heisenberg model on a triangular lattice*, Phys. Rev. B **41**, 11110 (1990).
- [118] I. Bose, *Two-dimensional spin models with resonating valence bond ground states*, Jour. Phys. **2**, 36 (1990).
- [119] K. Ueda, H. Kontani, M. Sigrist, and P. A. Lee, *Plaquette Resonating-Valence-Bond Ground State of CaV_4O_9* , Phys. Rev. Lett. **76**, 1932 (1996).
- [120] Y. Tang, A. W. Sandvik, and C. L. Henley, *Properties of resonating-valence-bond spin liquids and critical dimer models*, Phys. Rev. B **84**, 174427 (2011).
- [121] C. K. Majumdar and D. K. Ghosh, *On Next-Nearest-Neighbor Interaction in Linear Chain*, J. Math. Phys. **10**, 1388 (1969).
- [122] F. D. M. Haldane, *Exact Jastrow-Gutzwiller resonating-valence-bond ground state of the spin-1/2 antiferromagnetic Heisenberg chain with $1/r^2$ exchange*, Phys. Rev. Lett. **60**, 635 (1988).
- [123] L. Capriotti, F. Becca, A. Parola, and S. Sorella, *Resonating Valence Bond Wave Functions for Strongly Frustrated Spin Systems*, Phys. Rev. Lett. **87**, 097201 (2001).
- [124] S. Yan, D. A. Huse, S. R. White, *Spin-Liquid Ground State of the $S=1/2$ Kagome Heisenberg Antiferromagnet*, Science, **332**, 1173 (2011).
- [125] J. Wildeboer and A. Seidel, *Correlation Functions in $SU(2)$ -Invariant Resonating-Valence-Bond Spin Liquids on Nonbipartite Lattices*, Phys. Rev. Lett. **109**, 147208 (2012).
- [126] D. Poilblanc and N. Schuch, *Simplex Z_2 spin liquids on the kagome lattice with projected entangled pair states: Spinon and vison coherence lengths, topological entropy, and gapless edge modes*, Phys. Rev. B **87**, 140407(R) (2013).
- [127] R. Moessner and S. L. Sondhi, *Resonating Valence Bond Phase in the Triangular Lattice Quantum Dimer Model*, Phys. Rev. Lett. **86**, 1881 (2001).

- [128] T. K. Lee and S. Feng, *Doping dependence of antiferromagnetism in La_2CuO_4 : A numerical study based on a resonating-valence-bond state*, Phys. Rev. B **38**, 11809 (1988).
- [129] C. M. Ho, V. N. Muthukumar, M. Ogata, and P. W. Anderson, *Nature of Spin Excitations in Two-Dimensional Mott Insulators: Undoped Cuprates and Other Materials*, Phys. Rev. Lett. **86**, 1626 (1988).
- [130] Y. Fan and M. Ma, *Generating-function approach to the resonating-bond state on the triangular and square ladders*, Phys. Rev. B **37**, 1820 (1988).
- [131] G. Sierra and M. A. M. Delgado, *Short-range resonating-valence-bond state of even-spin ladders: A recurrent variational approach*, Phys. Rev. B **56**, 8774 (1997).
- [132] S. A. Kivelson, D. S. Rokhsar, and J. P. Sethna, *Topology of the resonating valence-bond state*, Phys. Rev. B **35**, 8865 (1987).
- [133] D. Poilblanc, N. Schuch, D. Perez-Garcia, and J. I. Cirac, *Resonating valence bond states in the PEPS formalism*, Phys. Rev. B **86**, 014404 (2012).
- [134] J. M. Stéphan, H. Ju, P. Fendley, and R. G. Melko, *Entanglement in gapless resonating valence-bond states*, New J. Phys. **15**, 015004 (2013).
- [135] D. Poilblanc, J. I. Cirac, and N. Schuch, *Chiral topological spin liquids with projected entangled pair states*, Phys. Rev. B **91**, 224431 (2015).
- [136] J. Wildeboer, A. Seidel, and R. G. Melko, *Entanglement entropy and topological order in resonating valence-bond quantum spin liquids*, Phys. Rev. B **95**, 100402(R) (2017).
- [137] D. Poilblanc, N. Schuch, and I. Affleck, *$SU(2)_1$ chiral edge modes of a critical spin liquid*, Phys. Rev. B **93**, 174414 (2016).
- [138] A. Chandran, D. Kaszlikowski, A. Sen(De), U. Sen, and V. Vedral, *Regional Versus Global Entanglement in Resonating-Valence-Bond States*, Phys. Rev. Lett. **99**, 170502 (2007).
- [139] R. Ramanathan, D. Kaszlikowski, M. Wiesniak, and V. Vedral, *Entanglement in doped resonating valence bond states*, Phys. Rev. B **78**, 224513 (2008).

- [140] H. S. Dhar, A. Sen(De), and U. Sen, *The density matrix recursion method: genuine multisite entanglement distinguishes odd from even quantum spin ladder states*, New J. Phys. **15**, 013043 (2013).
- [141] H. S. Dhar, A. Sen(De), and U. Sen, *Characterizing Genuine Multisite Entanglement in Isotropic Spin Lattices*, Phys. Rev. Lett. **111**, 070501 (2013).
- [142] H. S. Dhar and A. Sen(De), *Entanglement in resonating valence bond states: ladder versus isotropic lattices*, J. Phys. A: Math. Theor. **44**, 465302 (2011).
- [143] R. F. Werner, *Quantum states with Einstein-Podolsky-Rosen correlations admitting a hidden-variable model*, Phys. Rev. A **40**, 4277 (1989).
- [144] M. B. Plenio, S. Virmani, *An introduction to entanglement measures*, Quant. Inf. Comput. **7**,1 (2007).
- [145] M. Levin and X. G. Wen, *Detecting topological order in a ground state wave function*, Phys. Rev. Lett. **96**, 110405 (2006).
- [146] A. Kitaev and J. Preskill, *Topological Entanglement Entropy*, Phys. Rev. Lett. **96**, 110404 (2006).
- [147] C. H. Bennett, H. J. Bernstein, S. Popescu, and B. Schumacher, *Concentrating partial entanglement by local operations*, Phys. Rev. A **53**, 2046 (1996).
- [148] M. Srednicki, *Entropy and area*, Phys. Rev. Lett. **71**, 666 (1993).
- [149] F. Alet, S. Capponi, N. Laflorencie, and M. Mambrini, *Valence Bond Entanglement Entropy*, Phys. Rev. Lett. **99**, 117204 (2007).
- [150] R. W. Chhajlany, P. Tomczak, and A. Wójcik, *Topological Estimator of Block Entanglement for Heisenberg Antiferromagnets*, Phys. Rev. Lett. **99**, 167204 (2007).
- [151] A. B. Kallin, I. González, M. B. Hastings, and R. G. Melko, *Valence Bond and von Neumann Entanglement Entropy in Heisenberg Ladders*, Phys. Rev. Lett. **103**, 117203 (2009).
- [152] H. Tran and N. E. Bonesteel, *Valence bond entanglement and fluctuations in random singlet phases*, Phys. Rev. B **84**, 144420 (2011).
- [153] D. Schwandt, F. Alet, and M. Oshikawa, *Valence bond distribution and correlation in bipartite Heisenberg antiferromagnets*, Phys. Rev. B **89**, 104416 (2014).

- [154] A.W. Sandvik, *Ground State Projection of Quantum Spin Systems in the Valence-Bond Basis*, Phys. Rev. Lett. **95**, 207203 (2005).
- [155] M. A. Nielsen, *Conditions for a class of entanglement transformations*, Phys. Rev. Lett. **83** 436 (1999).
- [156] A. Peres, *Separability Criterion for Density Matrices*, Phys. Rev. Lett. **77**, 1413 (1996).
- [157] M. Horodecki, P. Horodecki, and R. Horodecki, *Separability of Mixed States: Necessary and Sufficient Conditions*, Phys. Lett. A **223**, 1 (1996).
- [158] K. Życzkowski, P. Horodecki, A. Sanpera, and M. Lewenstein, *Volume of the set of separable states*, Phys. Rev. A **58**, 883 (1988).
- [159] J. Lee, M. S. Kim, Y. J. Park, and S. Lee, *Partial teleportation of entanglement in a noisy environment*, J. Mod. Opt. **47**, 2151 (2000).
- [160] G. Vidal and R. F. Werner, *Computable measure of entanglement*, Phys. Rev. A **65**, 032314 (2002).
- [161] M. B. Plenio, *Logarithmic Negativity: A Full Entanglement Monotone That is not Convex*, Phys. Rev. Lett. **95**, 090503 (2005).
- [162] A. Sen(De) and U. Sen, *Channel capacities versus entanglement measures in multiparty quantum states*, Phys. Rev. A **81**, 012308 (2010).
- [163] A. Shimony, *Degree of entanglement*, Ann. NY Acad. Sci. **755**, 675 (1995).
- [164] H. Barnum and N. Linden, *Monotones and invariants for multi-particle quantum states*, J. Phys. A **34**, 6787 (2001).
- [165] T. Wei and P. M. Goldbart, *Geometric measure of entanglement and applications to bipartite and multipartite quantum states*, Phys. Rev. A **68**, 042307 (2003).
- [166] R. Orús, *Universal geometric entanglement close to quantum phase transitions*, Phys. Rev. Lett. **100**, 130502 (2008).
- [167] M. Blasone, F. Dell’Anno, S. DeSiena, and F. Illuminati, *Hierarchies of geometric entanglement*, Phys. Rev. A **77**, 062304 (2008).

- [168] R. Orús, S. Dusuel, and J. Vidal, *Equivalence of critical scaling laws for many-body entanglement in the Lipkin-Meshkov-Glick model*, Phys. Rev. Lett. **101**, 025701 (2008).
- [169] R. Orús, *Geometric entanglement in a one-dimensional valence-bond solid*, Phys. Rev. A **78**, 062332 (2008).
- [170] Q. Q. Shi, R. Orús, J. O. Fjærestad, and H. Q. Zhou, *Finite-size geometric entanglement from tensor network algorithms*, New J. Phys. **12**, 025008 (2010).
- [171] R. Orús and T. C. Wei, *Visualizing elusive phase transitions with geometric entanglement*, Phys. Rev. B **82**, 155120 (2010).
- [172] T. Das, S. S. Roy, S. Bagchi, A. Misra, A. Sen(De), and U. Sen, *Generalized geometric measure of entanglement for multiparty mixed states*, Phys. Rev. A **94**, 022336 (2016).
- [173] D. S. Rokhsar and S. A. Kivelson, *Superconductivity and the Quantum Hard-Core Dimer Gas*, Phys. Rev. Lett. **61**, 2376 (1988).
- [174] X. G. Wen, *Mean-field theory of spin-liquid states with finite energy gap and topological orders*, Phys. Rev. B **44**, 2664 (1991).
- [175] Y. Zhou, K. Kanoda, and T. K. Ng, *Quantum spin liquid states*, Rev. Mod. Phys. **89**, 025003 (2017).
- [176] E. H. Kim, G. Sierra, and D. Duffy, *Recurrent variational approach to the two-leg Hubbard ladder*, Phys. Rev. B **60**, 5169 (1999).
- [177] G. H. Hardy and E. M. Wright, *An introduction to the theory of numbers*, (Oxford University Press, Oxford, 1979).
- [178] R. A. Dunlap, *The Golden Ratio and Fibonacci Numbers*, (World Scientific, Singapore, 1997).
- [179] M. Livio, *The golden ratio: The story of phi, the world's most astonishing number*, (Broadway Books, New York, 2008).
- [180] H. Tasaki, *Order and disorder in the resonating-valence-bond state*, Phys. Rev. B **40**, 9183 (1989).
- [181] S. R. White, R. M. Noack, and D. J. Scalapino, *Resonating Valence Bond Theory of Coupled Heisenberg Chains*, Phys. Rev. Lett. **73**, 886 (1994).

- [182] F. G. S. L. Brandao and M. Horodecki, *An area law for entanglement from exponential decay of correlations*, *Nat. Phys.* **9**, 721 (2013).
- [183] X. G. Wen and P. A. Lee, *Theory of Underdoped Cuprates*, *Phys. Rev. Lett.* **76**, 503 (1996).
- [184] P. A. Lee and X. G. Wen, *Unusual Superconducting State of Underdoped Cuprates*, *Phys. Rev. Lett.* **78**, 4111 (1997).
- [185] T. Moriya and K. Ueda, *Antiferromagnetic spin fluctuation and superconductivity*, *Rep. Prog. Phys.*, **66**, 8 (2003).
- [186] P. A. Lee, N. Nagaosa, and X. G. Wen, *Doping a Mott insulator: Physics of high-temperature superconductivity*, *Rev. Mod. Phys.* **78**, 17 (2006).
- [187] G. Baskaran, *RVB States in doped Band Insulators from Coloumb forces: Theory and a case study of Superconductivity in BiS_2 Layers*, *Supercond. Sci. Technol.* **29**, 124002 (2016), and references therein.
- [188] E. Dagotto, J. Riera, and D. Scalapino, *Superconductivity in ladders and coupled planes*, *Phys. Rev. B* **45**, 5744 (1992).
- [189] S. R. White, R. M. Noack, and D. J. Scalapino, *Resonating Valence Bond Theory of Coupled Heisenberg Chains*, *Phys. Rev. Lett.* **73**, 886 (1994).
- [190] E. Dagotto, and T. M. Rice, *Surprises on the Way from 1D to 2D Quantum Magnets: the Novel Ladder Materials*, *Science* **271**, 618 (1996).
- [191] H. Yao and S. A. Kivelson, *Exact Spin Liquid Ground States of the Quantum Dimer Model on the Square and Honeycomb Lattices*, *Phys. Rev. Lett.* **108**, 247206 (2012).
- [192] S. Gopalan, T. M. Rice, and M. Sigrist, *Spin ladders with spin gaps: A description of a class of cuprates*, *Phys. Rev. B* **49**, 8901 (1994).
- [193] K. Modi, A. Brodutch, H. Cable, T. Paterek, and V. Vedral, *The classical-quantum boundary for correlations: Discord and related measures*, *Rev. Mod. Phys.* **84**, 1655 (2012).
- [194] X. Chen, Z. C. Gu, and X. G. Wen, *Local unitary transformation, long-range quantum entanglement, wave function renormalization, and topological order*, *Phys. Rev. B* **82**, 155138 (2010).

- [195] T. C. Wei, D. Das, S. Mukhopadhyay, S. Vishveshwara, and P. M. Goldbart, *Global entanglement and quantum criticality in spin chains*, Phys. Rev. A **71**, 060305(R) (2005).
- [196] T. R. de Oliveira, G. Rigolin, M. C. de Oliveira, and E. Miranda, *Multipartite Entanglement Signature of Quantum Phase Transitions*, Phys. Rev. Lett. **97**, 170401 (2006).
- [197] D. Buhr, M. E. Carrington, T. Fugleberg, R. Kobes, G. Kunstatter, D. McGillis, C. Pugh, and D. Ryckman, *Geometrical entanglement of highly symmetric multipartite states and the Schmidt decomposition*, J. Phys. A: Math. Theor. **44**, 365305 (2011).
- [198] M. F. Yang, *Reexamination of entanglement and the quantum phase transition*, Phys. Rev. A **71**, 030302 (2005).
- [199] X. F. Qian, T. Shi, Y. Li, Z. Song, and C. P. Sun, *Characterizing entanglement by momentum jump in the frustrated Heisenberg ring at a quantum phase transition*, Phys. Rev. A **72**, 012333 (2005).
- [200] M. N. Bera, R. Prabhu, A. Sen(De), and U. Sen, *Multisite Entanglement acts as a Better Indicator of Quantum Phase Transitions in Spin Models with Three-spin Interactions*, arXiv:1209.1523 [quant-ph].
- [201] H. Ju, A. B. Kallin, P. Fendley, M. B. Hastings, and R. G. Melko, *Entanglement scaling in two-dimensional gapless systems*, Phys. Rev. B **85**, 165121 (2012).
- [202] M. B. Hastings, I. González, A. B. Kallin, and R. G. Melko, *Measuring Renyi Entanglement Entropy in Quantum Monte Carlo Simulations*, Phys. Rev. Lett. **104**, 157201 (2010).
- [203] C. Lanczos, *An Iteration Method for the Solution of the Eigenvalue Problem of Linear Differential and Integral Operators*, J. Res. Natl. Bur. Stand. **45**, 255 (1950).
- [204] H. Nishimori, *Titpack—Numerical diagonalization routines and quantum spin Hamiltonians*, AIP Conf. Proc. **248**, 269 (1991).
- [205] M. Roncaglia, G. Sierra, and M. A. M. Delgado, *Dimer-resonating valence bond state of the four-leg Heisenberg ladder: Interference among resonances*, Phys. Rev. B **60**, 12134 (1999).

- [206] E. Orignac and T. Giamarchi, *Meissner effect in a bosonic ladder*, Phys. Rev. B **64**, 144515 (2001).
- [207] M. Atala, M. Aidelsburger, M. Lohse, J. T. Barreiro, B. Paredes, and I. Bloch, *Observation of chiral currents with ultracold atoms in bosonic ladders*, Nat. Phys. **10**, 588 (2014).
- [208] A. Petrescu and K. L. Hur, *Chiral Mott insulators, Meissner effect, and Laughlin states in quantum ladders*, Phys. Rev. B **91**, 054520 (2015).
- [209] I. Bloch, *Exploring quantum matter with ultracold atoms in optical lattices*, J. Phys. B: At. Mol. Opt. Phys. **38**, S629 (2005).
- [210] P. Treutlein, T. Steinmetz, Y. Colombe, B. Lev, P. Hommelhoff, J. Reichel, M. Greiner, O. Mandel, A. Widera, T. Rom, I. Bloch, and T. W. Hänsch, *Quantum information processing in optical lattices and magnetic microtraps*, Fortschr. Phys. **54**, 702 (2006).
- [211] D. Leibfried, R. Blatt, C. Monroe, and D. Wineland, *Quantum dynamics of single trapped ions*, Rev. Mod. Phys. **75**, 281 (2003).
- [212] H. Häffner, C. Roos, and R. Blatt, *Quantum computing with trapped ions*, Phys. Rep. **469**, 155 (2008).
- [213] K. Ki, M. S. Chang, S. Korenblit, R. Islam, E. E. Edwards, J. K. Freericks, G. D. Lin, L. M. Du, and C. Monroe, *Quantum simulation of frustrated Ising spins with trapped ions*, Nat. **465**, 590 (2010).
- [214] A. A. Guzik and P. Walther, *Photonic quantum simulators*, Nat. Phys. **8**, 285 (2012).
- [215] X. S. Ma, B. Dakic, W. Naylor, A. Zeilinger, and P. Walther, *Quantum simulation of the wavefunction to probe frustrated Heisenberg spin systems*, Nat. Phys. **7**, 399 (2011).
- [216] S. Nascimbène, Y. A. Chen, M. Atala, M. Aidelsburger, S. Trotzky, B. Paredes, and I. Bloch, *Experimental Realization of Plaquette Resonating Valence-Bond States with Ultracold Atoms in Optical Superlattices*, Phys. Rev. Lett. **108**, 205301 (2012).
- [217] H.A. Bethe, *On the theory of metals.*, Z. Phys. **71**, 205 (1931).

- [218] U. Schollwöck, *The density-matrix renormalization group*, Rev. Mod. Phys. **77**, 259 (2005).
- [219] W. M. C. Foulkes, L. Mitas, R. J. Needs, and G. Rajagopal, *Quantum Monte Carlo simulations of solids*, Rev. Mod. Phys. **73**, 33 (2001).
- [220] G. Misguich, D. Serban, and V. Pasquier, *Quantum Dimer Model on the kagomé Lattice: Solvable Dimer-Liquid and Ising Gauge Theory*, Phys. Rev. Lett. **89**, 137202 (2002).
- [221] B. S. Shastry and B. Sutherland, *Exact Ground State of a Quantum Mechanical antiferromagnet*, Physica **108B**, 1069 (1981).
- [222] H. J. Mikeska and A. K. Kolezhuk, *One-dimensional magnetism in: Quantum Magnetism*, eds. U. Schollwöck, J. Richter, D. J. J. Farnell and R.F. Bishop, Lecture Notes in Physics, **645** (Springer, Berlin, 2004).
- [223] M. Mambrini, A. Lauchli, D. Poilblanc, and F. Mila, *Plaquette valence-bond crystal in the frustrated Heisenberg quantum antiferromagnet on the square lattice*, Phys. Rev. B **74**, 144422 (2006).
- [224] B. Kumar, *Quantum spin models with exact dimer ground states*, Phys. Rev. B **66**, 024406 (2002).
- [225] I. Bose and A. Ghosh, *Exact ground and excited states of frustrated antiferromagnets on the CaV_4O_9 lattice*, Phys. Rev. B **56**, 3149 (1997).
- [226] K. S. Raman, R. Moessner, and S. L. Sondhi, *$SU(2)$ -invariant spin- $\frac{1}{2}$ Hamiltonians with resonating and other valence bond phases*, Phys. Rev. B **72**, 064413 (2005).
- [227] R. Moessner, S. L. Sondhi, and P. Chandra, *Phase diagram of the hexagonal lattice quantum dimer model*, Phys. Rev. B **64**, 144416 (2001).
- [228] G. Misguich, D. Serban, and V. Pasquier, *Quantum Dimer Model on the kagomé Lattice: Solvable Dimer-Liquid and Ising Gauge Theory*, Phys. Rev. Lett. **89**, 137202 (2002).
- [229] G. Misguich and C. Lhuillier, *Frustrated spin system* (World Scientific, Singapore, 2004).

- [230] J. Cano and P. Fendley, *Spin Hamiltonians with Resonating-Valence-Bond Ground States*, Phys. Rev. Lett. **105**, 067205 (2010).
- [231] B. Frischmuth, B. Ammon, and M. Troyer, *Susceptibility and low-temperature thermodynamics of spin- $\frac{1}{2}$ Heisenberg ladders*, Phys. Rev. B **54**, R3714(R) (1996).
- [232] Y. Nishiyama, N. Hatano, and M. Suzuki, *Hidden Orders and RVB Formation of the Four-Leg Heisenberg Ladder Model*, J. Phys. Soc. Japan **65**, 560 (1996).
- [233] H. C. Jiang, H. Yao, and L. Balents, *Spin liquid ground state of the spin- $\frac{1}{2}$ square J_1 - J_2 Heisenberg model*, Phys. Rev. B **86**, 024424 (2012).
- [234] L. Wang, Z. C. Gu, F. Verstraete, and X. G. Wen, *Spin-liquid phase in spin- $\frac{1}{2}$ square J_1 - J_2 Heisenberg model: A tensor product state approach*, arXiv:1112.3331 [quant-ph].
- [235] L. Wang, D. Poilblanc, Z. C. Gu, X. G. Wen, and F. Verstraete, *Constructing a Gapless Spin-Liquid State for the Spin- $\frac{1}{2}$ J_1 - J_2 Heisenberg Model on a Square Lattice*, Phys. Rev. Lett. **111**, 037202 (2013).
- [236] If we consider $|\phi_g\rangle$ as the exact ground state of the Hamiltonian, H_{int} , and $|\psi\rangle$ as the RVB state, corresponding to a quantum spin-1/2 ladder, then the fidelity between the two states is defined as $|\langle\phi_g|\psi\rangle|$. Further, the normalized relative difference in average energy is obtained using the relation, $\frac{E_g - \langle\psi|H_{int}|\psi\rangle}{E_g}$, where $E_g = \langle\phi_g|H_{int}|\phi_g\rangle$.
- [237] A. Y. Kitaev, *Fault-tolerant quantum computation by anyons*, Ann. Phys. **303**, 2 (2003).
- [238] E. H. Lieb and M. B. Ruskai, *Proof of the strong subadditivity of quantum-mechanical entropy*, J. Math. Phys. (N.Y.) **14**, 1938 (1973).
- [239] K. A. Chao, J. Spalek, and A. M. Oleś, *Kinetic exchange interaction in a narrow S-band*, J. Phys. C **10**, L271 (1977).
- [240] K. A. Chao, J. Spalek, and A. M. Oleś, *Canonical perturbation expansion of the Hubbard model*, Phys. Rev. B **18**, 3453 (1978).
- [241] F. C. Zhang and T. M. Rice, *Effective Hamiltonian for the superconducting Cu oxides*, Phys. Rev. B **37**, 3759(R) (1988).

- [242] V. J. Emery and G. Reiter, *Quasiparticles in the copper-oxygen planes of high- T_c superconductors: An exact solution for a ferromagnetic background*, Phys. Rev. B **38**, 11938(R) (1988).
- [243] A. Auerbach, *Interacting Electrons and Quantum Magnetism*, Springer, Berlin, 1998.
- [244] Another important derivation of the t - J model was obtained by Zhang and Rice from the three-band Hubbard model that describe the cuprate planes in high- T_c superconductors [241] (cf. [242]). The t - J model together with the one-band and three-band Hubbard models, in various limits, effectively describe the Hamiltonians for the study of high- T_c superconductivity, although disagreements exist [263, 264].
- [245] T. Barnes and J. Riera, *Susceptibility and excitation spectrum of $(VO)_2P_2O_7$ in ladder and dimer-chain models*, Phys. Rev. B **50**, 6817 (1994).
- [246] M. Sigrist, T. M. Rice, and F. C. Zhang, *Superconductivity in a quasi-one-dimensional spin liquid*, Phys. Rev. B **49**, 12058 (1994).
- [247] R. M. Noack, S. R. White, and D. J. Scalapino, *Correlations in a Two-Chain Hubbard Model*, Phys. Rev. Lett. **73**, 882 (1994).
- [248] D. V. Khveshchenko and T. M. Rice, *Spin-gap fixed points in the double-chain problem*, Phys. Rev. B **50**, 252 (1994).
- [249] B. Edegger, V. N. Muthukumar, and C. Gros, *Gutzwiller–RVB theory of high-temperature superconductivity: Results from renormalized mean-field theory and variational Monte Carlo calculations*, Adv. Phys. **927**, 1033 (2007).
- [250] M. Ogata, M. U. Luchini, and T. M. Rice, *Spin gap in a generalized one-dimensional t - J model*, Phys. Rev. B **44**, 12083(R) (1991).
- [251] M. Imada, *Spin-gap state and superconducting correlations in a one-dimensional dimerized t - J model*, Phys. Rev. B **48**, 550 (1993), and references therein.
- [252] M. Ogata, M. Luchini, S. Sorella, and F. Assaad, *Phase diagram of the one-dimensional t - J model*, Phys. Rev. Lett. **66**, 2388 (1991).
- [253] S. R. White and D. J. Scalapino, *Hole and pair structures in the t - J model*, Phys. Rev. B **55**, 6504 (1997).

- [254] S. R. White and D. J. Scalapino, *Density Matrix Renormalization Group Study of the Striped Phase in the 2D t - J Model*, Phys. Rev. Lett. **80**, 1272 (1998).
- [255] A. Moreno, A. Muramatsu, and S. R. Manmana, *Ground-state phase diagram of the one-dimensional t - J model*, Phys. Rev. B **83**, 205113 (2011).
- [256] S. Guertler and H. Monien, *Unveiling the Physics of the Doped Phase of the t - J Model on the Kagome Lattice*, Phys. Rev. Lett. **111**, 097204 (2013).
- [257] K. Sano, *Possible Phase Diagram of a t - J Ladder Model*, J. Phys. Soc. Jpn. **65**, 1146 (1996).
- [258] M. Troyer, H. Tsunetsugu, and T. M. Rice, *Properties of lightly doped t - J two-leg ladders*, Phys. Rev. B **53**, 251 (1996).
- [259] G. Sierra, M. A. M. Delgado, J. Dukelsky, S. R. White, and D. J. Scalapino, *Dimer-hole-RVB state of the two-leg t - J ladder: A recurrent variational ansatz*, Phys. Rev. B **57**, 11666 (1998).
- [260] F. D. M. Haldane, *‘Luttinger liquid theory’ of one-dimensional quantum fluids. I. Properties of the Luttinger model and their extension to the general 1D interacting spinless Fermi gas*, J. Phys. C: Solid State Phys. **14**, 2585 (1981).
- [261] N. Nagaosa and P. A. Lee, *Normal-state properties of the uniform resonating-valence-bond state*, Phys. Rev. Lett. **64**, 2450 (1990).
- [262] C. A. Hayward and D. Poilblanc, *Luttinger-liquid behavior and superconducting correlations in t - J ladders*, Phys. Rev. B **53**, 11721 (1996).
- [263] E. Dagotto, *Correlated electrons in high-temperature superconductors*, Rev. Mod. Phys. **66**, 763 (1994).
- [264] P. A. Lee, N. Nagaosa, and X. G. Wen, *Doping a Mott insulator: Physics of high-temperature superconductivity*, Rev. Mod. Phys. **78**, 17 (2006).
- [265] M. Hofmann, A. Osterloh, and O. G  hne, *Scaling of genuine multiparticle entanglement close to a quantum phase transition*, Phys. Rev. B **89**, 134101 (2014).
- [266] The counting of all possible dimer coverings with holes on a ladder configuration is not easily tractable using conventional exact methods. In fact, in a 2D quantum spin lattice, the arrangement of monomer and dimer coverings, as encountered in the doped RVB system, is *NP*-complete [139].

- [267] M. Jerrum, *Two-dimensional monomer-dimer systems are computationally intractable*, J. Stat. Phys. **48**, 121 (1987).
- [268] A. Eckardt and M. Lewenstein, *Controlled hole doping of a Mott insulator of ultracold fermionic atoms*, Phys. Rev. A **82**, 011606(R) (2010).
- [269] We develop a numerical algorithm, based on the Lanczos method, to exactly solve the composite hole-dimer qutrit system. By dividing the Hilbert space in different sub-spaces, according to the hole concentration and total S_z , exact ground state of the $t - J$ Hamiltonian can be obtained for moderate system size. The algorithm is implemented using codes written in MatLab and Fortran90.
- [270] J. G. Bednorz, and K. A. Müller, *Possible high T_c superconductivity in the Ba-La-Cu-O system*, Z. Phys. B **64**, 189 (1986).
- [271] B. Keimer, S. A. Kivelson, M. R. Norman, S. Uchida, and J. Zaanen, *From quantum matter to high-temperature superconductivity in copper oxides*, Nat. (London) **518**, 179 (2015).
- [272] N. F. Mott, *The Basis of the Electron Theory of Metals, with Special Reference to the Transition Metals*, Proc. Phys. Soc. A **62**, 416 (1949).
- [273] A. J. Leggett, *What DO we know about high T_c ?*, Nat. Phys. **2**, 134 (2006).
- [274] A. Mann, *High-temperature superconductivity at 25: Still in suspense*, Nat. (London) **475**, 280 (2011).
- [275] C. Gros, *Superconductivity in correlated wave functions*, Phys. Rev. B **38**, 931(R) (1988).
- [276] M. A. M. Delgado, *Entanglement and Concurrence in the BCS State*, arXiv:0207026 [quant-ph].
- [277] H. J. Kimble, *The quantum internet*, Nature **453**, 1023 (2008).
- [278] A. Zeilinger, A. Ekert, and D. Bouwmeester, eds., *The physics of quantum information : quantum cryptography, quantum teleportation, quantum computation* (Springer, Berlin, 2000).
- [279] S. Pirandola, J. Eisert, C. Weedbrook, A. Furusawa, and S. L. Braunstein, *Advances in quantum teleportation*, Nature Photon. **9**, 641 (2015).

- [280] C. Weedbrook, S. Pirandola, R. G. Patrón, N. J. Cerf, T. C. Ralph, J. H. Shapiro, and S. Lloyd, *Gaussian quantum information*, Rev. Mod. Phys. **84**, 621 (2012).
- [281] S. Bose, *Quantum communication through spin chain dynamics: an introductory overview*, Contemp. Phys. **48**, 13 (2007).
- [282] A. Key, *A Review of Perfect, Efficient, State Transfer and its Application as a Constructive Tool*, Int. J. Quantum Inform. **08**, 641 (2010).
- [283] L. C. Venuti, C. D. E. Boschi, and M. Roncaglia, *Long-Distance Entanglement in Spin Systems*, Phys. Rev. Lett. **96**, 247206 (2006).
- [284] L. Campos Venuti, C. Degli Esposti Boschi, and M. Roncaglia, *Qubit Teleportation and Transfer across Antiferromagnetic Spin Chains*, Phys. Rev. Lett. **99**, 060401 (2007).
- [285] R. Raussendorf and H. J. Briegel, *A one-way quantum computer*, Phys. Rev. Lett. **86**, 5188 (2001).
- [286] H. J. Briegel, D. E. Browne, W. Dür, R. Raussendorf, and M. Van den Nest, *Measurement-based quantum computation*, Nat. Phys. **5**, 19 (2009).
- [287] I. Bloch, J. Dalibard, and W. Zwerge, *Many-body physics with ultracold gases*, Rev. Mod. Phys. **80**, 885 (2008).
- [288] J. J. Morton and B. W. Lovett, *Hybrid Solid-State Qubits: The Powerful Role of Electron Spins*, Annu. Rev. Condens. Matter Phys. **2**, 189 (2011).
- [289] J. Wrachtrup and F. Jelezko, *Processing quantum information in diamond*, J. Phys. Condens. Matter **18**, S807 (2006).
- [290] M. V. G. Dutt, L. Childress, L. Jiang, E. Togan, J. Maze, F. Jelezko, A. S. Zibrov, P. R. Hemmer, and M. D. Lukin, *Quantum Register Based on Individual Electronic and Nuclear Spin Qubits in Diamond*, Science **316**, 1312 (2007).
- [291] J. H. Plantenberg, P. C. de Groot, C. J. P. M. Harmans, and J. E. Mooij, *Demonstration of controlled-NOT quantum gates on a pair of superconducting quantum bits*, Nat. **447**, 836 (2007).

- [292] L. DiCarlo, J. M. Chow, J. M. Gambetta, Lev S. Bishop, B. R. Johnson, D. I. Schuster, J. Majer, A. Blais, L. Frunzio, S. M. Girvin, R. J. Schoelkopf, *Demonstration of two-qubit algorithms with a superconducting quantum processor*, Nat. **460**, 240 (2009).
- [293] F. Mallet, F. R. Ong, A. Palacios-Laloy, F. Nguyen, P. Bertet, D. Vion, and D. Esteve, *Single-shot qubit readout in circuit quantum electrodynamics*, Nat. Phys. **5**, 791 (2009).
- [294] S. Pirandola and S. L. Braunstein, *Unite to build a quantum Internet*, Nature **532**, 169 (2016).
- [295] D. I. Schuster, A. P. Sears, E. Ginossar, L. DiCarlo, L. Frunzio, J. J. L. Morton, H. Wu, G. A. D. Briggs, B. B. Buckley, D. D. Awschalom, and R. J. Schoelkopf, *High-Cooperativity Coupling of Electron-Spin Ensembles to Superconducting Cavities*, Phys. Rev. Lett. **105**, 140501 (2010).
- [296] Y. Kubo, F. R. Ong, P. Bertet, D. Vion, V. Jacques, D. Zheng, A. DrÄlau, J.-F. Roch, A. Auffeves, F. Jelezko, J. Wrachtrup, M. F. Barthe, P. Bergonzo, and D. Esteve, *Strong Coupling of a Spin Ensemble to a Superconducting Resonator*, Phys. Rev. Lett. **105**, 140502 (2010).
- [297] T. J. Kippenberg and K. J. Vahala, *Cavity Optomechanics: Back-Action at the Mesoscale*, Science **321**, 1172 (2008).
- [298] P. Rabl, S. J. Kolkowitz, F. H. L. Koppens, J. G. E. Harris, P. Zoller, and M. D. Lukin, *A quantum spin transducer based on nanoelectromechanical resonator arrays*, Nat. Phys. **6**, 602 (2010).
- [299] F. Bussieres, C. Clausen, A. Tiranov, B. Korzh, V. B. Verma, S. W. Nam, F. Marsili, A. Ferrier, P. Goldner, H. Herrmann, C. Silberhorn, W. Sohler, M. Afzelius, N. Gisin, *Quantum teleportation from a telecom-wavelength photon to a solid-state quantum memory*, Nat. Phot. **8**, 775 (2014).
- [300] P. Richerme, Z.-X. Gong, A. Lee, C. Senko, J. Smith, M. Foss-Feig, S. Michalakakis, A. V. Gorshkov, and C. Monroe, *Non-local propagation of correlations in quantum systems with long-range interactions*, Nat. **511**, 198 (2014).
- [301] M. F. Feig, Z. X. Gong, C. W. Clark, and A. V. Gorshkov, *Nearly Linear Light Cones in Long-Range Interacting Quantum Systems*, Phys. Rev. Lett. **114**, 157201 (2015).

- [302] A. Bayat and V. Karimipour, *Thermal effects on quantum communication through spin chains*, Phys. Rev. A **71**, 042330 (2005).
- [303] J. M. Cai, Z. W. Zhou, and G. C. Guo, *Decoherence effects on the quantum spin channels* Phys. Rev. A **74**, 022328 (2006).
- [304] D. Burgarth and S. Bose, *Universal destabilization and slowing of spin-transfer functions by a bath of spins*, Phys. Rev. A **73**, 062321 (2006).
- [305] C. K. Burrell, J. Eisert, and T. J. Osborne, *Information propagation through quantum chains with fluctuating disorder*, Phys. Rev. A **80**, 052319 (2009).
- [306] L. Adamska, M.B. S. Neto, and C. M. Smith, Phys. Rev. B **75**, 134507 (2007).
- [307] A. Niederberger, T. Schulte, J. Wehr, M. Lewenstein, L. S. Palencia, and K. Sacha, *Disorder-induced order in two-Component Bose-Einstein condensates*, Phys. Rev. Lett. **100**, 030403 (2008).
- [308] A. Niederberger, J. Wehr, M. Lewenstein, and K. Sacha, *Disorder-induced phase control in superfluid Fermi-Bose mixtures*, Euro. Phys. Lett. **86**, 26004 (2009).
- [309] A. Niederberger, M. M. Rams, J. Dziarmaga, F. M. Cucchietti, J. Wehr, and M. Lewenstein, *Disorder-induced order in quantum XY chains*, Phys. Rev. A **82**, 013630 (2010).
- [310] D. Petrosyan, G. M. Nikolopoulos, and P. Lambropoulos, *State transfer in static and dynamic spin chains with disorder*, Phys. Rev. A **81**, 042307 (2010).
- [311] A. Bayat and S. Bose, *Entanglement transfer through an antiferromagnetic spin chain*, Adv. Math. Phys. **2010**, 127182 (2010).
- [312] S. Yang, A. Bayat, and S. Bose, *Spin-state transfer in laterally coupled quantum-dot chains with disorders*, Phys. Rev. A **82**, 022336 (2010).
- [313] D. I. Tsomokos, T. J. Osborne, and C. Castelnovo, *Interplay of topological order and spin glassiness in the toric code under random magnetic fields*, Phys. Rev. B **83**, 075124 (2011).
- [314] J. Jeske, N. Vogt, and J. H. Cole, *Excitation and state transfer through spin chains in the presence of spatially correlated noise*, Phys. Rev. A **88**, 062333 (2013).

- [315] M. S. Foster, H. Y. Xie, and Y. Z. Chou, *Phys. Rev. B*, *Topological protection, disorder, and interactions: Survival at the surface of three-dimensional topological superconductors*, **89**, 155140 (2014).
- [316] P. Villa Martín, J. A. Bonachela, and M. A. Muñoz, *Quenched disorder forbids discontinuous transitions in nonequilibrium low-dimensional systems*, *Phys. Rev. E* **89**, 012145 (2014), and references therein.
- [317] M. Murao, D. Jonathan, M. B. Plenio, and V. Vedral, *Quantum telecloning and multiparticle entanglement*, *Phys. Rev. A* **59**, 156 (1999).
- [318] D. J. Klein, *Exact ground states for a class of antiferromagnetic Heisenberg models with short-range interactions*, *J. Phys. A* **15**, 661 (1982).
- [319] C. Nayak and K. Shtengel, *Microscopic models of two-dimensional magnets with fractionalized excitations*, *Phys. Rev. B* **64**, 064422 (2001).
- [320] V. Scarani, S. Iblisdir, N. Gisin, and A. Acín, *Quantum cloning*, *Rev. Mod. Phys.* **77**, 1225 (2005).
- [321] C. Nayak, S. H. Simon, A. Stern, M. Freedman, and S. D. Sarma, *Non-Abelian anyons and topological quantum computation*, *Rev. Mod. Phys.* **80**, 1083 (2008).
- [322] F. Wilczek, *Quantum Mechanics of Fractional-Spin Particles*, *Phys. Rev. Lett.* **49**, 957 (1982).
- [323] M. A. Nielsen and C. M. Dawson, *Fault-tolerant quantum computation with cluster states*, *Phys. Rev. A* **71**, 042323 (2005).
- [324] D. V. Else, I. Schwarz, S. D. Bartlett, and A. C. Doherty, *Symmetry-protected phases for measurement-based quantum computation*, *Phys. Rev. Lett.* **108**, 240505 (2012).
- [325] F. Verstraete and J. I. Cirac, *Renormalization algorithms for quantum-many body systems in two and higher dimensions*, arXiv:cond-mat/0407066 [quant-ph].
- [326] F. Verstraete and J. I. Cirac, *Valence-bond states for quantum computation*, *Phys. Rev. A* **70**, 060302 (2004).
- [327] N. Schuch, D. Poilblanc, J. I. Cirac, and D. Pérez-García, *Resonating valence bond states in the PEPS formalism*, *Phys. Rev. B* **86**, 115108 (2012).

- [328] R. Raussendorf and T. C. Wei, *Quantum computation by local measurement*, Annu. Rev. Condens. Matter Phys. **3**, 239 (2012).
- [329] L. C. Kwek, Z. Wei, and B. Zeng, *Measurement-Based Quantum Computing with Valence-Bond-Solids*, Int. J. Mod. Phys. B **26**, 1230002 (2012).
- [330] X. Chen, B. Zeng, Z. C. Gu, B. Yoshida, and I. L. Chuang, *Gapped two-body hamiltonian whose unique ground state is universal for one-way quantum computation*, Phys. Rev. Lett. **102**, 220501 (2009).
- [331] D. Jennings, A. Dragan, S. D. Barrett, S. D. Bartlett, and T. Rudolph, *Quantum computation via measurements on the low-temperature state of a many-body system*, Phys. Rev. A **80**, 032328 (2009).
- [332] T. C. Wei, I. Affleck, and R. Raussendorf, *Affleck-Kennedy-Lieb-Tasaki state on a honeycomb lattice is a universal quantum computational resource*, Phys. Rev. Lett. **106**, 070501 (2011).
- [333] A. Miyake, *Quantum computational capability of a 2D valence bond solid phase*, Ann. Phys. **326**, 1656 (2011).
- [334] A. S. Darmawan, G. K. Brennen, and S. D. Bartlett, *Measurement-based quantum computation in a two-dimensional phase of matter*, New J. Phys. **14**, 013023 (2012).
- [335] T. C. Wei, P. Haghnegahdar, and R. Raussendorf, *Hybrid valence-bond states for universal quantum computation*, Phys. Rev. A **90**, 042333 (2014).
- [336] R. Kaltenbaek, J. Lavoie, B. Zeng, S. D. Bartlett, and K. J. Resch, *Optical one-way quantum computing with a simulated valence-bond solid*, Nat. Phys. **6**, 850 (2010).
- [337] K. Liu, W. D. Li, and Y. J. Gu, *Measurement-based quantum computation with an optical two-dimensional Affleck-Kennedy-Lieb-Tasaki state*, J. Opt. Soc. Am. B **31**, 2689 (2014).
- [338] S. Nascimbène, Y. A. Chen, M. Atala, M. Aidelsburger, S. Trotzky, B. Paredes, and I. Bloch, *Experimental Realization of Plaquette Resonating Valence-Bond States with Ultracold Atoms in Optical Superlattices*, Phys. Rev. Lett. **108**, 205301 (2012).